Weldability and Degradation Study of Coated Electrodes for Resistance Spot Welding

By

Kevin Randall Chan

A thesis
presented to the University of Waterloo
in fulfillment of the
thesis requirement for the degree of
Master of Applied Science
in
Mechanical Engineering

Waterloo, Ontario, Canada

I hereby declare that I am the sole author of this thesis.
I authorize the University of Waterloo to lend this thesis to other institutions or individuals for the purpose of scholarly research.

Kevin R. Chan

I further authorize the University of Waterloo to reproduce the thesis by photocopying or other means, in total or in part, at the request of other institutions or individuals for the purpose of scholarly research.

Kevin R. Chan

The University of Waterloo requires the signatures of all persons using or photocopying this thesis. Please sign below, and give address and date.

Abstract

In resistance spot welding of hot dipped galvanized steel sheet, the effect of a TiC metal matrix composite coated electrode on weldability, electrode life and degradation processes was studied. A review of the resistance spot welding process is given, followed by a literature study of the known issues when welding zinc coated steels and some of the methods explored to address those issues.

Coated and uncoated Class II CuCrZr domed-flat 'B' nose electrodes were used to conduct welding trials. To study the weldability of the coated electrodes compared to the uncoated electrodes, both types were subjected to increasing weld current and time while monitoring resultant weld size. Overall, the coated electrodes showed an improved weldability over the uncoated electrode. Testing revealed that the coated electrode was able to form welds at lower weld current and lower weld time than the uncoated electrode. The range of acceptable weld current and weld time was also increased when using the coated electrode. All other welding parameters were held constant for both electrode types. The cause of the improvement stemmed from the TiC composite electrode coating changing both the electrical and thermal circuit of the welding system. The higher electrical and thermal resistance of the coating material caused the coating to act primarily as a thermal barrier to insulate the heat generated at the faying surface from escaping too quickly through the electrodes.

Electrode life testing has shown the TiC composite coating capable of double the tip life of uncoated electrodes. Electrode degradation mechanisms were observed and it was found that the coated electrode was able to delay the zinc-copper interaction, hence the rate of tip wear and length reduction thereby reducing the rate of tip face diameter growth. Cu deposition on the sheet steel was reduced in the early stages of tip life by use of the coated electrodes. With the coating in place, the interaction between the zinc and the copper was hindered and material transfer was prevented even after alloys formed beneath the TiC coating.

Study of the degradation mechanisms of the coated electrode revealed that electrode tip growth was due to more than the typical alloying and material loss as well as gross electrode deformation. A unique process involving microscopic deformation and plastic

flow of alloy layers formed underneath the electrode coating was found to contribute to tip growth while contributing little to electrode length reduction. This process also worked to embed the fragments of electrode coating into the softer underlying alloy layer. Eventual damage to the electrode coating and penetration of zinc caused the loss of the TiC coating, and degradation of the electrode then proceeded as for an uncoated electrode.

Acknowledgments

I wish to thank my academic supervisors, Dr. Y. Norman Zhou, Dr. Scott Lawson, and Dr. Yuquan Ding for their time, guidance, support and assistance in this endeavor. Their knowledge and wisdom have guided and encouraged me through the exploration of this research into the realm of welding as well as my own character.

Nigel Scotchmer, and the other members at Huys Ind. also deserve thanks and appreciation for their assistance and input to this project. I hope that this work will be able to assist Huys with their future ventures and developments.

Financial contributions to this research project included direct funding from Huys Ind., and the Auto 21 Research Initiative. Consumable welding material supplies for research were also provided generously from Huys Ind. as well as Dofasco, without which, this work would not have been possible.

My family and friends, and the advanced materials joining group at the University of Waterloo who quickly became my friends have all helped and supported me during this work. I truly appreciate all that they have done in questioning, answering, assisting and enjoying this journey with me.

Table of Contents

List of Figures

List of Tables

Chapter 1

Introduction

Resistance spot welding (RSW) is the main method for joining sheet steel components in the automotive and domestic appliance industries. Within these industries, use of zinc coated steels has increased significantly over the past decade, owing to their good corrosion resistance and relatively low cost. However, the zinc coating has increased the difficulty of welding due to its lower electrical resistance and melting temperature [24]. This has led to a drastic reduction in weldability as well as electrode tip life [2,3,5,6,9]. Poor weldability requires more care to be taken when setting weld parameters. A short electrode tip life brings about the need to change tips frequently and can be costly due to the time needed to change the tip and the cost of the tips themselves [2]. These issues are of great concern for manufacturers. A novel welding electrode employing a TiC MMC surface coating has been proposed to increase the tip life when welding zinc coated steels. The purpose of this work is to explore the performance and wear behaviour of the TiC coated electrode.

1.1 Resistance Spot Welding

The RSW process involves the clamping of two or more worksheets together by the welding electrodes, and then the passing of electrical current through the electrodes and sheets to generate heat and cause fusion at the faying interface of the worksheets. Each weld sequence consists of four main stages: 1) clamping of the work, 2) applying the weld force required for welding, 3) applying the weld current necessary for fusion of the

workpieces, 4) and then retraction of the electrodes after the molten nugget has solidified. This process is shown schematically in Figure 1.1.

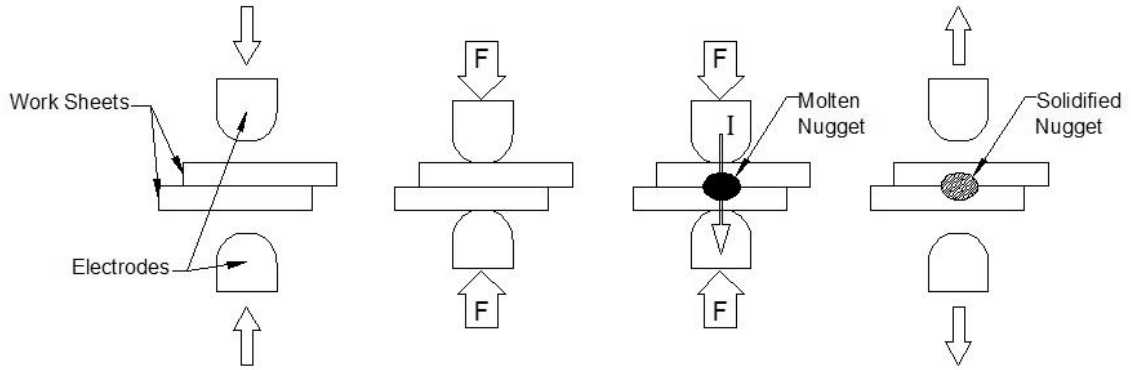

Figure 1.1: Schematic diagram of RSW process

The welding electrodes are internally water cooled. The amount of heat generated by the contact resistance at the interfaces and bulk resistances in the work-piece is governed by Equation 1.1.

$$H=I^2Rt \qquad (1.1)$$

H is the total heat, *I* the weld current, *R* the total circuit resistance, and *t* the weld time. The quality of the weld formed is directly dependent on the localized heat generation, or *H/A*, where *A* is the area of the contact face of the electrode. This is in turn influenced by *I/A* known as current density. With the weld current set and held constant, the quality of the welds is determined by the contact area. The contact area and rate of tip face growth are tracked with carbon tip imprinting and can be used to compare the wear rate of electrodes.

Fundamentally, degradation of the electrodes is the loss of ability to perform its functions. The three functions of the resistance welding electrode are to provide the necessary weld force, weld current density, and cooling. Typical electrode degradation occurs when the tip diameter of the electrode grows too large to convey adequate current density to the workpiece. This leads to insufficient heating of the workpiece and undersized nuggets.

Weld quality is typically measured by means of a peel test, where welds are destroyed to reveal a peel button. The peel button is representative of the actual weld nugget. As measurement of the actual weld nugget is difficult with non-destructive testing, peel testing and button diameter measurements are accepted as sufficient means of assessing weld quality.

1.2 Steel Coatings

Metallic coatings can be applied to steels in several manners. The three main coating processes are hot-dip [HDG], electroplating (also called electrogalvanized [EG]) and dip-annealing (also called galvannealed [GA]). Each of these coatings requires slightly different welding conditions due to the extent of alloy formation between the coating and the steel substrate. The HDG coating consists of mainly zinc with some Al and Pb to control the iron-zinc alloying and to refine the spangle pattern of the solidified coating respectively. The strip steel is drawn through a molten bath of the coating and allowed to cool and solidify. The GA coating composition is typically very similar to the HDG coating except that the sheet is drawn through a furnace as it emerges from the zinc bath to allow the coating to fully alloy with the steel base. This produces a two phase alloy coating consisting of a high and low iron alloy at the steel interface and surface respectively [21]. The EG coatings are produced by electrolytic deposition of zinc metal ions. This is a low temperature process and so yields a thin coating with little to no alloying at the interface of the steel.

1.3 Thesis Outline

This work is aimed at exploring and understanding the formation of welds and the electrode degradation when making resistance spot welds on hot dip galvanized steels using TiC metal matrix composite coated electrodes. Chapter 1 introduces the resistance spot welding process. Chapter 2 presents a literature review on related subjects, such as the degradation mechanisms of electrodes when welding zinc coated steels as seen by other researchers. A gathering of approaches to combat the problem of rapid electrode

degradation is also given. Chapter 3 introduces the experimental setup and procedures. Chapter 4 deals with the welding behaviour of the TiC MMC coated electrode in terms of weldability and electrode tip life. In Chapter 5, the degradation mechanisms of the coated electrodes are investigated. The coating was found to serve a dual purpose in improving the weldability and tip life of the electrode. Finally, Chapter 6 summarizes the knowledge gained and proposes future work.

Chapter 2

Literature Review

2.1 Welding Galvanized Steels

2.1.1 Nugget Formation

The low electrical resistance and low melting point coating on the steel create an electrical resistance system of six layers instead of two. Figure 2.1 shows resistance spot welding schematic for both uncoated and coated steels with their respective electrical resistances. The sheet coating changes the process of nugget formation and can have adverse effects on the electrode wear character as well [12]. Upon heating, the coating will melt first [47], and the molten coating at each of the interfaces serves to reduce and equalize the contact resistances as shown in Figure 2.2 compared to uncoated steels [22]. The molten zinc at the faying interface is pushed to the periphery of the contact area where it forms an annulus which serves to shunt the weld current further reducing the resistance of the circuit [2]. This effect is not seen to the same extent on the electrode-sheet interface due to the lower temperature at this interface as well as the geometry of the electrode contact faces.

The change in resistance affects the formation of the weld nugget also. Studies have shown that the weld nugget in coated steels can develop as an annulus which grows to the full spheroid shape only if enough heat is supplied. Figures 2.3 and 2.4 show the formation of this annulus as well as an uncoated weld nugget cross section [14,23]. If insufficient heat is supplied to fully fuse the entire weld area, buttons are created that could have a hidden defect. As the electrode degrades and current density is decreased, this change in nugget development produces irregular buttons and rapid electrode failure.

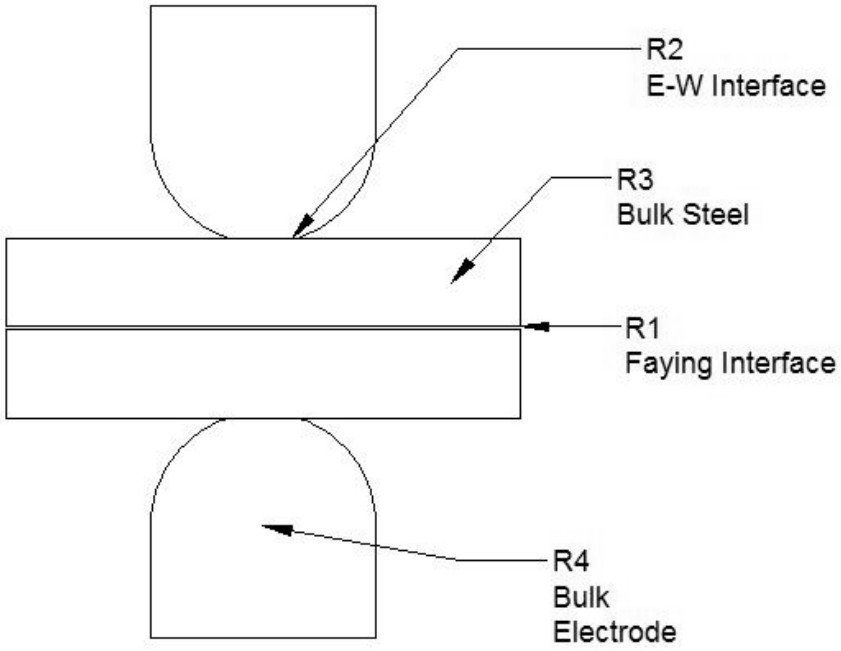

a)

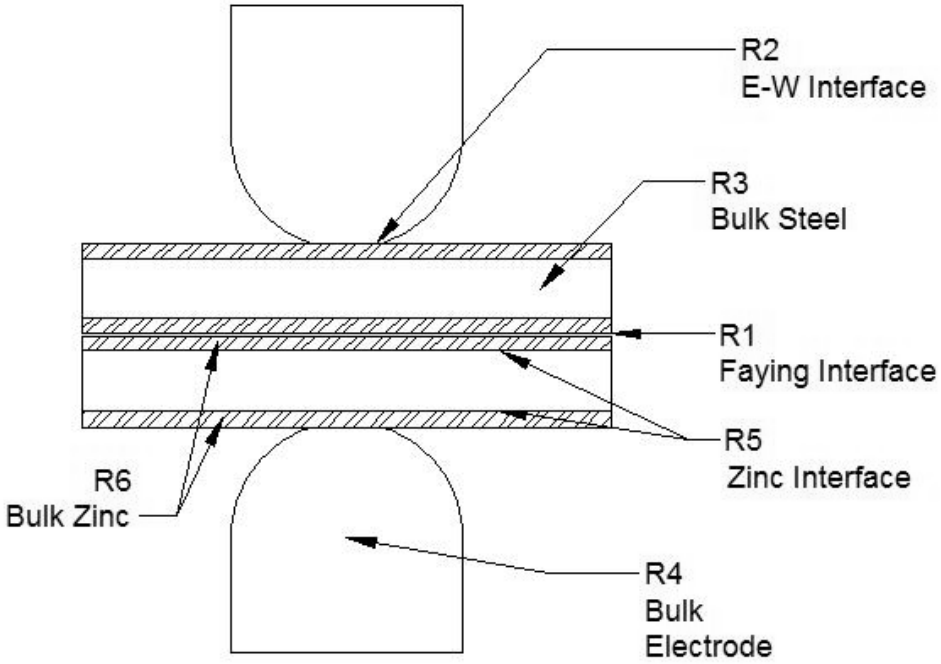

b)

Figure 2.1: RSW system and resistances for a) uncoated and b) coated steels.

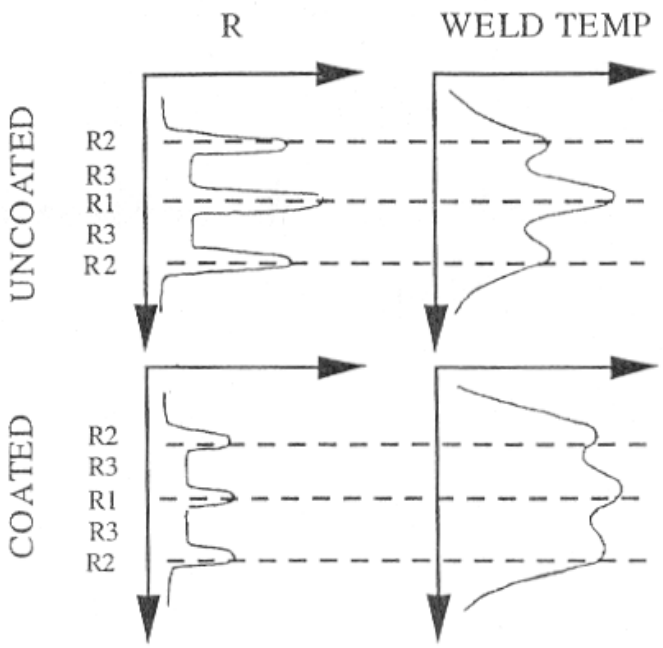

Figure 2.2: Resistance and resultant temperature profile for coated and uncoated steel systems [22]

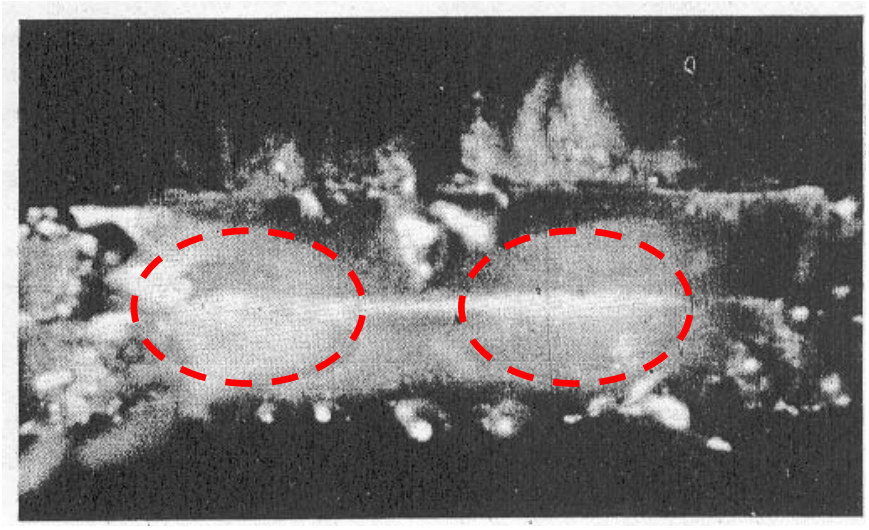

Figure 2.3: In process photo of annular molten zone forming in HDG steel. Outlined areas represent the initiation of melting [14]

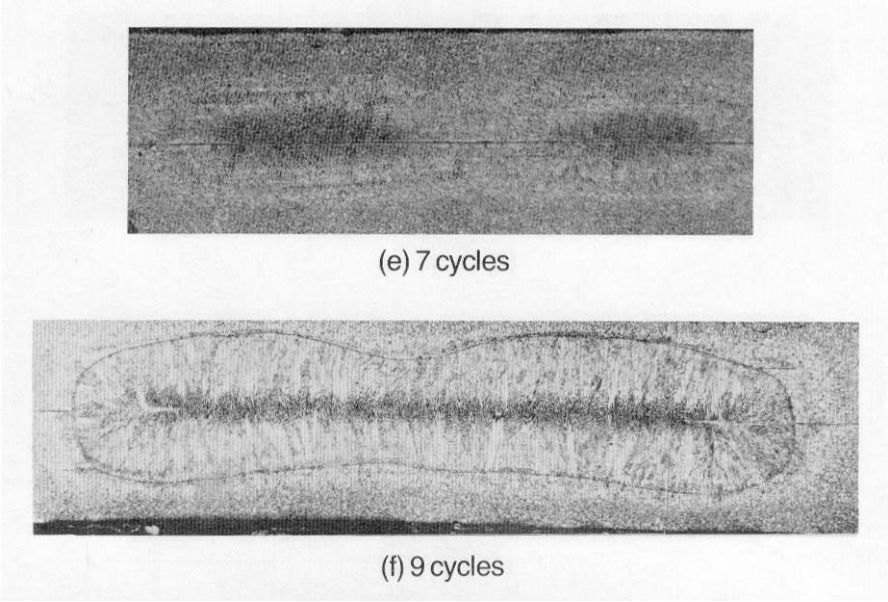

a)

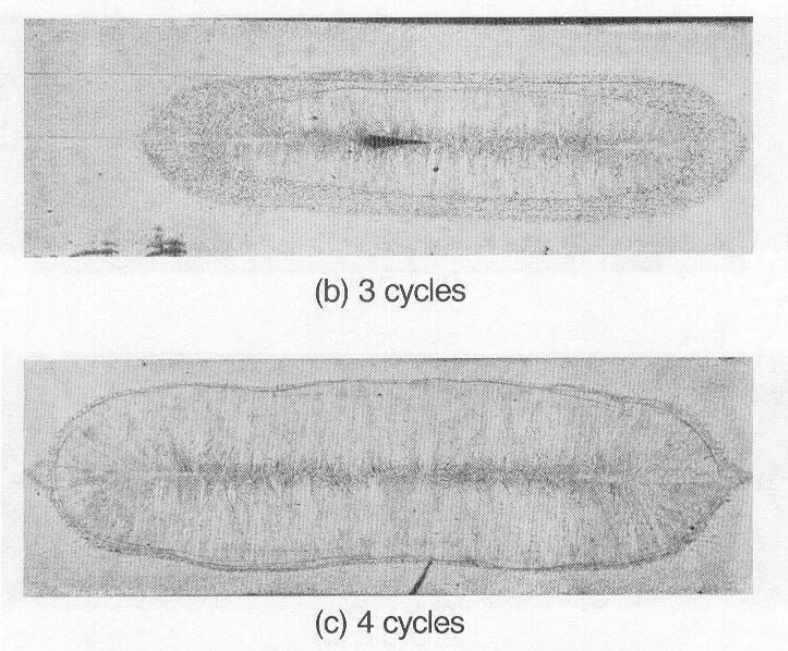

b)

Figure 2.4: Cross sections of welds in a) HDG steel showing the annular molten zone at increasing weld times, b) uncoated steel showing the central molten zone progression at increasing weld times. [23]

Although this phenomenon occurs generally when welding coated steels, it may not be true for all cases.

Full development of the weld nugget may be restricted by the extraction of heat through the electrodes. Although the resistance at the interfaces has shifted due to the presence of zinc, the thermal gradient across the weld parallel to the electrode axis to the electrode may still be rather small. To approximate the speed of propagation of a transient thermal wave into a body from the surface from which that heat was generated, the basic solution for the standard one-dimensional transient thermal diffusion equation may be of use. Consider the case of a semi-infinite body initially at temperature T_1 which has one of its surfaces suddenly heated/cooled to a new temperature T_2 at time t = 0. The solution (transient temperature inside the body as a function of time and the distance x from the surface that was heated) is given by [51]:

$$\frac{T - T_2}{T_1 - T_2} = erf\left(\frac{x}{2\sqrt{\alpha t}}\right) \tag{2.1}$$

where *erf* is the integral of the Gauss curve, and α is thermal diffusivity (m^2/s). Since *erf*(1.0) = 0.84, the position in space-time where $(x/2\sqrt{\alpha t}) = 1.0$ can approximate the front edge of a thermal wave moving through the body. This would mean that the time taken for a thermal wave to propagate through a thickness ***x*** of a material is of the order of $t = \left(x^2/4\alpha\right)$. Using thermal diffusivities for Fe and Cu (22.1 and 118 $x10^{-6}m^2/s$ respectively [52]), to approximate that of the RSW system, a transient thermal wave will travel through 0.297 and 0.687mm respectively in 1ms. With weld cycle times on the order of 182ms (11 cycles), it is clear that the thermal gradient across the sheet thickness is very small. The effect of heat extraction through the electrodes may become crucial to the formation of the weld nugget.

2.1.2 Weldability

Quantifying how the coated steel system affects the welding of coated steels compared to uncoated steels can be done by comparing the weldability lobes and electrode lives of the steels. Weldability lobes present the upper and lower limits of the system with respect to weld current and weld time parameters that are able to produce

satisfactory weld buttons. The position and width of these lobes will determine the relative power needed to form welds as well as the robustness of the system. Figure 2.5 shows the typical welding lobes for uncoated and coated steels [22]. The galvanized weld lobe is shifted to a higher current range and longer weld times. The width of the lobe is also reduced allowing less flexibility between the minimum weld size and the expulsion limit [47]. A weld current lobe can be used to compare the performance and weldability of welding systems for a given steel substrate. A section of the full current-time weld lobe is tested at a fixed weld time to assess the range of weld current that will yield viable nuggets. The range of weld current and nominal weld current of one electrode can be compared to that of another electrode to assess weldability. The electrode with larger weld current range and lower nominal current would be judged superior.

Figure 2.6 shows the relative differences between the weld lobe and electrode life for the different types of galvanized coatings. The HDG steels were found to yield the widest welding lobes, yet the shortest tip lives. The GA steels showed the narrowest welding lobes, and the longest tip lives [2]. The EG steels had a weldability and tip life in between the HDG and GA steels.

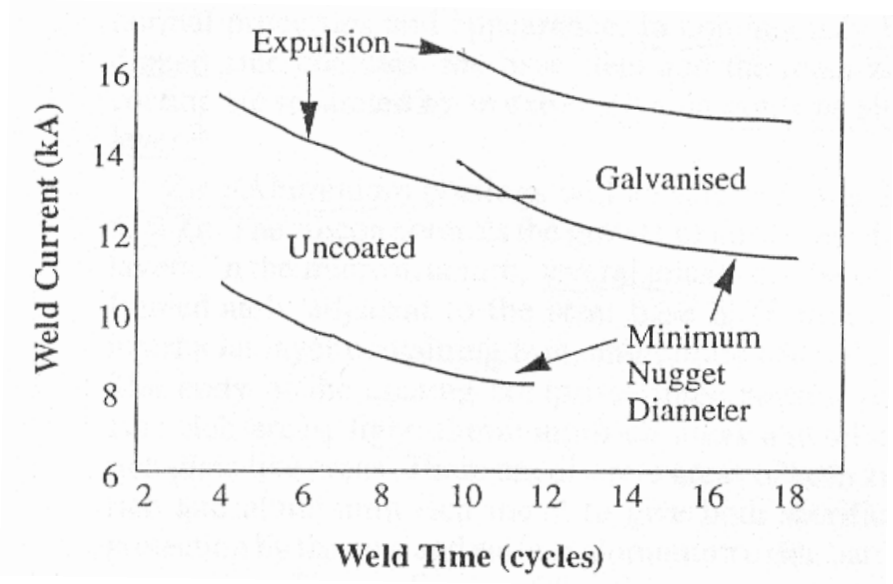

Figure 2.5: Typical weld lobes for the uncoated and galvanized steel systems showing the shift to higher currents and weld time for the galvanized steels [22]

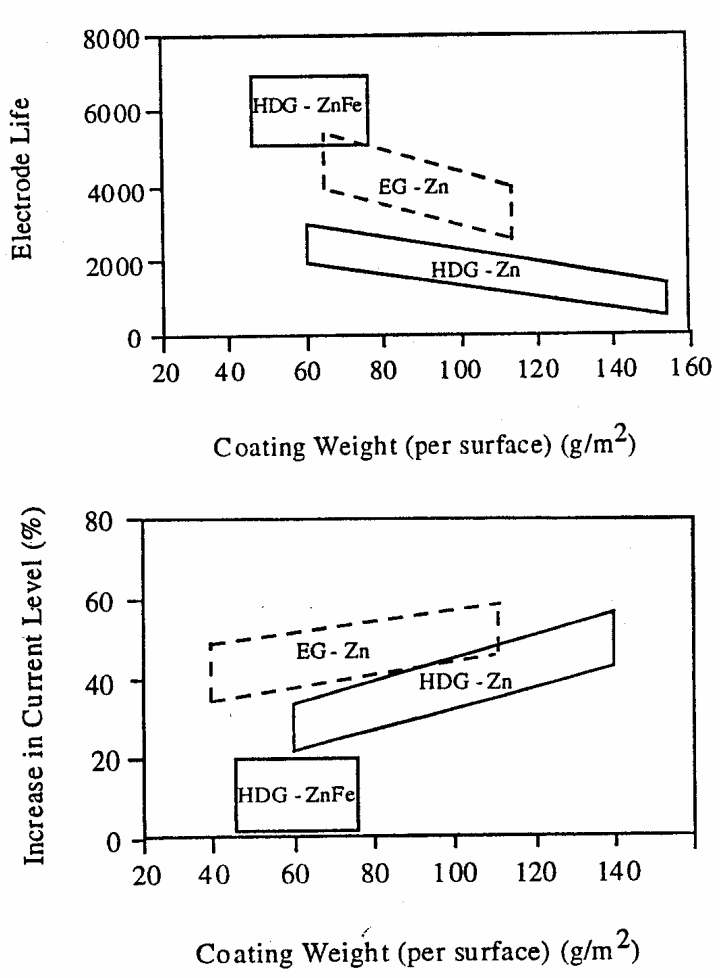

Figure 2.6: Relative shifts in weld lobe and electrode life for HDG, EG and HDG-ZnFe (GA) steels [22]

2.2 Welding Parameters

Weld parameters for resistance spot welding have been explored for many years the results of which have contributed to the standardization of recommended parameters for a given sheet thickness. Recommended weld parameters for the welding of galvanized steel sheets are given in the "Recommended Practices for Test Methods for Evaluating the Resistance Spot Welding Behaviour of Automotive Sheet Steel Materials" (ANSI/AWS/SAE/D8.9-97) [15]. The following sections present the findings of past researchers when welding galvanized steels and their contributions to the standards.

2.2.1 Weld current

Adjustments of the welding parameters to suit the galvanized coatings have been studied by various authors. The presence of the low resistance zinc coating at the faying interface requires a higher welding current to be used to form satisfactory weld nuggets. Orts [26] has reported that an increase in the welding current is needed due to the displaced molten zinc ring increasing the contact area. Other findings have put the amount of weld current increase need from 25-100% [10,35]. Morita et al [27] and Tanaka et al [11] have each reported that electrode tip life increases linearly with increasing weld current to a maximum, above which the heating and cooling cycle is severe enough to reduce electrode life.

2.2.2 Weld Time

Weld time is normally set dependent on the thickness of the sheet being welded. Weld time must be increased to allow time for the molten zinc coating to be displaced from the weld area. Dickenson [28] reported that a 50-100% increase was needed over uncoated steels, and Kimchi and Gould [29] noted that too short a weld time will cause a severe heating cycle and too long a weld time will lead to higher overall electrode temperatures and longer diffusion times.

2.2.3 Weld Force

Weld force required also tends to increase to help facilitate the removal of the coating from the weld area. Although a higher force is needed to displace the coating more rapidly so that weld times can be reduced, a higher weld force also yields a lower contact resistance which must be compensated for by either longer weld times or higher weld current. Saito [9], Nealon and Lake [30], and Jud [31] have shown an increase in the electrode tip life by increasing the weld force 20%-50% over that of uncoated steels.

These findings have contributed to the creation of weld parameter guidelines for a given RSW application. The AWS/SAE/ASME recommends a set of base welding parameters dependent on the thickness of the coated steel sheet to be welded [15]. The weld current is to be determined per application by experimentation and is further explained in Chapter 3 of this work.

2.3 Welding Electrodes

The welding electrode is the most important component of the welding process. It must transmit the welding force, convey the welding current, and draw excess heat from the weld. This three-fold function requires the electrode material to be one with a high electrical conductivity, high thermal conductivity, and high hot strength to resist deformation under the welding force at elevated temperatures. If the electrode material resistance is too large, heat generation will be shifted to the electrode and not the workpiece as well as require a higher voltage. In the extreme case, the electrodes would melt due to overheating. If the thermal conductivity is too low, heat will build up in the electrode and can accelerate material flow and loss of shape of the electrode. It is important to note that the cooling of the electrodes typically by cooling water flow, is mainly to cool the electrodes themselves and not the weld. Heat extraction too quickly can lead to the formation of martensite in steels and is undesirable. If the material has a low hot strength it will easily flow and deform under the heat and pressure of repeated welding cycles.

Special copper alloys are traditionally employed in this role and are divided into classes depending on their strength suited for the application [1]. Class II precipitation hardened Cu-Cr-Zr alloys are typically specified for welding coated steels. Table 2.1 shows the typical material properties for the different classes of electrode materials. Although copper alloys possess the requisite characteristics for the welding application, the affinity to alloy with zinc to form brass phases causes rapid degradation of the electrode when welding zinc coated materials.

Table 2.1: Electrode Material Specifications [1]

MECHANICAL AND PHYSICAL PROPERTIES FOR RWMA MATERIALS

GROUP A (Copper Base Alloys)	HARDNESS (Rockwell) (Minimum)			CONDUCTIVITY (Percent IACS) (Minimum)			YIELD STRENGTH (kpsi) (Typical) (5 Percent Ext. Under Load)			TENSILE STRENGTH (kpsi) (Minimum)			ELONGATION (Minimum Percent) (In 2-in Or 4-in diam)		
	Class 1	Class 2	Class 3	Class 1	Class 2	Class 3	Class 1	Class 2	Class 3	Class 1	Class 2	Class 3	Class 1	Class 2	Class 3
ROUND ROD — (Cold Worked)															
Up to 1-in diameter	65B	75B	90B	80	75	45	45	55	90	60	65	95	13	13	9
1-in to 2-in diameter	60B	70B	90B	80	75	45	45	55	90	55	59	92	14	13	9
2-in to 3-in diameter	55B	65B	90B	80	75	45	45	55	90	50	55	88	15	13	9
SQUARE, RECTANGULAR AND HEX — (Cold Worked)															
Up to 1-in Thickness	55B	70B	90B	80	75	45	45	45	90	60	65	95	13	13	9
Over 1-in Thickness	50B	65B	90B	80	75	45	45	40	90	50	55	90	14	13	9
FORGINGS															
Up to 1-in Thickness	55B	65B	90B	80	75	45	45	45[1]	50	60	55	94	12	13	9
1-in to 2-in Thickness	50B	65B	90B	80	75	45	45	45[1]	50	50	55	90	13	13	9
Over 2-in Thickness	50B	65B	90B	80	75	45	45	40[1]	50	50	55	88	13	13	9
CASTINGS															
All	N/A	55B	90B	N/A	70	45	N/A	20	45	N/A	45	75	N/A	12	5

• 1. Hot worked and heat treated — but not cold worked

Figure 2.7 shows the most common geometries of electrode tips used in RSW. For welding coated steels, the truncated cone electrode is typically recommended with an included angle between 90° and 120°. This geometry is used due to its low geometric tip growth rate, however it is subject to macro-deformation or "mushrooming". Mushrooming is commonly dealt with by machining the electrode tip in situ, or dressing the electrode. Another common geometry of electrode used is the domed electrode, although this electrode has a higher geometric growth rate, it is able to comply with machine/electrode misalignments. This geometry also does not suffer from severe macro-deformation as the truncated electrode does.

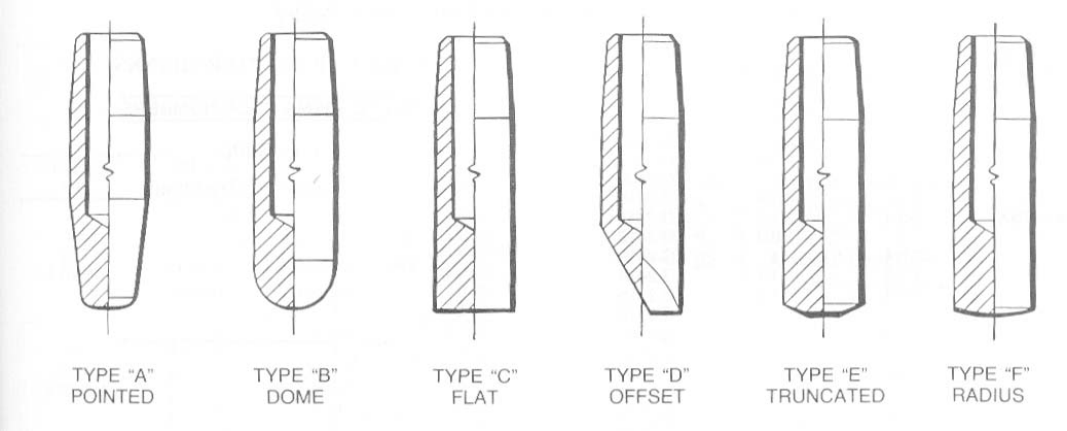

Figure 2.7: Typical RSW electrode tip geometries [1]

2.4 Electrode Degradation

The presence of a zinc based coating on the steel surfaces presents an obstacle not only for weldability, but for the electrodes as well. The use of copper alloys for electrode materials presents a diffusion couple when combined with the zinc present in the coating. The change in contact resistance as shown in Figure 2.2 causes the generation of more heat at the electrode-work interface, which leads to higher temperatures experienced by the electrodes [22]. The increased heat at the electrode-work interface affects the electrode life in a twofold manner. 1: The high temperature has been shown to melt and even vaporize the zinc coating in contact with the electrode [24]. This leads to rapid inter-diffusion of the copper and zinc, forming alloy phases. 2: The elevated temperature also causes local softening of the electrode material and accelerates the plastic deformation of the electrode tip by the repeated stress of the weld force cycle. Both of

these mechanisms work to increase the tip contact area and thereby decrease the current density until the electrode is no longer able to form satisfactory weld nuggets. Failure of the electrodes occurred when the pullout button diameter falls below the minimum weld size (MWS), $4\sqrt{t}$ where *t* is the thickness of the steel sheet.

2.4.1 Alloy Formation

Zinc interactions and alloy formation at the electrode sheet interface have been the topic of several studies [5, 9, 11, 12, 19]. Babu et al. had shown that when liquid zinc comes in contact with copper, the rate of penetration was 500 times faster than that of solid-state diffusion [19]. These interactions lead to material property changes of the electrode and eventual mass transport to occur between the electrode and steel sheet. Brass alloys reduce the hardness and melting temperatures of the electrode face. Figure 2.8 shows a binary phase diagram of the copper-zinc system [24]. As zinc concentration increases, the FCC alpha phase with zinc in solid solution becomes BCC beta brass (β, CuZn) at approximately 33.6 wt% Zn. Beta brass has a melting temperature around 900°C depending on the amount of zinc and is ochre to gold in colour [45]. Gamma (γ, Cu_5Zn_8) brass begins to form when the zinc content reaches 50.6 wt%, forming a hard brittle layer with a complex double cubic crystal structure [45]. Tanaka et al. [11] stated that the electrode life campaign is greatly dependent on the reaction products formed at the tip surface.

Saito [9] and Morita [27] have identified two distinct alloy layers on the electrode surface during welding of coated steels. Using X-ray diffraction, these layers were found to be a gamma brass layer, over a beta brass layer. The gamma brass was typically cracked due to the high hardness relative to the beta and copper base. Parker et al. [5] had shown these layers to be present in as few as 10 welds. Subsequent layers of ε brass and zinc oxide have also been seen by Tanaka et al. [11]. The layers formed on the electrode surface were not uniform across the entire electrode surface. Uneven surface profiles and slight electrode misalignments lead to uneven current distribution across the electrode surface. This causes the formation of these alloy layers to occur unevenly yielding different alloy thickness over the surface. Figure 2.9 shows the stacking of the

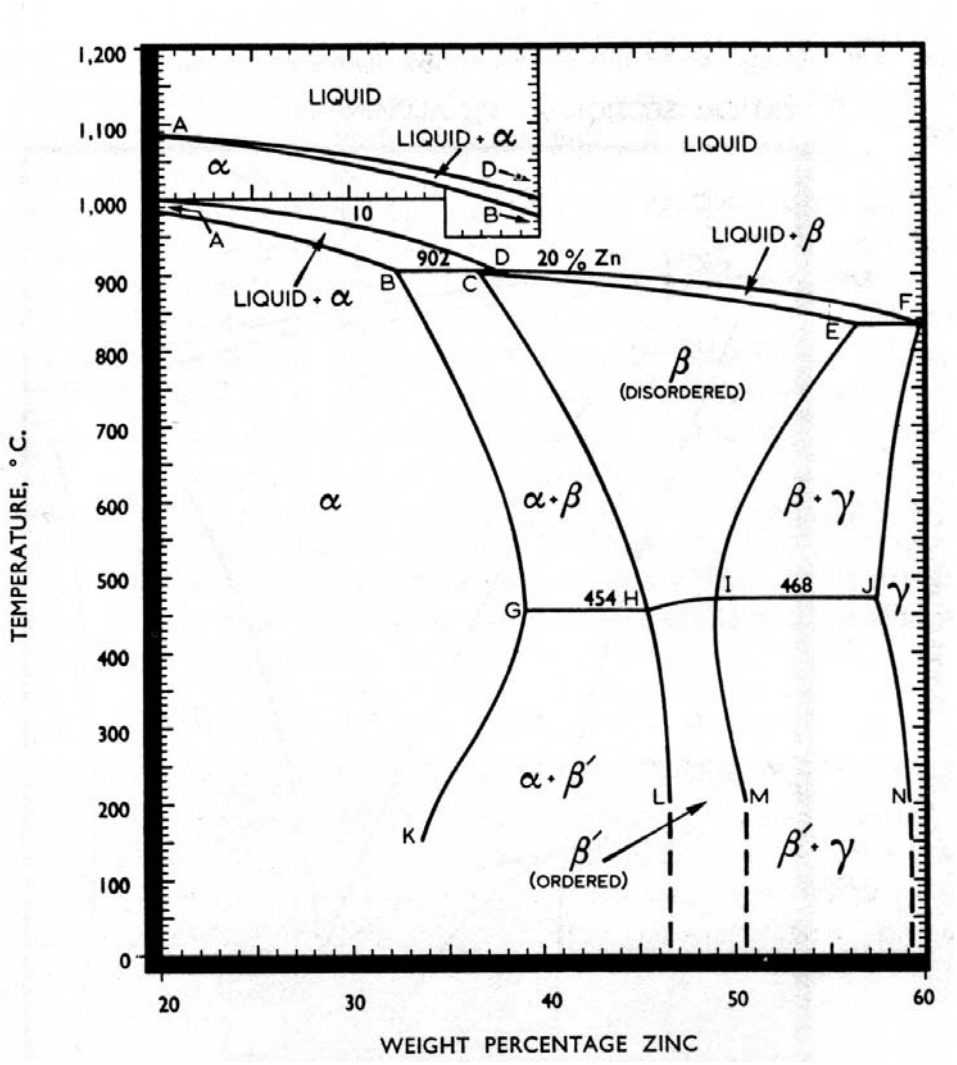

Figure 2.8: Binary phase diagram for Copper-Zinc [45]

Copper
Beta Brass
Gamma Brass
Outer Layer
Zinc

Figure 2.9: Typical electrode alloy layer schematic [5]

alloy layers on the electrode surface. The gamma phase of brass is thought to be the layer that is continually lost to the sheet and reformed as more zinc is introduced to the system. The more rapidly the gamma phase is able to form, the faster the wear rate of the electrode will be [9,27].

An iron-zinc alloy layer was also seen on the surface when welding galvannealed steels and the longer life of the electrode was attributed to this [12,27]. This iron-zinc alloy layer was suggested to slow the formation of the gamma brass phase and hence slow the rate of electrode wear [22].

2.4.2 Wear Mechanisms

Gould et al. [35] have given a summary of the basic wear mechanism of electrodes when welding coated steels. Zinc adheres to the electrode surface from the very first weld and is present as a reservoir to facilitate the diffusion couple. Occasional bonding of the electrode and the workpiece (sticking) occurs when the zinc or brass layers form a braze at the interface or the electrode is forge bonded to the steel. Retracting the electrodes after welding then causes the removal of copper and copper alloys as seen by the copper left on the steel sheet. This net loss of mass from the electrode causes length reduction which in turn causes geometric growth. As the periphery of the electrode experiences a concentration of both force and current, it tends to wear faster than the center of the electrode face. The melting and vaporization of zinc can often lead to zinc flash at the electrode-work interface. The cooled electrodes provide a very effective solidification and condensation surface for the zinc. By this mechanism of zinc melting and expulsion from the sheet surface, zinc and brass alloys can be found to build up around the periphery of the electrode, increasing the net mass of the electrode.

Holliday et al. has summarized the processes contributing to the wear of electrodes when welding zinc coated steels as follows [6]:

(i) Recrystallization of the surface of the cold worked electrodes resulting in softening.
(ii) Mushrooming or electrode face growth
(iii) Alloying between the zinc steel coating and the electrode
(iv) Pitting at the electrode surface

For the welding of HDG steels, Holliday et al. have found that length reduction due to material transfer contributed roughly 50% to the tip growth of the electrode with electrode softening and deformation causing the remaining 50% [6]. It was also noted that this contribution proportion would be dependant on the electrode geometry and type of steel coating used.

In addition to the shift in weld parameters and the interaction of zinc and copper, Saito [9] also adds that the wear pattern of the electrode is key to the electrode life and depends on the type of steel coating being welded. Testing was done using truncated cone electrodes. It was noted that when welding galvannealed steel, the tip wore in an irregular convex pattern, and although wear seemed to be more rapid, the tip diameter remained constant and hence tip life was extended. If the electrode wore in a concave pattern, as in the case with hot dipped or electrogalvanized steels, the tip life would be short. Figure 2.10 illustrates Saito's findings [9].

Cracks in the surface layer both axial and along the alloy layer interface of the electrode cause it to be easily broken off and deposited to the steel sheet. This stripping of the electrode surface causes erosion and/or pitting which leads to a length reduction of the electrode [4,5,6]. With continued erosion, the tip diameter grows due to geometry as shown in Figure 2.11 for a typical domed electrode. The geometric tip growth due to length reduction will vary with the electrode geometry. The domed electrode experiences this geometric growth severely, which the truncated cone electrodes do much less so depending on the included angle of the cone. This however may not occur across the entire alloy layer at once. Areas of the contact face are affected by the welding cycle differently making the prediction of exact electrode wear phenomena extremely difficult [22].

Deformation processes cause the contact face to grow by the flow of material to the periphery. Deformation also has an associated length reduction which contributes to tip growth. The softening of the base electrode material due to heating has been shown to accelerate the deformation process [19]. The plastic flow of unalloyed material to the tip periphery will cause the formation of wings and hence increase the effective tip face diameter, which has been traditionally referred to as mushrooming. Figure 2.12 shows an example of severe mushrooming on a truncated cone electrode [50]. Build up of alloyed

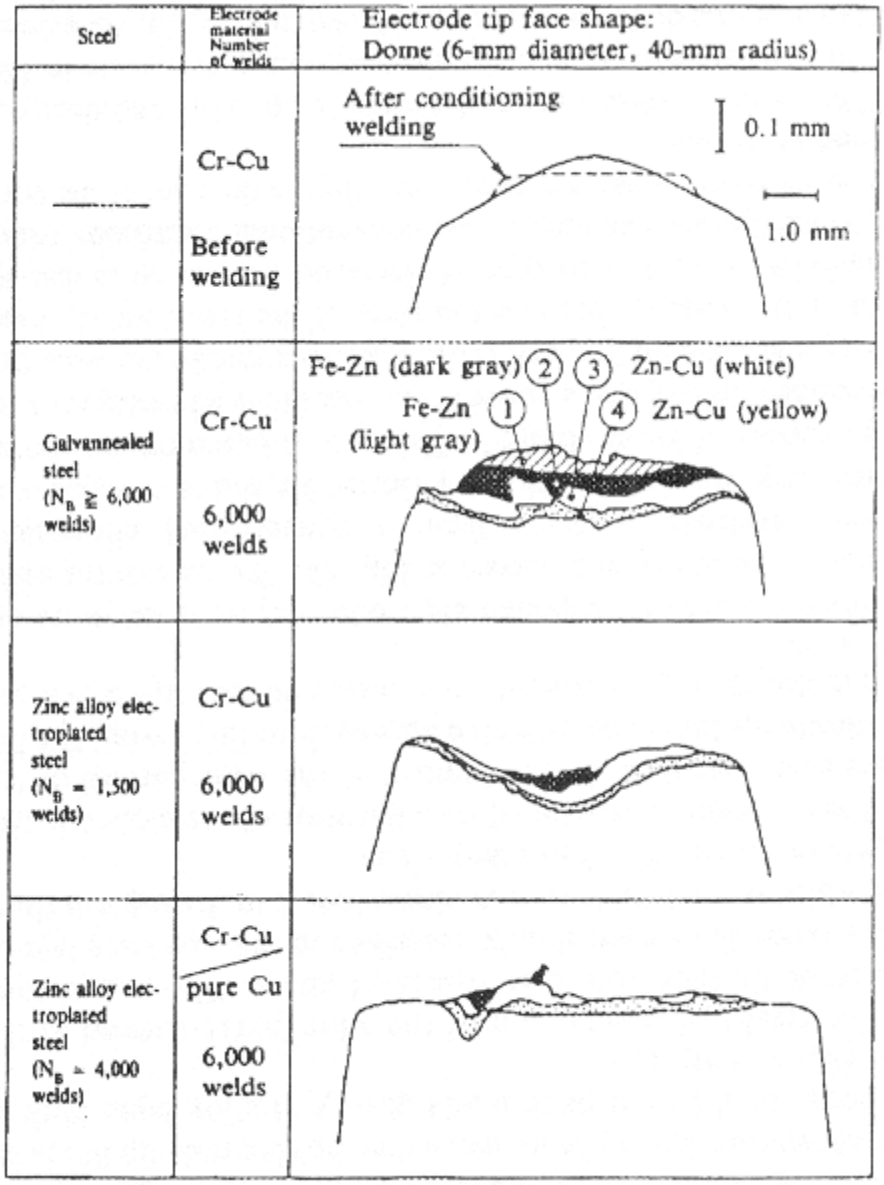

Figure 2.10: Electrode tip shape after consecutive welds (roughness meter recording and optical microscope sketch). Saito et al. [9].

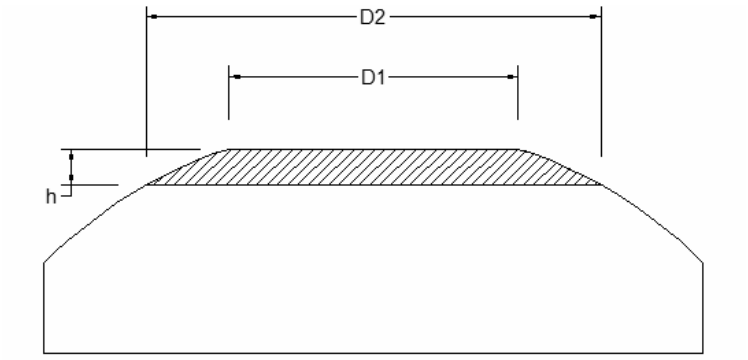

Figure 2.11: Tip growth mechanism by length reduction. *D1* is the initial tip diameter, *D2* the final tip diameter, and *h* the length reduction.

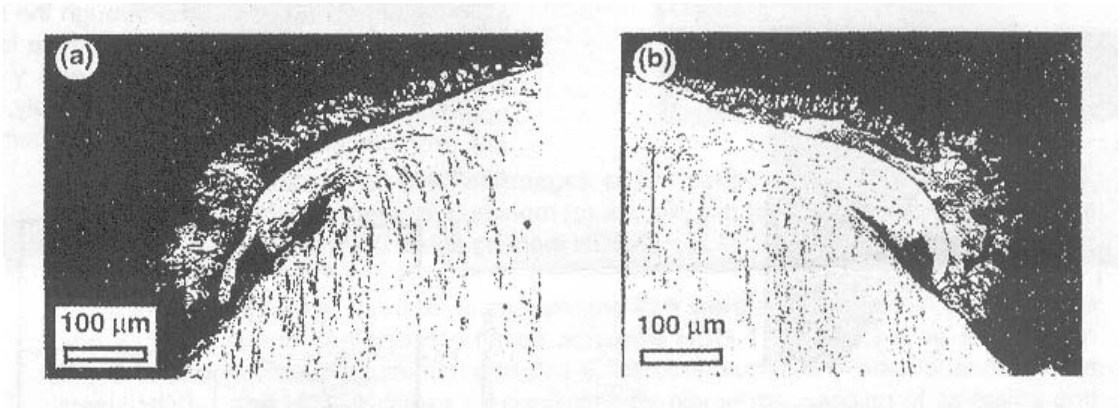

Figure 2.12: Severe macro-deformation or mushrooming on a truncated cone electrode. Optical micrographs of electrodes tested to a) 1000 welds and b) 2000 welds on steel HDG-4 [50].

product and/or zinc at the periphery of the electrode contact face results in an increase in the effective diameter. Electrode softening is primarily due to the overaging and recovery processes in Class II copper materials [5]. The cooling rate of the electrodes due to geometry may have a great effect on the softening behaviour of the electrode under the same welding conditions. The degree of electrode softening can only be measured on cross sectioned electrodes. Micro-hardness profiles are taken beginning at the electrode contact face and traversing into the electrode axially. Figure 2.13 shows the typical Vickers hardness indentation traverse. Severe softening of the electrode material can also cause the entire electrode to deform and flatten out enlarging the contact area and failing the electrode. The use of domed electrodes has been shown to reduce the degree of mushrooming that the electrode experiences [5].

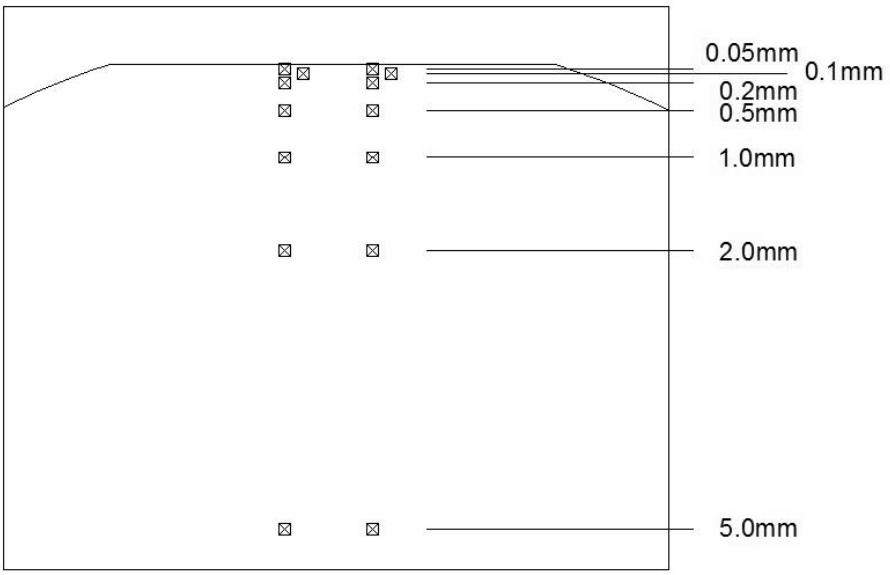

Figure 2.13: Vickers hardness testing on cross sectioned electrode measuring degree of electrode softening.

With various mechanisms contributing to the growth of the electrode tip face, the total wear rate could be approximated by the rate at which the electrode tip face grew. Measured tip diameters throughout an electrode tip life test yielded a growth curve, the slope of which was used to approximate tip grow rate.

2.5 Tip Life Improvement Methods

2.5.1 Improved Steel Coatings

Howe [13] and Tanaka [11] have both individually explored the use of ZnNi steel coatings. Both studies have shown an increase in the electrode tip life using ZnNi EG sheets with a minimum of double the life of typical Zn EG or GA sheets. The increased tip life was suggested to be due to the Ni present on the electrode surface, which acted as a diffusion barrier layer preventing the zinc from penetrating into the copper. *Tanaka* performed a specific test for this and has shown that the depth of Zn penetration was indeed reduced on an electrode which was welding ZnNi coated steel sheet [11]. With less Zn penetration the brass alloy layers that typically form on the electrode surface and cause it to degrade are reduced, extending the life of the electrode by preventing the zinc-copper interaction. A summary of the electrode alloy layers is seen in Figure 2.14 [11].

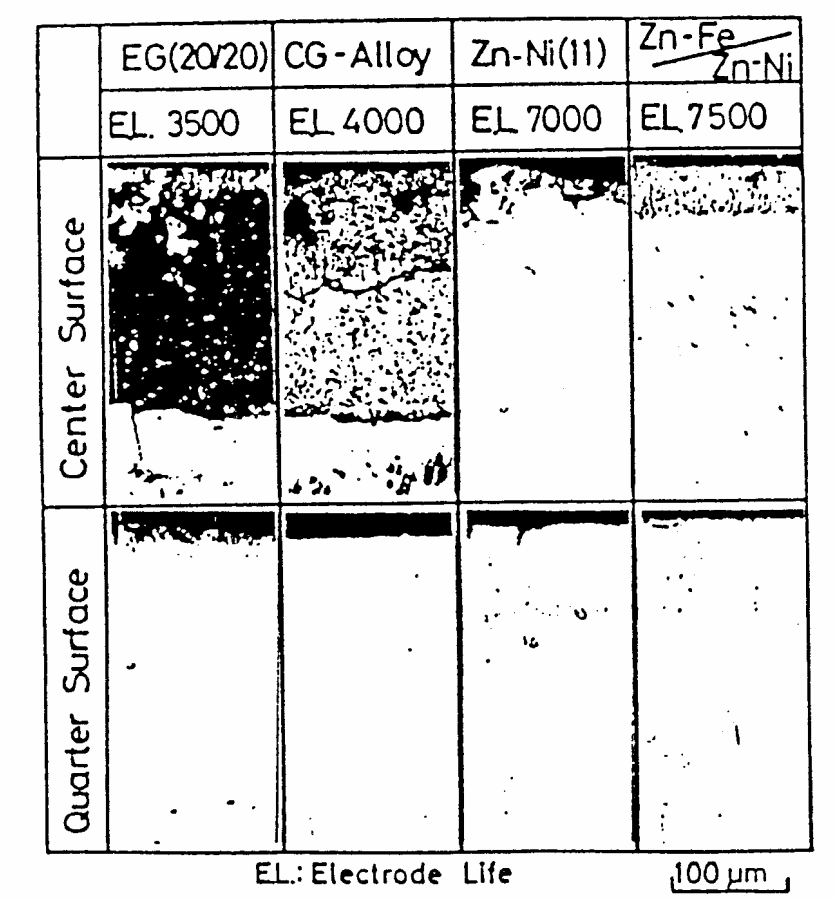

Figure 2.14: Summary of alloy layers found on the electrode surface when welding EG (EG-2020), GA (CG-Alloy) and two ZnNi sheets (Zn-Ni(11), and the double layer Zn-Fe/Zn-Ni). The greatly reduced alloy layer formation is seen when welding the ZnNi sheets as compared to the traditionally galvanized sheets. [11]

Howe has attributed the effectiveness of the ZnNi coating to the formation of a special dual layer alloy on the electrode surface when welding ZnNi sheets. This dual layer was able to minimize the interaction between the zinc and copper of the electrode as observed by Tanaka. The dual layer consisted of a brittle intermetallic outer layer consisting of zinc, iron, nickel and small amounts of copper, and a ductile brass inner layer. The primary wear mechanism for electrodes welding this type of steel was observed to be a gradual plastic deformation of the contact face. The erosion commonly seen to occur was greatly reduced. As deformation is the primary mechanism, factors affecting the heat experienced by the electrode face would in turn affect the deformation

rates. Additionally, Howe found that the current ranges for this type of steel coating was typical for EG coated steels without Ni.

2.5.2 New Electrode Geometry

As an easy method to extend electrode tip life and reduce downtime due to tip changing, Chatterjee [38] has used a modified electrode design with an optimized tip dressing unit. Tip dressing is the machining of the electrode face to remove some or all of the alloy layers that have formed as well as reshape the tip face. A traditional electrode can only be dressed a certain number of times before the material between the contact face, and the cooling channel becomes too thin to support the weld force. Chatterjee has fashioned an electrode with a longer shank to provide more material between the cooling channel face and the contact face, thus allowing more dressing operations to take place. This new electrode has 30mm between the tip face and the cooling face compared to the 10mm on traditional electrode designs.

The change in geometry would be expected to cause a change in the cooling rate of the electrode which in turn would affect the contact face temperature when welding changing the wear character. Temperature profile simulation tests shown in Figure 2.15 show that the new electrode face temperature was actually predicted to be 100°C lower than that of traditional electrodes [38]. This result illustrated how the copper electrode was able to draw heat away form the weld very quickly. The increased thermal mass provided by the extended electrode shank was able to dissipate the heat generated by the weld faster than the traditional electrode thereby decreasing the surface temperature of the electrode. The effect of this result on the wear character of the electrode was not studied, but rather used to validate the new design in terms of face cooling. When used on schedules already incorporating tip dressing, with the same tip dressing frequency, the new electrode designs were able to provide longer total time between tip changes and thereby decrease downtime. Figure 2.16 shows the life testing results using the new electrode and dressing schedule. The new design electrode was able to achieve approximately double the life of a standard electrode using the same dressing schedule on HDG steel.

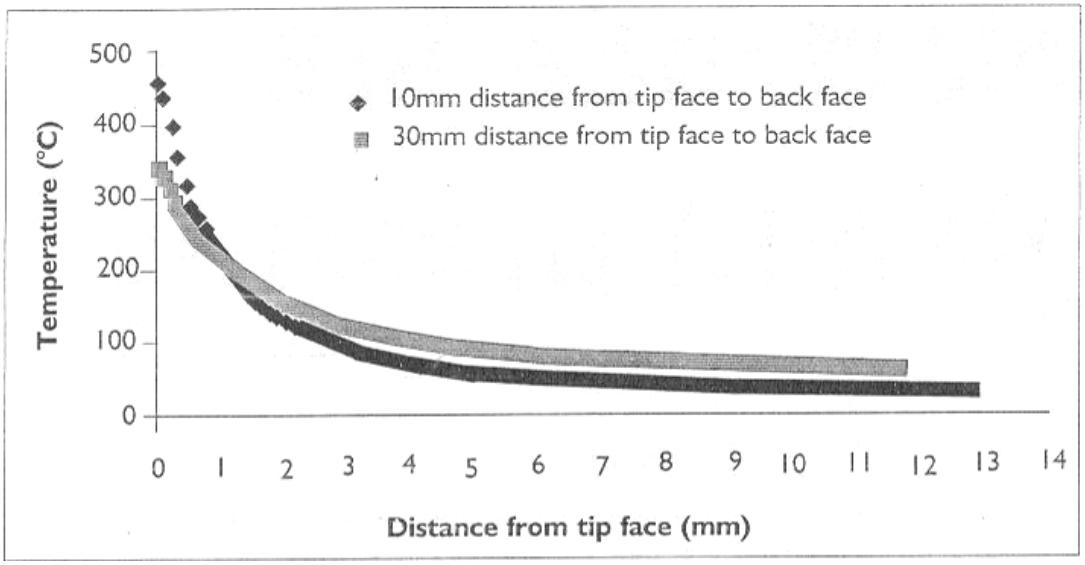

Figure 2.15: Surface temperature distribution for traditional and new (30mm distance) electrode design [26]

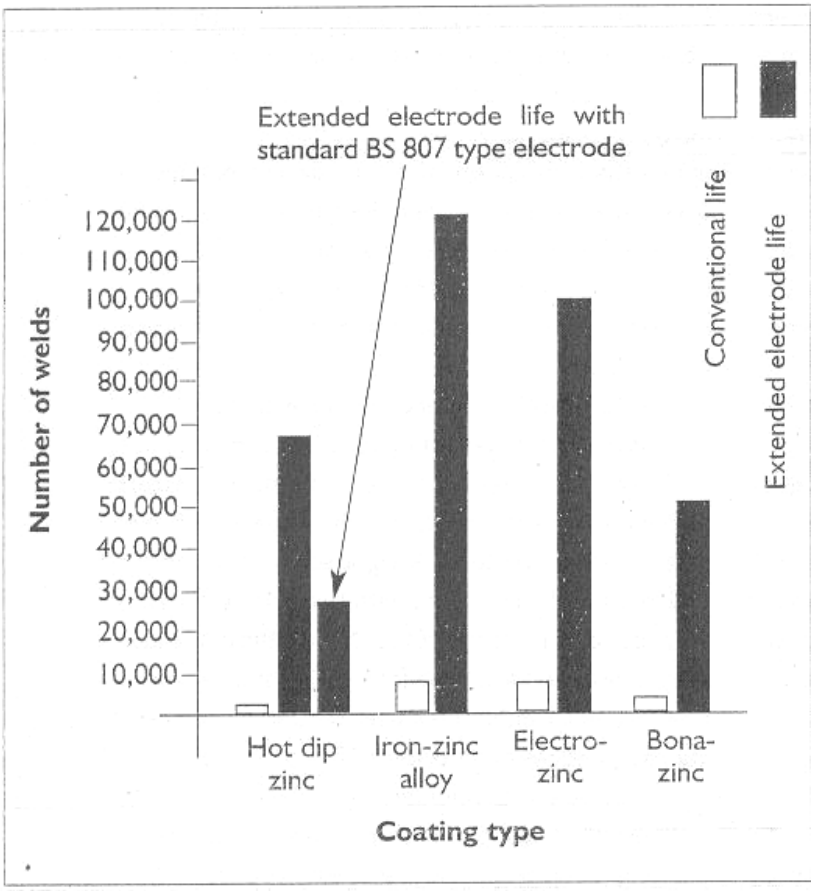

Figure 2.16: Electrode lives obtained for various steels comparing the conventional electrode to the new design electrode. [26]

2.5.3 Spin Electrodes

Takahashi and Saito [39] have developed spin electrode spot welding, which rotates electrodes set on an angle to the workpiece. This action serves to create multiple facets on the electrode surface which were rotated every 100 welds. Figure 2.17 shows the spin electrode setup. This specialized welding equipment may limit its range of applications due to the additional elements needed to form the weld. The electrodes were held at an axial incline angle of 10° and rotation was made every 100 welds through various rotation angles to produce different electrode face geometries. Figure 2.18 shows the electrode after welding with varying rotation angles. It is seen from this figure that the longest tip life was experienced using a rotation angle of 60° forming 6 facets on the electrode face. The contact faces of the electrode were no longer circular in shape, but wedge shaped. This wedge shape was still able to produce sound buttons as seen in Figure 2.19 showing the pullout buttons from each of the rotation angles. Figure 2.20 shows the corresponding electrode carbon imprints at progressing stages in life. The wedge shape was seen to develop early in the life and remain relatively constant in the 60° rotation case. The 30° rotation electrode developed very narrow wedges and hence elongated nuggets. This geometry did not yield an electrode life as long as the 60° rotation.

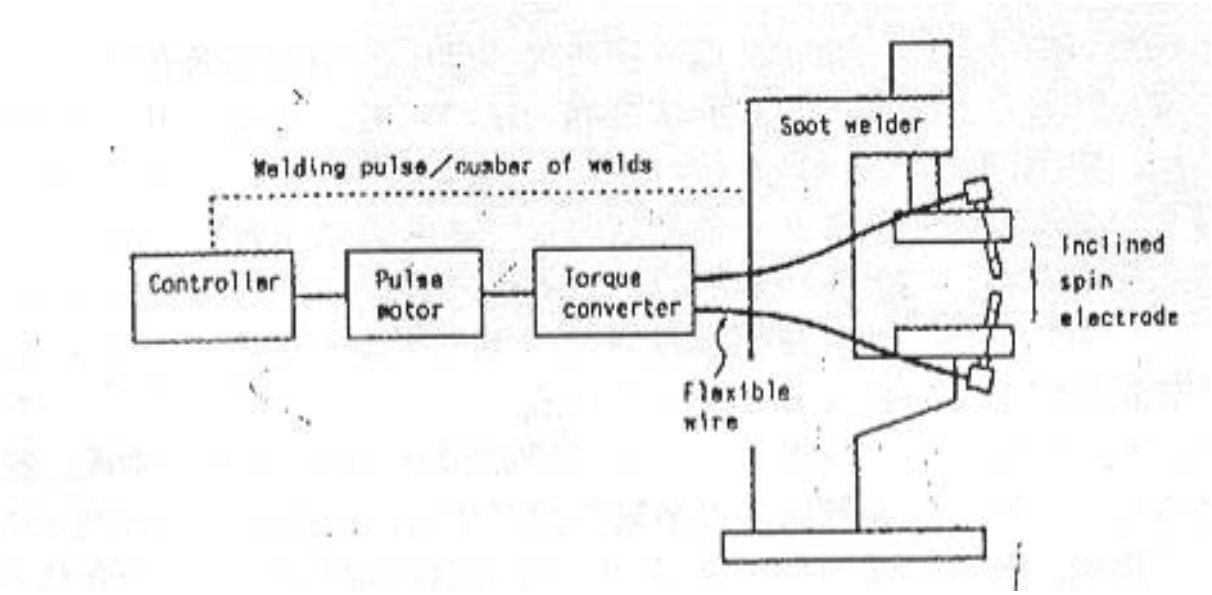

Figure 2.17: Schematic diagram of Spin Electrode Welding system [27]

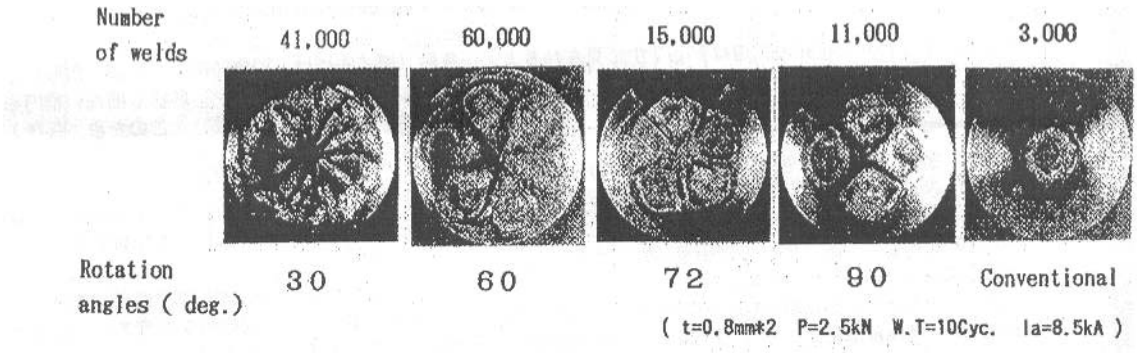

Figure 2.18: Electrode contact face images for varying rotation angles [27]

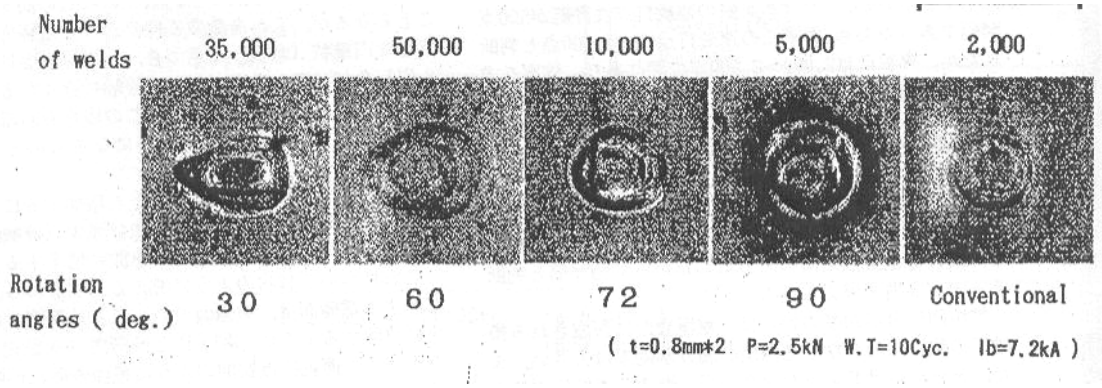

Figure 2.19: Weld peel buttons for varying electrode rotation angles at corresponding weld number [27]

10mm

Rotation angles(deg.)	Number of contact faces	Number of welds							
		1	2,500	5,000	10,000	20,000	30,000	40,000	50,000
30	12	●							
60	6	●							
72	5	●							
90	4	●							
Conventional	1	●							

(t=0.8mm*2 P=2.5kN W.T=10Cyc. Ia=8.5kA)

Figure 2.20: Electrode carbon tip imprints for varying rotation angles at progressing welds [27]

The mechanism for the extended life was found to the “self dressing” [39] of the spin electrodes. Each time a weld face was rotated, the face growth served to reshape the previous enlarged face due to the fixed geometry. The fixed number of weld faces on the surface of the electrode restricted the directions in which the weld face could grow. This is shown diagrammatically in Figure 2.21. The only direction for the contact area to increase was outward to the edge of the electrode. Takahashi and Saito have theoretically taken the number of faces on the electrode (1/6) and the restricted face growth directions (1/3) and estimated that the growth rate of the contact area would be 1/18 that of conventional electrodes using a 60° rotation angle. This has been verified in his trials as the 60° rotation electrode exhibited a 50,000 weld life whereas the conventional electrode yielded only 2,500 welds. Figure 2.22 shows the electrode life curve for both the 60° spin electrode and conventional electrode. The life curves experienced a sharp drop and then stabilization, with fluctuations and eventually the nugget diameter dropped below the minimum. The spin electrode method does not directly address the problems of alloying and deformation associated with welding zinc coated steels, but accepts that they will occur and achieves gains in electrode life by changing the welding process. Further gains could be made if other technologies that address the zinc problem are used in conjunction with the spin electrode method.

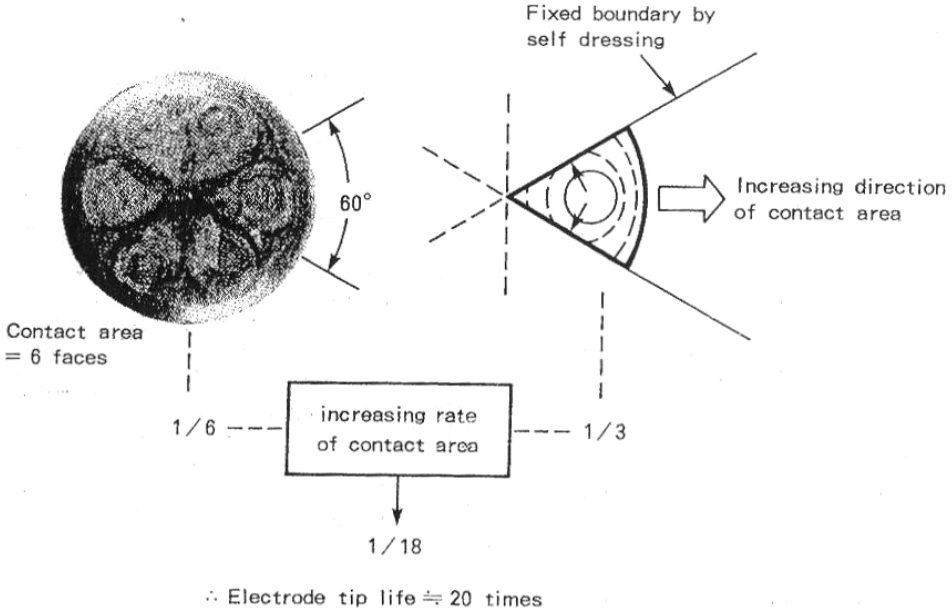

Figure 2.21: Self dressing schematic diagram of spin electrodes at 60° rotation angle yielding 18:1 tip life over traditional electrodes. [27]

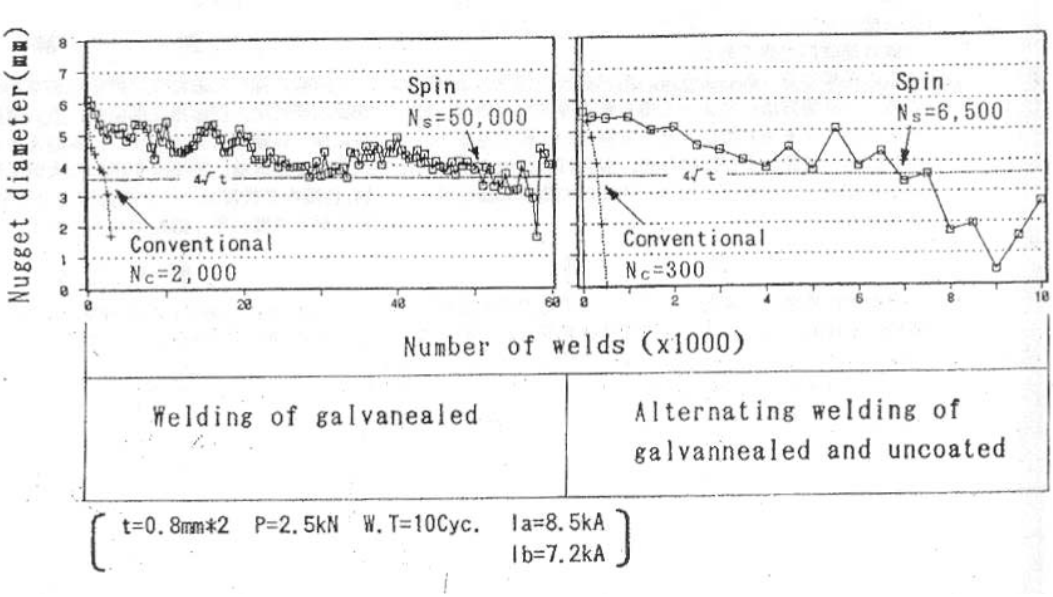

Figure 2.22: Electrode life curve for conventional and 60° rotation spin electrode on both GA steel and alternating GA and uncoated steels. [27]

2.5.4 New Electrode Materials

Nadkarni and Weber [40] have considered using dispersion strengthened copper (trademarked *GlidCop*) for welding electrodes. The dispersion strengthened copper (DSC) material has outstanding resistance to softening at elevated temperatures as well as short term high temperature tensile strength. The DSC copper is made by a patented [*Glidden Metals Group of SCM Corporation*] process where aluminum dissolved in the copper matrix is oxidized to form alumina. This creates a very finely dispersed metal matrix composite material which is then hot extruded to rod form where it can then be fashioned into welding electrodes. Initial industrial testing has shown that with modifications to the maintenance and current stepping programs, the DSC electrodes were able to yield a tip life 4 to 5 times that of Class II welding electrodes. An attribute of note was that the DSC electrodes reportedly did not stick to HDG steel sheets where this was a problem for Class II electrodes [40].

Nadkarni [41] later published another study on the DSC electrodes concentrating on the sticking behaviour when welding galvanized steels. Using two DSC electrodes with different alumina content and Class II CuCr, and CuCrZr electrodes, welding current was increased until the electrode became stuck to the weld sheet. This test was conducted using domed B nose, pointed A nose, and truncated E nose geometries on EG and HDG

steels. It was shown that the B nose geometry resisted sticking the most, and that HDG steels tend to stick less than EG steels. Overall, the DSC electrodes outperformed the Class II electrodes as many tests were terminated before a sticking current could be achieved. Figure 2.23 shows the sticking current charts for the A, B and E nose electrodes on HDG steel.

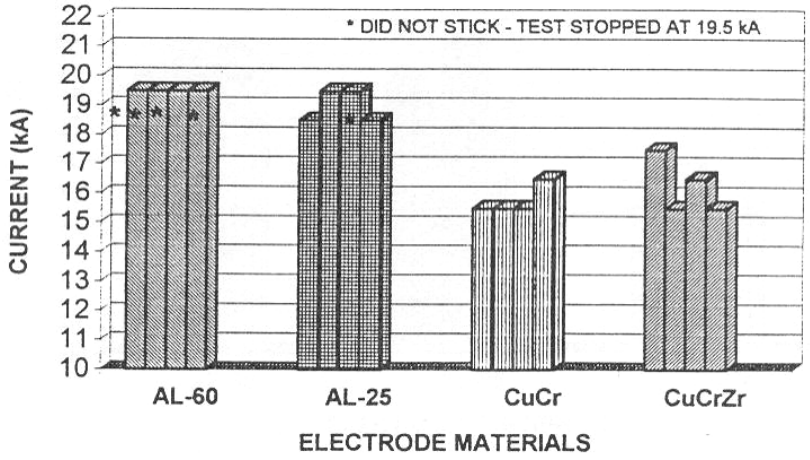

a)

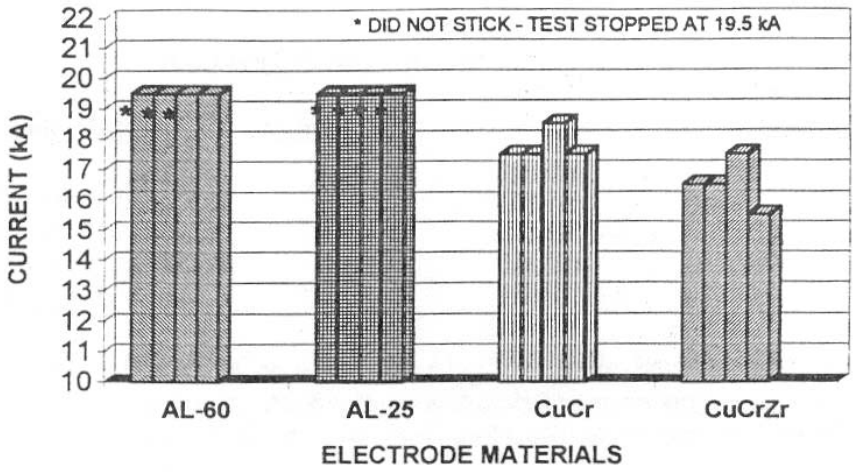

b)

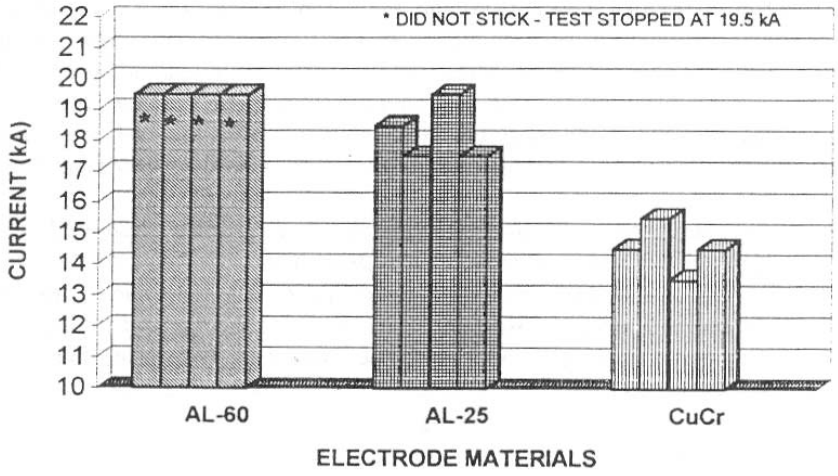

c)

Figure 2.23: Sticking current chart on HDG steel for a) for A nose electrodes b) B nose electrodes and c) E nose electrodes [29]

Although the theory of the DSC electrode is attractive to improve tip life, many studies have shown the DSC electrode to perform no better than traditional Class II electrodes [32,33]. The cost of DSC electrodes is also approximately four times that of Class II electrodes, not making them an effective solution in many applications [22].

2.5.5 Compound Electrodes

Key and Courtney [42] have used sintered metal inserts in electrodes to improve tip life and weld quality. Refractory metal matrix composites using molybdenum or tungsten in a copper matrix were used as inserts in a CuZr electrode shell, Figure 2.24. It was determined that a ratio of 32 vol. % W in a Cu matrix sintered for one hour yielded the longest life. The copper matrix is continuous while the tungsten particles are not continuous in this material. The presence of the refractory particles, while retaining a high percentage of copper at the contact face to conduct current and reduce heat generation was the proposed reasoning behind the electrode life improvements seen in Figure 2.25. The tip face growth rate of the electrodes was slightly improved yet still rapid in the initial stage of life. The compound electrode in this case showed what

appeared to be a steady state period where the face diameter did not grow substantially. It was in this region that the life improvement was gained.

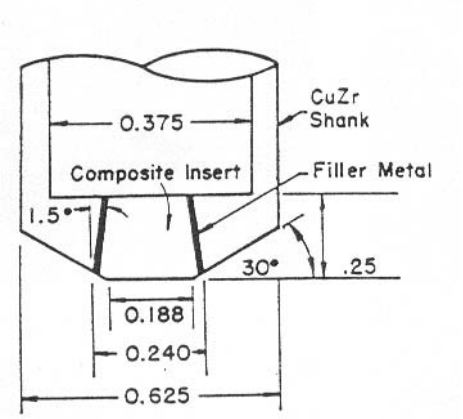

Figure 2.24: Refractory metal matrix composite insert compound electrode geometry. [30]

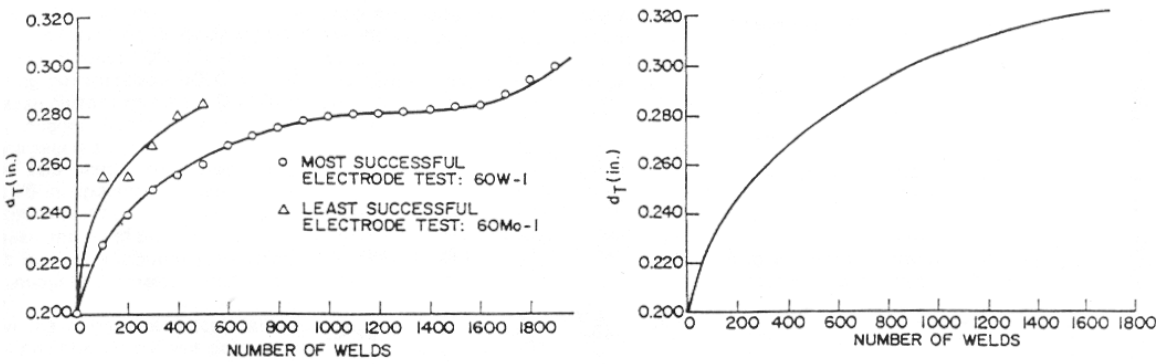

Figure 2.25: Electrode life curves for compound and conventional electrode. Tip Diameter vs. weld number. [30]

This was explained by a change in the degradation mechanism of the electrode. *Key* describes how the zinc environment is no longer the key factor for the failure of the compound electrodes. The melting of the matrix at the contact face was the mechanism of failure. It was found that the interfacial temperatures at the contact face were high enough to melt a band of the copper matrix of the composite. This band of copper would then be partially extruded to the periphery of the electrode face leaving the refractory particles in the band unsupported. This then resulted in rapid tip face growth as the composite insert was quickly eroded. When the insert has eroded to the point where the copper shank supporting the insert was exposed, a partial shunting of the current occurred

through the copper shank. This current shunting decreased the heat experienced by the contact face and was responsible for the decrease in the tip growth rate of the electrode after the initial high growth stage. Figure 2.26 shows a diagram of the result of the copper loss from the contact face which caused the rapid erosion and tip growth of the electrode.

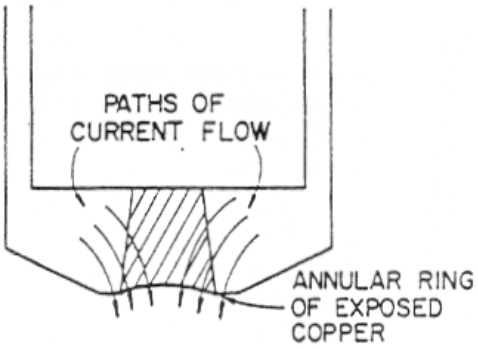

Figure 2.26: Schematic diagram of degradation mechanism showing rapid erosion of insert and exposure of copper sheath. [30]

The changes in degradation mechanism of the electrode and the lack of substantial gains in tip life have kept this compound electrode from industrial use. The addition of another wear mechanism to the alloying and deformation has made the refractory metal matrix composite compound electrode a poor option.

Tanaka and Noguchi [43] have made a compound electrode using a DSC core hot extruded into an oxygen free copper sheath. This process strongly bonded the DSC core to the copper shell and yielded an electrode with better conductivity than a conventional CuCr electrode and better wear and softening resistance. Life testing of this compound electrode in Figure 2.27 has shown it to at least double the life of the CuCr electrodes. X-ray elemental analysis of the electrode tips after the life test revealed that the zinc had not been able to penetrate as deep into the compound electrode as it had in the CuCr electrode. A hardness profile of the electrodes after failure was also taken and shown in Figure 2.28. The compound electrode showed a smaller central region of softened material and a lesser degree of softening as the original hardness was lower than that of the CuCr electrode. The improved tip life using this compound electrode was attributed to the reduced wear and damage on the electrode surface. It was not made clear whether

this reduced wear was caused by the greater resistance to softening or the improved conductivity which reduced the alloying effects of wear. *Tanaka* suggested that this type of compound material will be useful in various applications in the future as the degradation mechanisms typically seen when welding galvanized coatings have been reduced to yield reduced wear and longer electrode life.

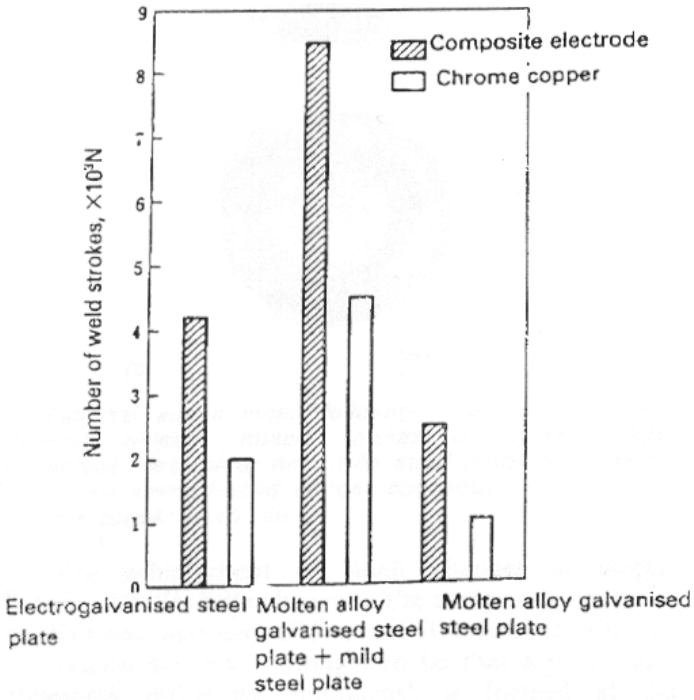

Figure 2.27: Electrode Life charts showing life improvement on various steels when welding with DSC composite compound electrode vs. conventional CuCr electrodes [31]

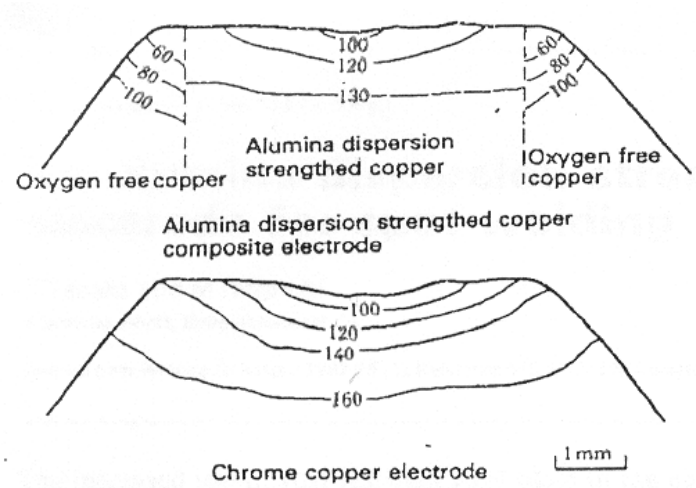

Figure 2.28: Hardness profile showing increased resistance for softening resistance for DSC compound electrode over conventional CuCr electrodes [31]

De et al [44] have made a compound electrode using a solid tungsten insert at the center of a domed electrode. The tungsten insert enhanced the mechanical strength of the electrode during welding in an effort to reduce the deformation that was experienced by the copper base electrode material. The tungsten greatly reduced the thermal conductivity of the electrode as well as electrical conductivity which worked to raise the temperature experienced by the electrode face and to promote deformation. This balance required optimization to achieve the proper size of insert for the application. It was to this end that *De* also developed a numerical model to try and simulate the thermo-mechanical system of the electrode wear process. This may have helped to determine insert size at the beginning of electrode life, however the model did not consider effects of alloying and material interaction. Experimental life testing of two different insert sizes as well as a plain electrode with no insert was conducted. The 1.0mm W insert showed the longest tip life which was slightly more than double that of the conventional electrode. Figure 2.29 shows tip diameter growth representing electrode life curves. It is interesting to note that all three electrodes reached the same tip diameter at approximately 700 welds; however the compound electrode was able to continue to make satisfactory welds. The deformation of the compound electrode face was noted to be less than that of the conventional electrode. The presence of zinc on the electrode surface was not studied and ultimate compound electrode degradation mechanisms were not explored.

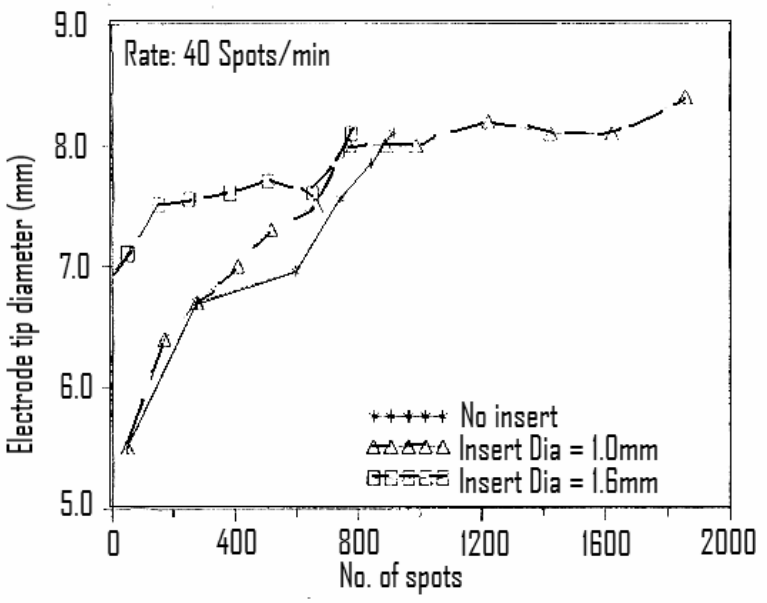

Figure 2.29: Growth in contact face during electrode life testing of W insert compound electrodes of different insert diameter and conventional electrode. [32]

2.5.6 Electrode Coating

The interaction of zinc from the steel coating with the copper of the electrode had been identified as a key factor in the degradation of the electrodes. The formation of alloy layers requires the presence of zinc to diffuse into the copper. If the zinc were not allowed to come in contact with the electrode base material, the interaction could be prevented. This could be achieved by using an electrode coating to serve as a diffusion barrier. Coating the surface of the electrode could allow the use of current steel coatings and current electrode materials. Design of the coating process and material may allow an electrode coating to be a cost effective solution to extend tip life and improve weldability. The challenge is to find a coating material that will not alloy with the zinc and remain intact to protect the electrode without affecting the weldability of the electrode in a negative manner.

Industrial processes such as physical vapour deposition (PVD), chemical vapour deposition (CVD), thermal spray and high velocity oxygen fuel spray (HVOF) may be used to deposit coatings on surfaces for cosmetic and corrosion protection. These processes typically require the base material to be heated. The nature of the welding electrode duty cycle requires a surface coating that will withstand the repeated impact and thermal cycles without delamination. The sensitivity to overaging of the precipitation hardened base material also restricts the temperature at which the coating process can be carried out at. These limitations have generally made electrode coatings a tedious and expensive undertaking.

In a study carried out by Finlay et al [46], PVD of chromium using unbalanced magnetron sputtering and filtered arc was used to coat a Cu-Cr electrode. This coating was shown to extend the life of the electrode by 100% when welding Al-45%Zn coated steel sheet.

Dong and Zhou [25] have shown that a TiC metal matrix composite (MMC) coated electrode from Huys Industries was able to reduce sticking, local bonding and materials transfer when micro-resistance welding nickel plated steel sheets. Cu-Cr-Zr and Cu-Al_2O_3 electrodes were coated with the TiC MMC using a patented electrospark deposition process [20]. The TiC coating was able to reduce the rate of electrode tip

growth as seen in Figure 2.30. This improvement in tip growth rate resulted in extended tip life seen in the plot of button diameter vs. number of welds in Figure 2.31.

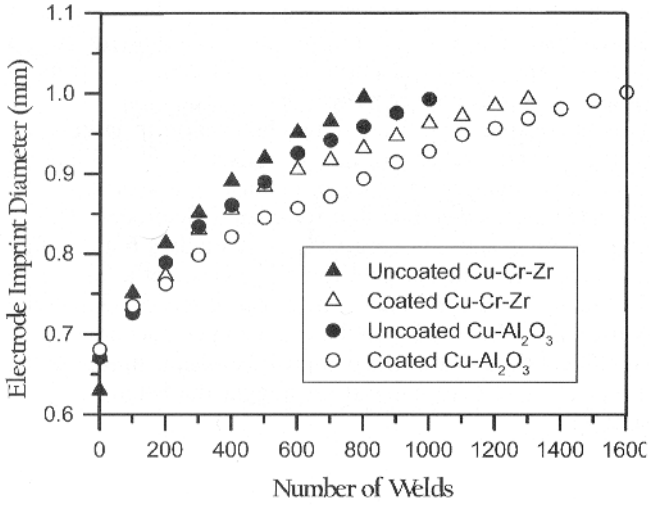

Figure 2.30: Electrode imprint diameter (tip diameter) plot versus number of welds illustrating reduced growth rate for TiC coated electrodes [20].

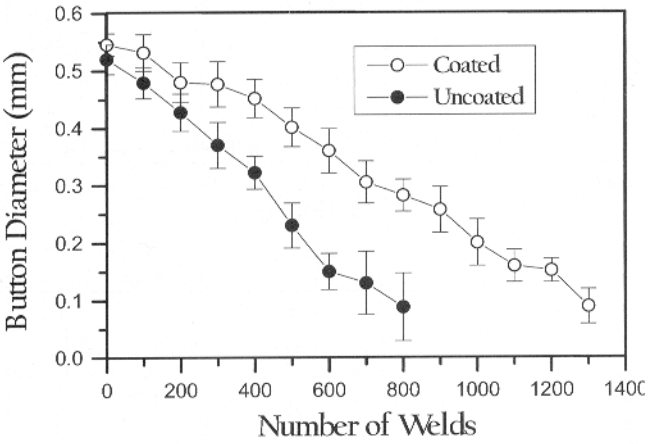

Figure 2.31: Button diameter versus number of welds. [20]

Titanium carbide is a strong, hard ceramic material that has been used in the tooling and machining applications industry for some time and is noted for its resistance to wear. The good electrical and thermal conductivity combined with high hardness and strength made TiC ideal for the resistance spot welding electrode wear problem. Using a surface engineering solution to restrict the zinc from the copper and hence prevent the electrode wear problems associated with zinc coated steels became a reasonable approach. Huys Industries has adopted this approach and has been producing TiC MMC coated electrodes

which have been in use in industry for several years. The improvement over uncoated electrodes when welding zinc coated steels has been shown in the field however fundamental understanding of how the electrode coating interacts with the zinc coating and eventually degrades is lacking.

2.6 Summary

The problem of reduced weldability and greatly reduced electrode tip lives when welding galvanized steel is due to the severe welding parameters required to form a nugget and the zinc-copper alloy formation. The increased heat generated at the electrode sheet interfaces work to rapidly degrade the electrode in a twofold manner:

1. The zinc interacts with copper leading to alloying and rapid erosion of the electrode face.
2. The increased heating leads to electrode softening and deformation of the copper electrode as well as alloy layers.

Through the development of new materials and processes, the tip life can be improved somewhat. Developments of new steel coatings that are able to resist corrosion and yet have less of a negative effect on the welding process are effectively attacking the problem at the source, the galvanized coating. New processes such as the Spin Electrode welding system and new electrode designs accept that the degradation of the electrode will occur and instead work around the problem. Increasing the length of the electrode tip was shown to decrease the surface temperature of the electrode during welding by more than 100°C. New electrode material developments choose to attack the problem by reducing the negative effect the galvanized coating has on the electrode by adapting the electrode to be more resistant to the zinc coating. These methods may or may not be suitable to every application in the wide range of resistance welding processes and may not be cost effective. The coated electrode chooses to leave the galvanized coating and copper electrode material alone, allowing cost effective mainstream use, and addresses the problem of the interaction by working to prevent the zinc and copper from coming into contact.

The methods and studies presented above are the much needed ventures into the realm of discovery that is still at an early stage. The weldability and tip life are not yet approaching that of welding uncoated steel systems. Eventual degradation by the effects of the zinc coating is currently not able to be stopped. However the TiC MMC coated electrode presents an intriguing approach to a solution of the problem. This work is focused on investigating the how a TiC MMC coated electrode degrades in terms of alloy formation and erosion, and softening and deformation associated with the traditional uncoated electrode.

Chapter 3

Experimental Methods

Welding trials were conducted on hot-dip coated steels using both coated and uncoated electrodes. Weldability testing was carried out to investigate the ability of the coated electrode to make acceptable welds. Electrode life tests were conducted to study electrode degradation. Additional life tests were performed sacrificing the electrodes before failure at periodic intervals for analysis. All test data recorded can be found in Appendix A. Results presented in the following chapters are selected from particular test sequences that were believed to be representative and typical of the behaviour patterns observed.

3.1 Material

Sheet steel used was hot dip galvanized high strength low alloy steel as specified in Table 3.1. Two sheet thicknesses were used for experimentation. A 1.0mm thick sheet was used for weldability testing, while 0.7mm thick steel was used for electrode life testing. Welding coupons were cut as per guidelines specified in the "Recommended Practices for Test Methods for Evaluating the Resistance Spot Welding Behaviour of Automotive Sheet Steel Materials" (ANSI/AWS/SAE/D8.9-97) [15]. Light wiping of all steel surfaces was conducted prior to welding to remove loose dirt and evenly distribute any machine oil. All of the steel sheets were of the same batch for their respective thickness. Details of the coupon dimensions for peel testing and life testing are shown in Figure 3.1.

Table 3.1: Sheet Steel Specifications

Steel Type	HSLA
Coating Type and Thickness	Hot Dip – 60G
Sheet Thickness	0.7mm / 1.0mm
Tensile Strength	296 MPa

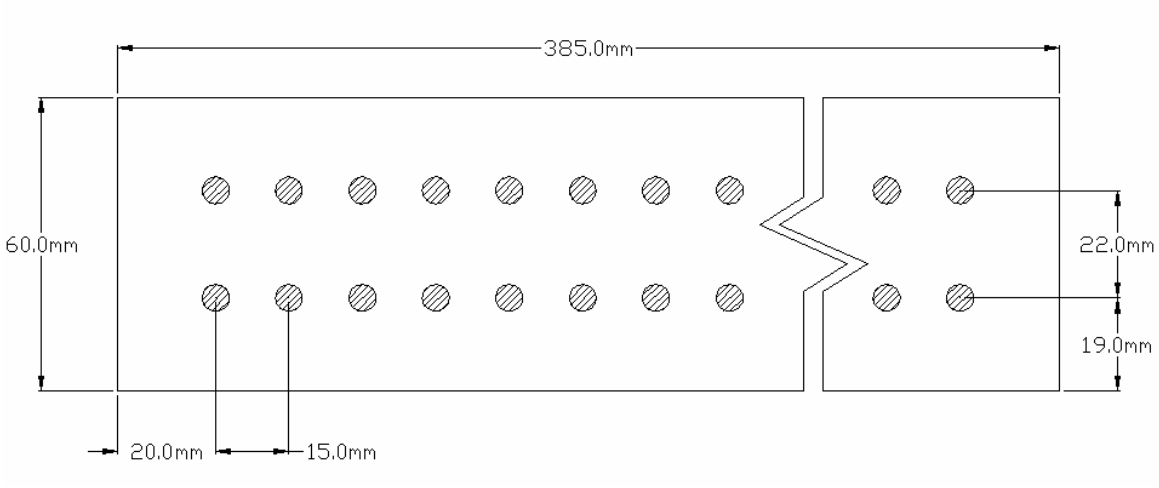

a)

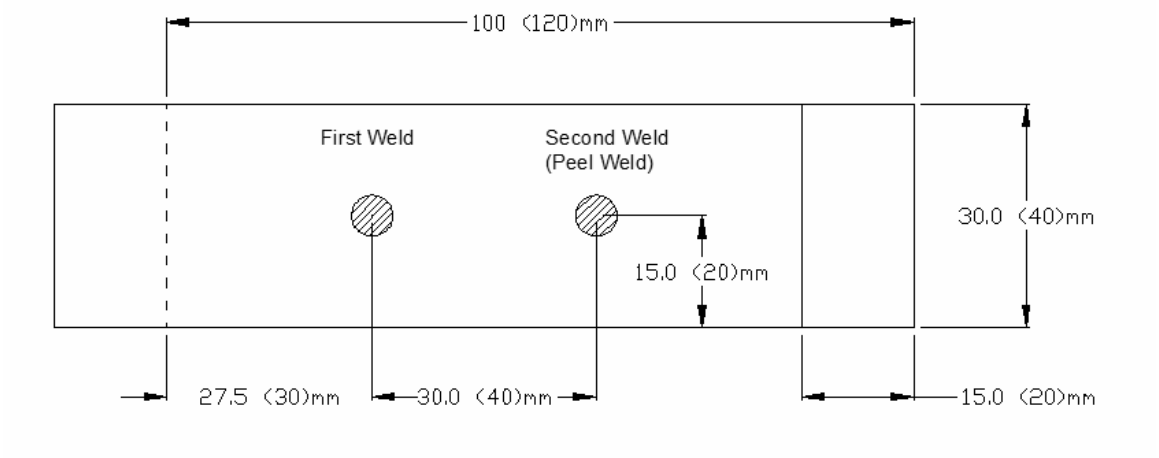

b)

Figure 3.1: Steel coupon specifications for a) endurance life testing, b) peel testing. Dimensions in parenthesis are for 1.0mm thick steel sheets. [15]

3.2 Electrodes

3.2.1 Uncoated Electrodes

Welding electrodes used in this study were RWMA Group A, Class II, Cu-Cr-Zr domed-flat nose, female caps (Part# FB-25). Electrodes were cold formed to the final welding geometry. The contact face of the electrode was machined to 4.80±0.5mm and 6.0±0.5mm to suit the steel thickness as per recommended practices [15]. A schematic drawing of the electrode dimensions is given in Figure 3.2. The 6.0mm face diameter electrode was machined to the nominal face diameter from the cold forged 4.8mm electrode. This resulted in a 0.2mm loss of electrode length.

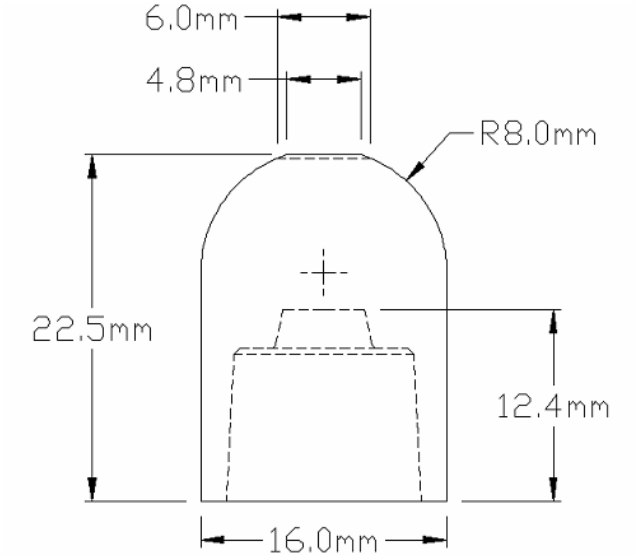

Figure 3.2: Electrode schematic diagram. Tip face diameter was cold forged to 4.8mm nominal and machined to 6.0mm nominal, where required. Machining also reduced the total electrode length by 0.2mm.

3.2.2 Coated Electrodes

The Coated electrodes used in this study were identical to the uncoated electrodes save the TiC MMC coating (hereinafter referred to simply as the *TiC coating*) applied to the domed surface. The TiC coating composition is shown in Table 3.2. It should be noted that carbon was not included in the table as the EDS was not able to detect elemental carbon. The coating thickness was observed to vary across the contact surface of the same electrode from 20 to 40μm. The coating covers the flat area as well as the

surrounding domed area of the electrode face. Figure 3.3 shows the coated electrode and the uncoated electrode caps.

Table 3.2: TiC MMC Coating Composition. Carbon content not included.

	Ti	Ni	Mo	W	Cu
TiC Coated Layer	59.3	22.4	13.13	1.02	4.14

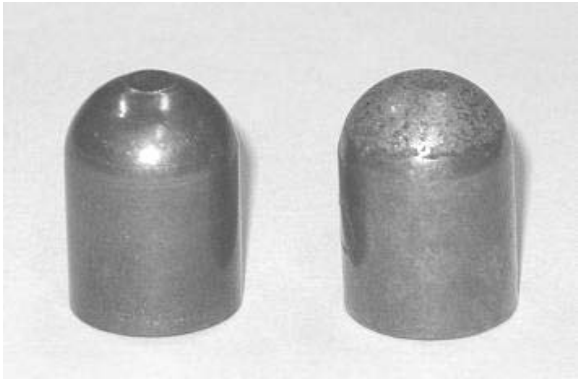

Figure 3.3: Photograph of uncoated and coated electrode caps used. Left uncoated, right coated.

Coating of the electrodes was performed manually on uncoated electrodes in the as received condition with no surface cleaning or conditioning prior to coating. All coated electrodes were coated offsite by the manufacturer. The coating material in the form of a sintered rod is applied to the surface of the electrode using a patented [20] intermittent arc electro-spark deposition. This process causes the local melting and fusing of both coating rod and base material. The intermittent nature of the process however causes the coating to be deposited in discrete droplets which are built up to form the coating thickness. The coated layer contains the TiC particles in suspension with a matrix composed mainly of Ni with some Mo, W and Cu mixed in from the base material. Measured hardness of the coating rod, coated layer, and base electrode were found to be 2250, 980, and 148 (HV_{200}) respectively.

3.3 Welding Trial Procedures

3.3.1 Weldability Study

The weldability study was aimed at determining if any, the differences in the nugget formation between the uncoated and coated electrode. Two sets of test trials were conducted for each electrode type for both weld current and weld time. All weldability testing was done using 1.0mm steel sheet. The thicker steel was used to facilitate metallographic analysis. Welds were made on peel sample coupons, and weld quality was determined by peel testing and weld cross-sectioning and etching. Peel testing was performed using a custom built machine to peel the samples as shown in Figure 3.4. Weld current was determined for each electrode type while holding all other parameters constant and the point of fusion, MWS and weld expulsion were recorded. The evolution of the weld nugget was then studied by increasing the weld time one cycle at a time from one with no hold time while holding weld current at a nominal setting for both electrode types. The point of sheet fusion, MWS, and expulsion were recorded. This technique of weld time ramping allows for the complete weld sequence to be stopped and analysed at each weld cycle.

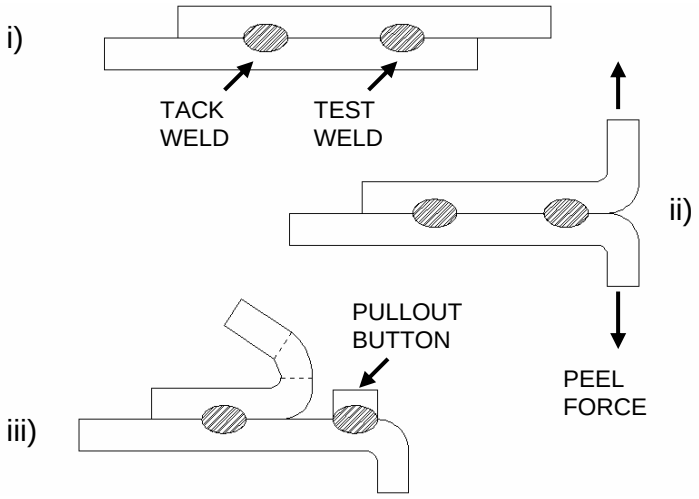

Figure 3.4: Peel Test Schematic. i) the peel test sample is welded tack weld first, then test weld. ii) the ends of the sample on the test weld side are bent back and a peel force is applied. iii) the weld is pulled to failure and either interfacial failure occurs yielding no button, or weld pullout occurs yielding a peel button.

3.3.2 Electrode Life Trials

Four life tests were conducted per electrode type on 0.7mm coated steel. Life trials were carried out until the button diameter fell below the MWS of $4(t)^{0.5}$, where t is the steel sheet thickness. At this point, the electrodes were determined to have reached end of life and were removed for analysis. Additional welding trials were terminated at various points in the electrode life for analysis.

A new pair of electrodes was selected and installed for each new trial. Six welds yielding three peel samples, each in a different orientation [15], as well as carbon tip imprints, electrode tip photographs, electrode mass and length were measured at 100 weld intervals. Weld quality was monitored by measuring the peel button size. Electrode displacement was measured during each weld using an LVDT sensor with an accuracy of 0.001mm and a data acquisition system linked to a personal computer. Electrode mass was measured before and after the life test using a digital weigh scale accurate to 0.001g.

Analysis of electrodes and welds was carried out on samples that were terminated after a certain number of welds or when end of life had been reached. Carbon tip imprints were taken using an imprint coupon made by fixing strips of carbon typing paper to a steel endurance coupon covered with plain white paper on both surfaces (top and bottom). The electrodes were then allowed to apply the weld force to the imprint coupon without weld current to transfer the carbon ink to the paper. Imprints were viewed with a stereoscope and measurements recorded using a *Futaba Pullscale* digital scale connected to the stereoscope stand. Figure 3.5 illustrates the tip imprint coupon with electrode impressions.

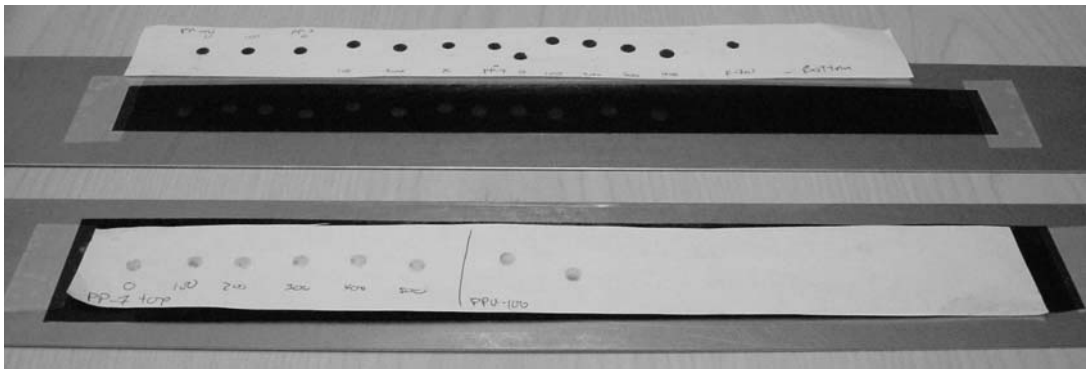

Figure 3.5: Carbon imprint coupon photograph. Top image shows transferred imprints.

3.4 Welding Trial Parameters

Welding was conducted on a 250kVA, air operated, single phase AC, pedestal type spot welding machine. The welder was manufactured by Centerline, Windsor ON., and located at the University of Waterloo. Weld force, weld time, cooling water flow, welding rate, and hold time were specified by recommended practices [15] and are listed in Table 3.3. Weld voltage was applied as a single pulse at 70-80% power factor with weld current being determined for each type of electrode using the process outlined in AWS recommended practices [15], and given in the table. The process to determine weld current involves slowly increasing the weld current while holding all other parameters constant until the minimum weld size is reached, at that point, the current is deemed I_{min}. Then proceeding to increase current until expulsion or severe electrode sticking is experienced on the second weld of a peel sample, I_{max} was determined. The weld current (I_{op}) is then the I_{max} value less 200A.

Table 3.3: Electrode Test Weld Parameters

	Weldability Study		Electrode Life Study
	Current Tests	Time Tests	
Weld Current (kA)	10000 - 11100	10500	9200 Uncoated / 8500 Coated
Weld Force (kN / lbf)	2.8 / 623	2.8 / 623	2.0 / 445
Weld Time (ms / cycles)	217 / 13	17-283 / 1-17	11
Welding Rate (welds/minute)	15	15	20
Hold Time (cycles)	5	0	5
Cooling Water (L/min , gal/min)	4 /1	4 / 1	4 / 1

3.4.1 Weldability Study

The weldability study was split into two sets of experiments, the weld current range tests, and the weld time range tests. To determine the weld current operating range, all other parameters were held constant and weld current was increased from 10000A to 11100A in 100A stages. Weld time was held at 13 cycles (217ms) as recommended for the sheet thickness [15]. The weld time tests were carried out at 10500A while increasing

weld time from 1 cycle (17ms) to 17 cycles (283ms) in one cycle (16.6ms) increments. All other parameters were constant for both studies.

3.4.2 Electrode Life Trials

Weld current was determined for each electrode type as described above. Weld time was the same for both electrode types as outlined in life test procedures of recommended practices [15]. It is noted that the weld current in Table 3.3 was substantially different for the uncoated and coated electrode. This was due to the initial results of the weldability study and will be discussed later in this study.

3.5 Static Resistance

Static resistance of the weld systems of both uncoated and coated electrodes were measured using an *AVO Ducter DLRO 10X Digital Low Resistance Ohmmeter* four point micro-resistance meter. Probe leads were setup as shown in Figure 3.6 and attached to the electrode shanks using stainless steel hose clamps. Measurements were taken with the electrodes held together under the weld force without weld current. Readings with no steel sheet, a single sheet and two sheets were taken.

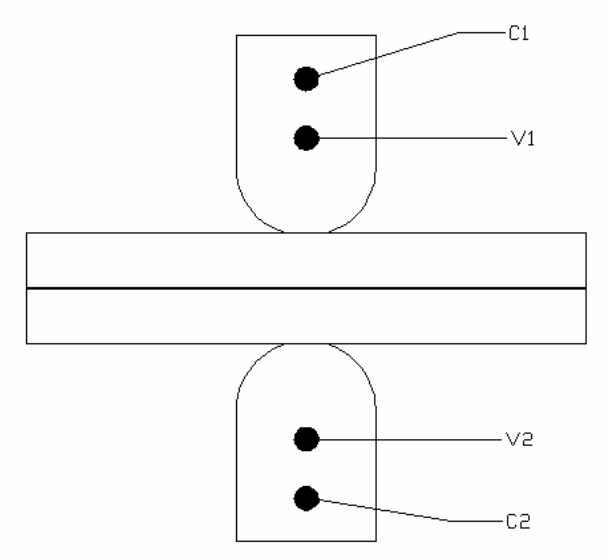

Figure 3.6: Static resistance four point probe schematic. C1 and C2 leads connected to current terminals on tester. V1 and V2 leads connected to voltage terminals on tester.

3.6 Hardness Testing

Micro hardness testing was performed on cross-sectioned electrodes using a *LECO MHT Series 200* Vickers micro-hardness tester. Test load was 100g and indentations were made 0.05, 0.1, 0.2, 0.5, 1.0, 2.0, and 5.0mm from the electrode surface as shown in Figure 2.13. Indentation traverses were taken at the center of the electrode face. Indentation diagonal measurements and HV calculations were done with optical microscopy with the aide of image analysis software *Image Pro 5*.

3.7 Microscopy

Scanning electron microscopy (SEM) was performed on a *Jeol JSM 6460* with an attached *Oxford Instruments INCA-350* for energy dispersive spectroscopy (EDS) analysis. Analysis of welding electrodes was performed on the contact face as well as surface cross sections. SEM and optical microscopy were used to observe the surface profile as well as alloy layer development. Energy dispersive spectroscopy was used to analyse the progression of zinc into the electrode material as well as track the presence of TiC on the coated electrode surface. Elements were monitored for their presence in the scan area only, as the EDS scan is not meant for detailed quantitative analysis. According to the Monte Carlo electron trajectory simulation [49], the depth of penetration of an EDS scan is no more than 1.5μm on a copper sample. X-Ray diffraction analysis was used to identify the phases formed on the surface of the electrode.

Chapter 4

Welding Behaviour Study

Uncoated and coated electrodes were tested to observe the difference in weldability and tip life behaviour. Results are divided in two sections, the first dealing with the formation of the weld nugget, and the second dealing with the electrode life. Degradation mechanisms of the electrodes are discussed in the following chapter. Welding parameters and data collection procedures as described in Chapter 3 were used to characterize the electrodes. All measured data can be found in Appendix A.

4.1 Nugget Formation

The following investigations were performed to observe how the coated electrode nugget formation sequence differed from that of the uncoated electrode. This section is involved with the electrical and thermal interaction of the electrode with the steel.

4.1.1 Weld Current Study

Weld current was determined for each of the electrode types using the procedure outlined in Section 3.4. Weld time was held at 13 cycles for both electrode types and weld current was increased at 100A intervals until interfacial fusion, MWS, and expulsion conditions were reached. Table 4.1 shows the current tests results for both electrode types. The ability of the coated electrode to form acceptable welds at lower currents indicated its improved weldability over the uncoated electrode. The increased range of weld current over which the coated electrode was able to form welds was also indicative of its superior weldability.

Table 4.1: Weld Current Test Results at 13 cycle Weld Time

	Button Size / Joint Condition	
Weld Current (A)	Coated Electrode	Uncoated Electrode
10000	No Fusion	No Fusion
10100	Interfacial Failure	No Fusion
10200	3.1	No Fusion
10300	4.2 (MWS)	No Fusion
10400	4.84	No Fusion
10500	5.6	Interfacial Failure
10600	5.8	3.6
10700	6.16	4.5 (MWS)
10800	6.2	5.57
10900	6.5 (Expulsion)	5.8
11000		6.3
11100		6.45 (Expulsion)

4.1.2 Weld Time Study

It was seen in previous trials that the coated electrodes would require less weld current to produce satisfactory nuggets. In an effort to determine if the processes for nugget formation were different for coated and uncoated electrodes, weld time was set to terminate the weld current before the completion of the weld sequence to freeze the weld at each cycle of the sequence. Table 4.2 shows the weld time in cycles required to achieve fusion of the steel, form a weld that meets minimum weld size, and cause expulsion. Both electrodes under the same weld schedule were also observed to have melted the zinc coating at the faying interface after 2 cycles of weld current. The large difference in character was the number of cycles required to achieve fusion of the workpieces. Almost double the weld time was required for the uncoated electrode at 13 cycles compared to the 7 cycles for the coated electrode. Minimum weld sizes were achieved at 10 and 14 cycles for the coated and uncoated electrodes respectively. Expulsion occurred at 15 and 17 cycles for the coated and uncoated electrodes

respectively. The number of weld current cycles between the fusion point and the expulsion point can give an indication of the weldability of the electrode. The coated electrode was able to form welds between 7 and 15 cycles yielding an 8 cycle range. The uncoated electrode time range was only from 13 to 17 cycles, half that of the coated electrode.

Table 4.2: Weld Time Test Results at 10500A Weld Current

	Button Size / Joint Condition	
Weld Cycles	Coated Electrode	Uncoated Electrode
1	No Fusion	No Fusion
2	No Fusion	No Fusion
3	No Fusion	No Fusion
4	No Fusion	No Fusion
5	No Fusion	No Fusion
6	No Fusion	No Fusion
7	Interfacial Failure	No Fusion
8	3.46	No Fusion
9	3.74	No Fusion
10	4.7 (MWS)	No Fusion
11	5.09	No Fusion
12	5.2	No Fusion
13	5.6	Interfacial Failure
14	6.15	4 (MWS)
15	6.53 (Expulsion)	5.2
16		6.46
17		6.6 (Expulsion)

Figure 4.1 shows the cross section of a weld stopped at 7 cycles of current using uncoated electrodes. At this point, the uncoated sample showed a slight heat affected zone at the faying interface outlined in a). The higher magnification view in b) shows the change in microstructure with no evidence of melting or fusion between the steel sheets.

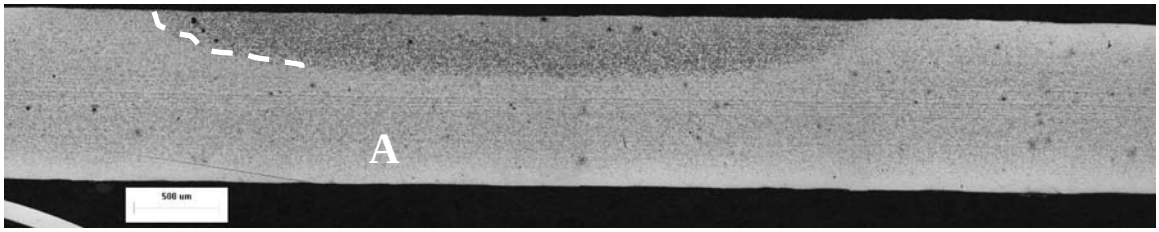

a)

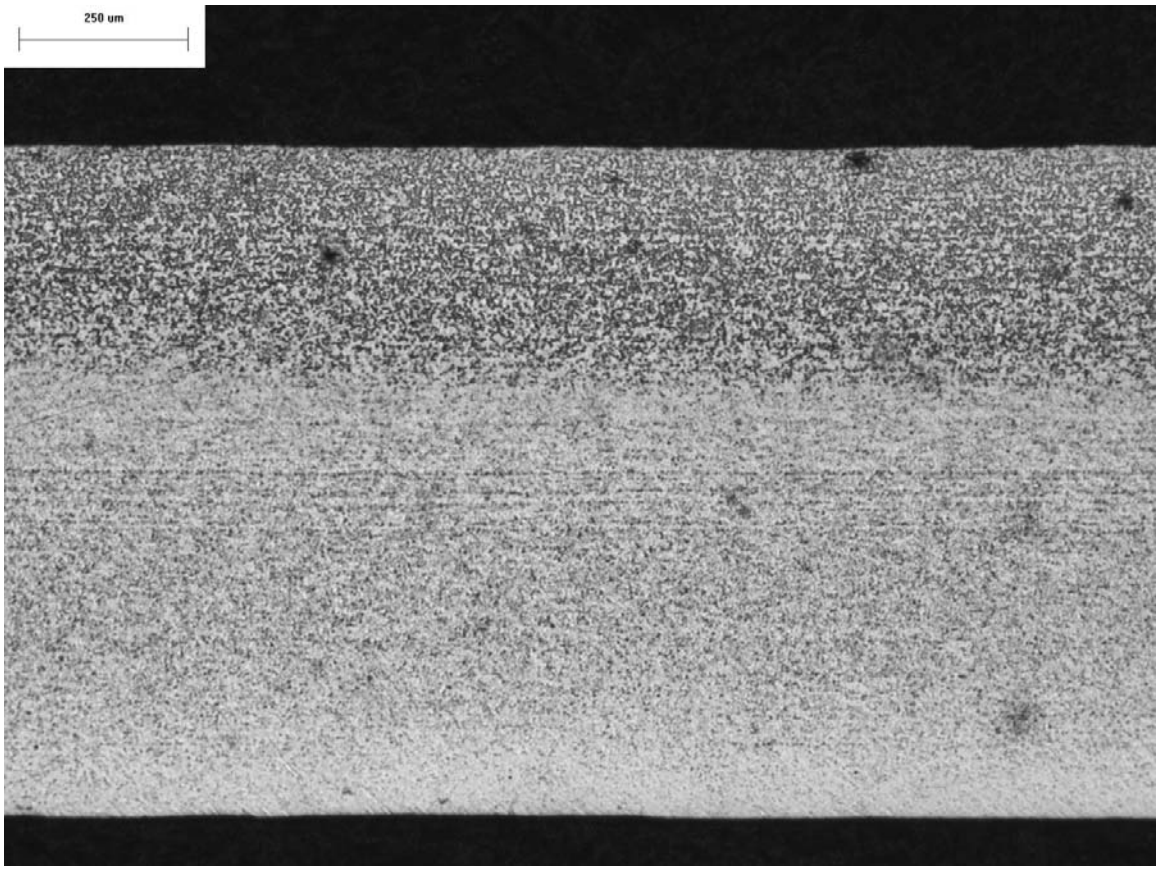

b)

Figure 4.1: Uncoated electrode weld sheet after 7 cycles of weld current at 10500A. Region A shown in high magnification in b). The top surface is the faying interface.

As shown in Table 4.2, the uncoated electrode required almost double the weld time to melt the steel at the faying interface. Under the same conditions, the steel sheet welded with the coated electrode is shown in Figure 4.2. A clear heat affected zone has progressed through the thickness of the sheet and evidence of melting was present at the faying interface. Peel testing had shown that a weld nugget had formed and the sheets had fused and then fractured along the faying interface. The higher magnification view in b) clearly shows the solidification microstructure as well as the fracture region. Under similar weld conditions and weld parameters, the coated electrode was able to produce fusion where the uncoated electrode was not.

Figure 4.3 shows the welds at 14 cycles of current. At this point, both coated and uncoated electrodes were able to form welds. The uncoated weld in a) shows the button measured as 4.0mm. The fusion nugget penetration was approximately 30% as shown on the figure. The coated weld shown in b) displayed a much larger nugget with a measured button of 6.15mm. The penetration of this nugget was approximately 60%, double that of the uncoated electrode. Again, the coated electrode displayed the ability to produce larger welds under the same welding parameters.

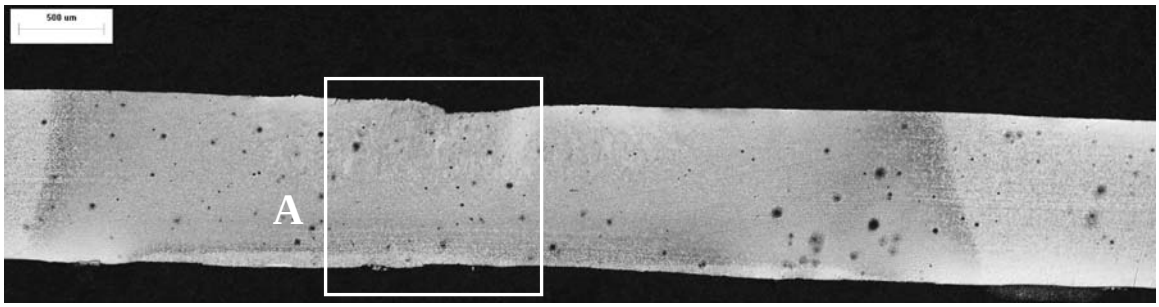

a)

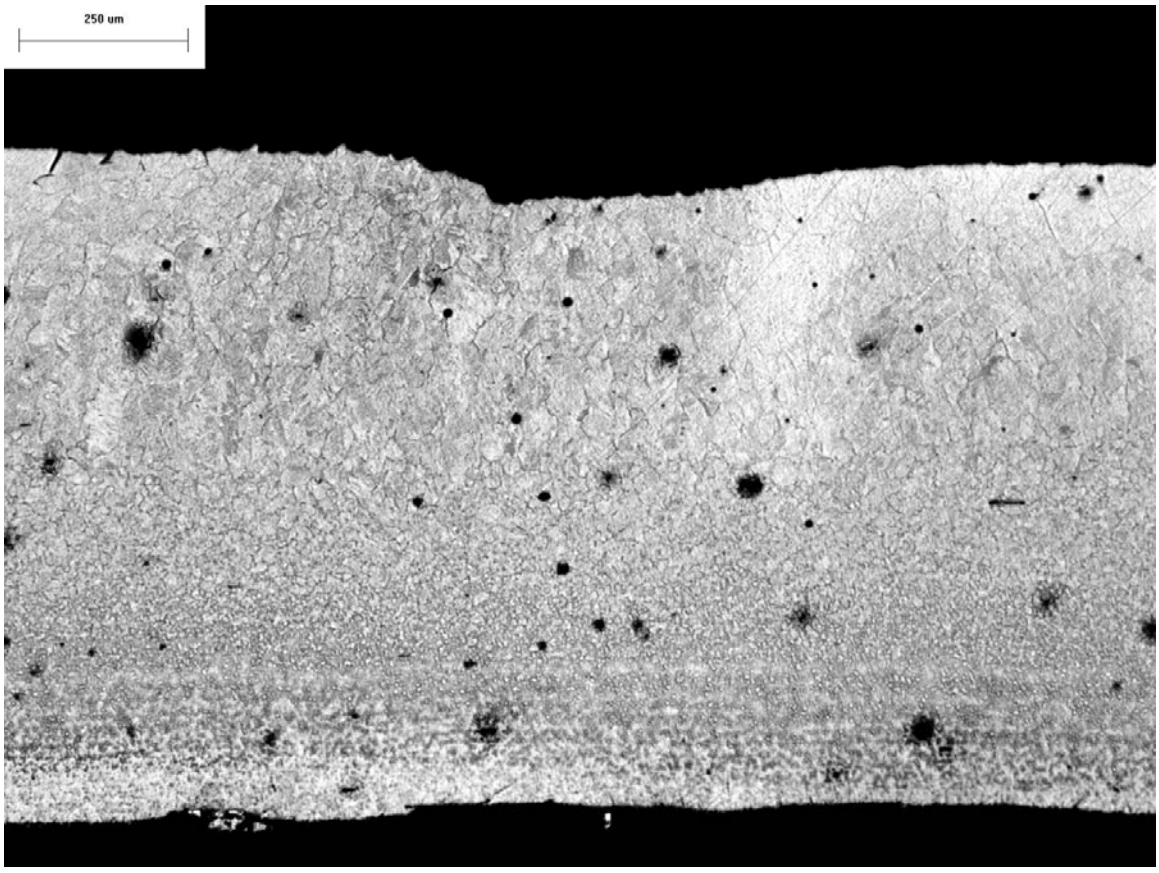

b)

Figure 4.2: Coated electrode weld at 7cycles of weld current at 10500A. Region A shown in high magnification in b). The top surface is the faying interface.

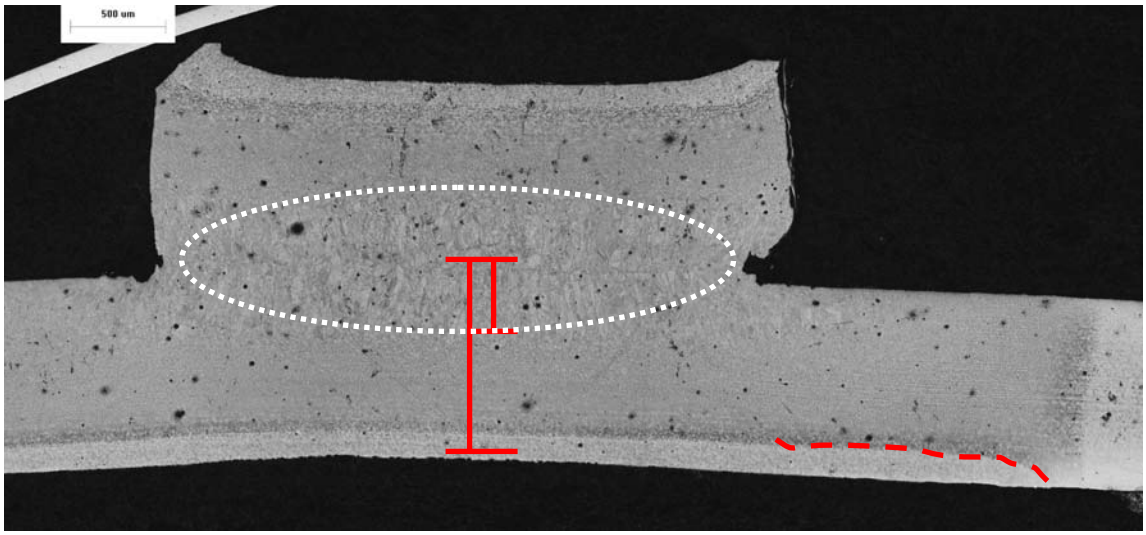

a)

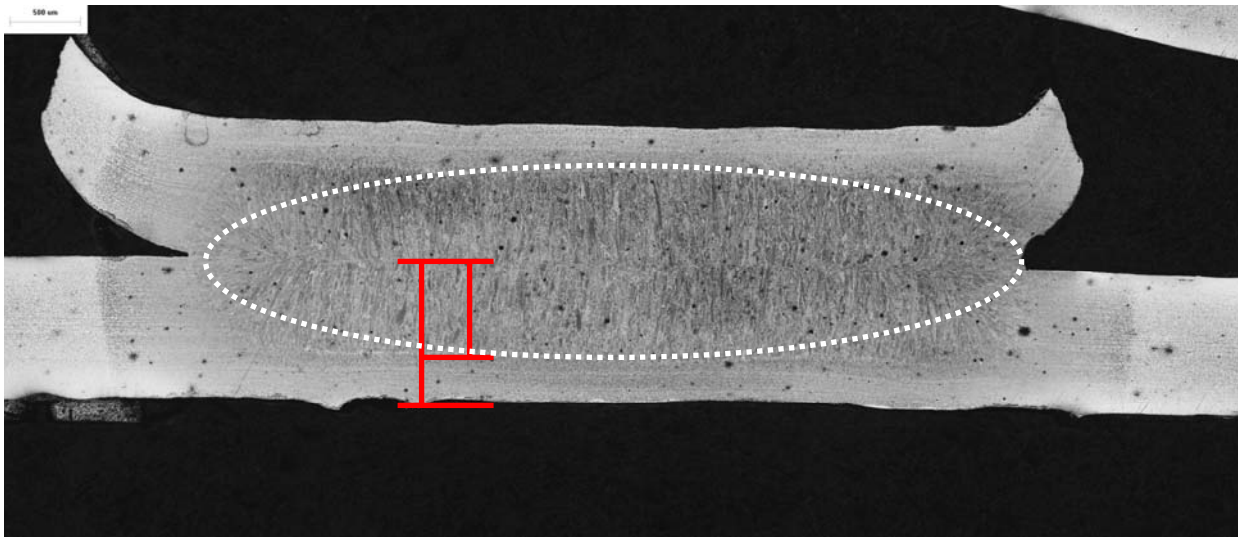

b)

Figure 4.3: Weld cross sections at 14 cycles of weld current after peel testing. a) uncoated, b) coated.

4.1.3 Coating Resistance

The presence of a thin film on the surface of the electrode will affect the resistance of the electrode and could influence the welding behaviour. With the coating-electrode interface added to the system, and a thin film resistance from the coating itself, the RSW system for welding coated steels with coated electrodes has become more complex and is represented schematically in Figure 4.4.

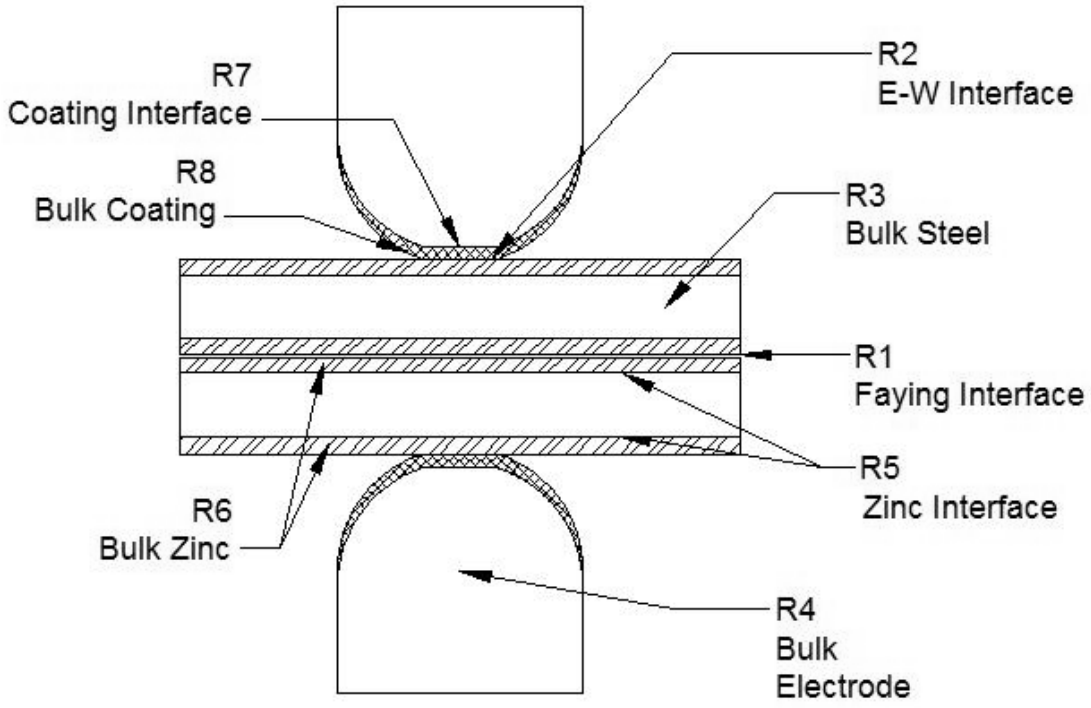

Figure 4.4: Coated electrode resistance circuit. R7 and R8 are added to the system due to the electrode coating.

Static resistance measurements of the uncoated and coated electrodes were taken while setup on the welder. Resistance was measured across the electrode contact faces without a weld sheet while pressed together under the weld force, across the electrodes and a single steel sheet, and across the electrodes and two steel sheets as the complete welding circuit. Measurements were then averaged to yield a nominal resistance with one standard deviation above and below. Results were tabulated in Table 4.3. Without a steel sheet between the electrodes, measurements reflect the bulk resistivity of the electrodes as well as their contact resistance under the weld force. The coated electrode resistance was more than double that of the uncoated electrode at 36.1 and 12.5 μohm respectively. The resistance of the bulk coating rod was also measured by the four point probe and resistivity was calculated to be approximately 918μohm*mm. For an average coating thickness of 30μm, the coating would theoretically add 1.7μohm to the system. The much higher coated resistance measured was most likely due to poor contact between the coated electrode faces.

Table 4.3: Electrode Static Resistance at Beginning of Life

Static Resistance (micro ohm)			
	Electrode Only	One Sheet	Two Sheets
Uncoated Electrodes	12.5 ±0.6	22.8 ±0.9	32.5 ±1.2
Coated Electrodes	36.1 ±1.5	33.9 ±0.8	36.0 ±0.5

With one sheet added to the resistance circuit the uncoated electrodes experienced an increase to 22.8μohm, rising approximately 10μohm most likely due to the bulk resistance of the steel. The coated electrodes decreased slightly in resistance, at 33.9μohm. With the zinc coating to facilitate intimate contact of the two surfaces, the resistance would experience a drop. The addition of the bulk resistance of the steel worked to offset the drop due to improved contact and yielded the total resistance seen.

With two steel sheets in the circuit representing the resistance experienced during welding, the electrodes yielded an average resistance of 33.5μohm and 36.0μohm for uncoated and coated electrodes respectively. The uncoated electrode resistance increased approximately 10μohm again due to the bulk steel. The coated electrodes have approached the original resistance without any steel sheets. As the bulk resistance of the steel sheets must be present, this suggests that the presence of the sheets works to reduce the poor contact resistance experienced by the rough coating.

From the heat input equation [Eq. 1.1], the heat input to the system is governed by weld current, circuit resistance and weld time. As the weld current, weld time, and tip area are identical for both electrodes during the weldability tests, the resistance of the weld circuit remains the variable that could influence the heat input to the system. As seen above, the total circuit resistance for the coated electrodes was only approximately 3μohm higher than the uncoated system. Again referring to Eq. 1.1, the ratio of the change in heat input becomes the ratio of the resistance of the entire circuit. Using the measured system resistances from Table 4.3, the increase in heat input due to the coating is 8.4%. The weld time needed to achieve similar weld sizes is nearly double for the uncoated electrode, meaning that an approximate heat input increase of 85% was required to form similar welds using the uncoated electrode. The 8.4% increase in heat input due

to increased resistance does not fully account for the performance improvement of the coated electrode. This is explored later in this chapter.

4.1.4 Electrode Softening

The additional heat generated by the electrode coating occurs at the electrode work interface, and therefore increases the heating experienced by the electrode. This heating could lead to softening of the electrode base material and deformation causing rapid tip growth and failure. Hardness profiles as outlined in Section 3.6 were taken on cross-sectioned electrodes at various stages in electrode life and are presented in Figure 4.5. Electrode base material softening was seen at the surface of the electrode face with increasing hardness at greater distances from the electrode face. The degree of softening can be roughly measured by the depth at which the base material has experienced a significant drop in hardness. With increasing life, the softened region was shown to penetrate deeper into the electrodes. At 24 welds, the uncoated electrode had experienced greater softening at the surface due to the zinc interaction. At 100 welds, both electrodes seem to have undergone similar degrees of softening, however the overall hardness of the coated electrode was higher. At the end of life condition, the softening was again similar for both coated and uncoated electrodes. In each case, the uncoated electrode showed a lower hardness at the surface, and generally a lower overall hardness as the life of the electrode progressed. Contrary to the additional heat generated at the electrode surface, the coated electrode appeared to have been able to protect the base material from the heat input to the weld.

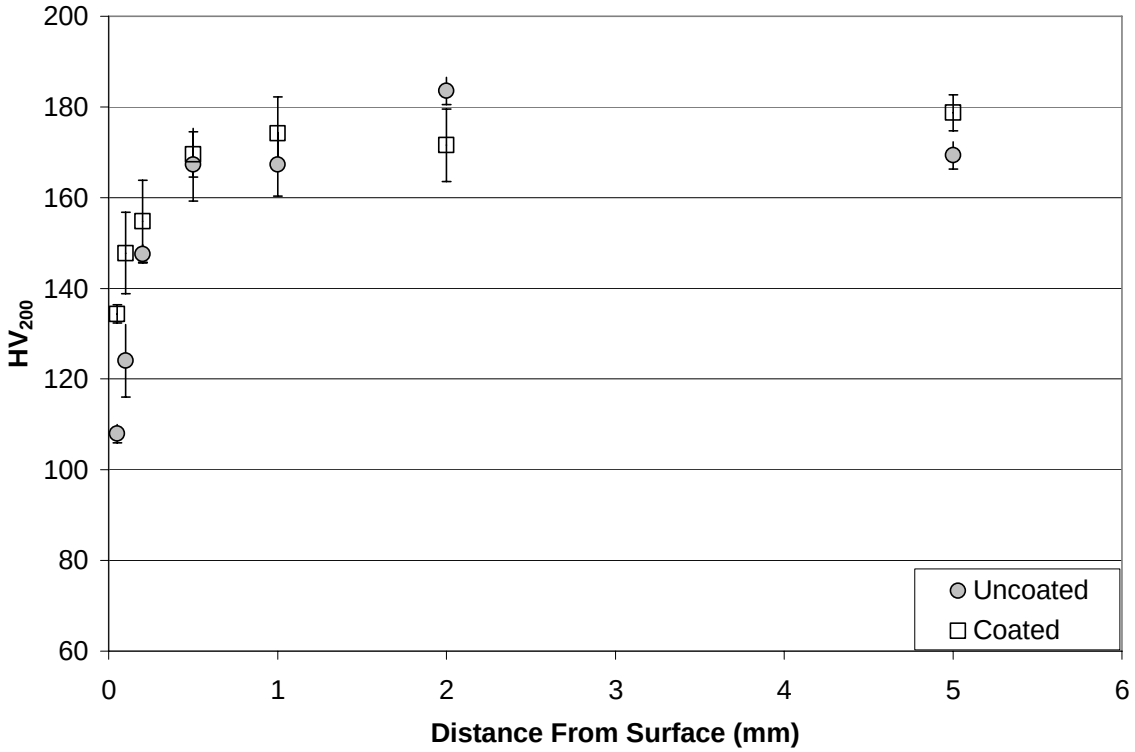
200
180
160
140
120
100
80
60
HV200
0
1
2
3
4
5
6
Distance From Surface (mm)
Uncoated
Coated

a)

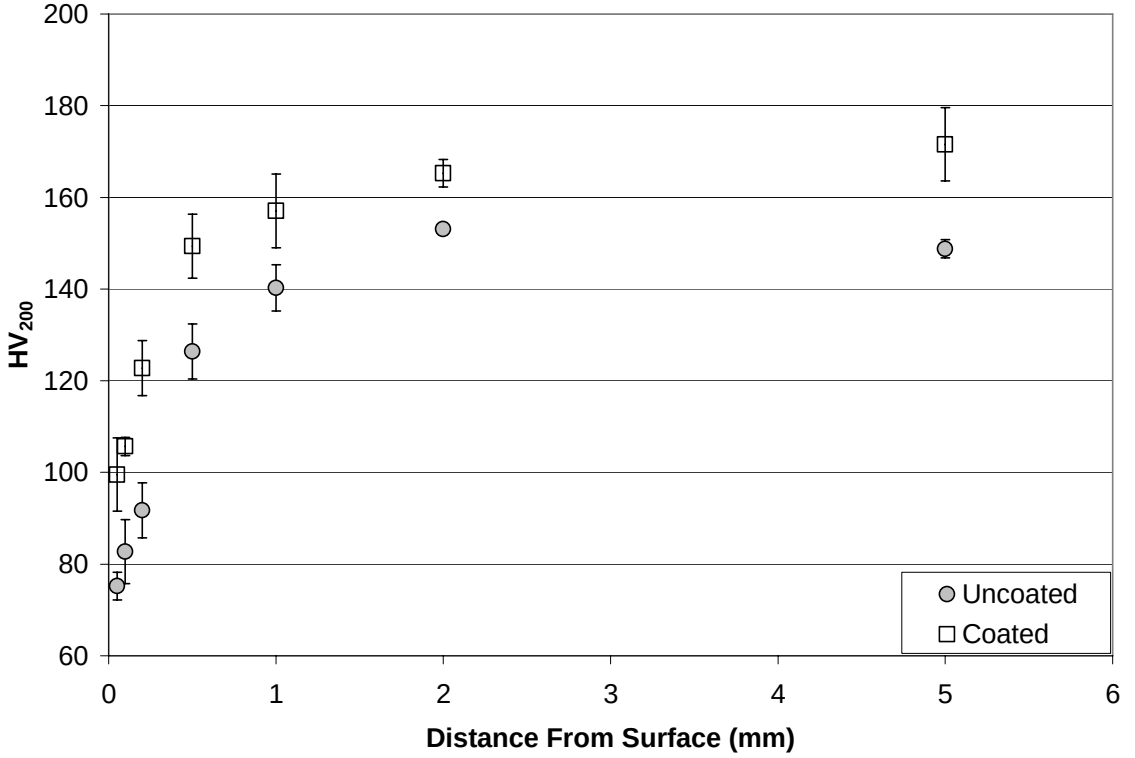
200
180
160
140
120
100
80
60
HV200
0
1
2
3
4
5
6
Distance From Surface (mm)
Uncoated
Coated

b)

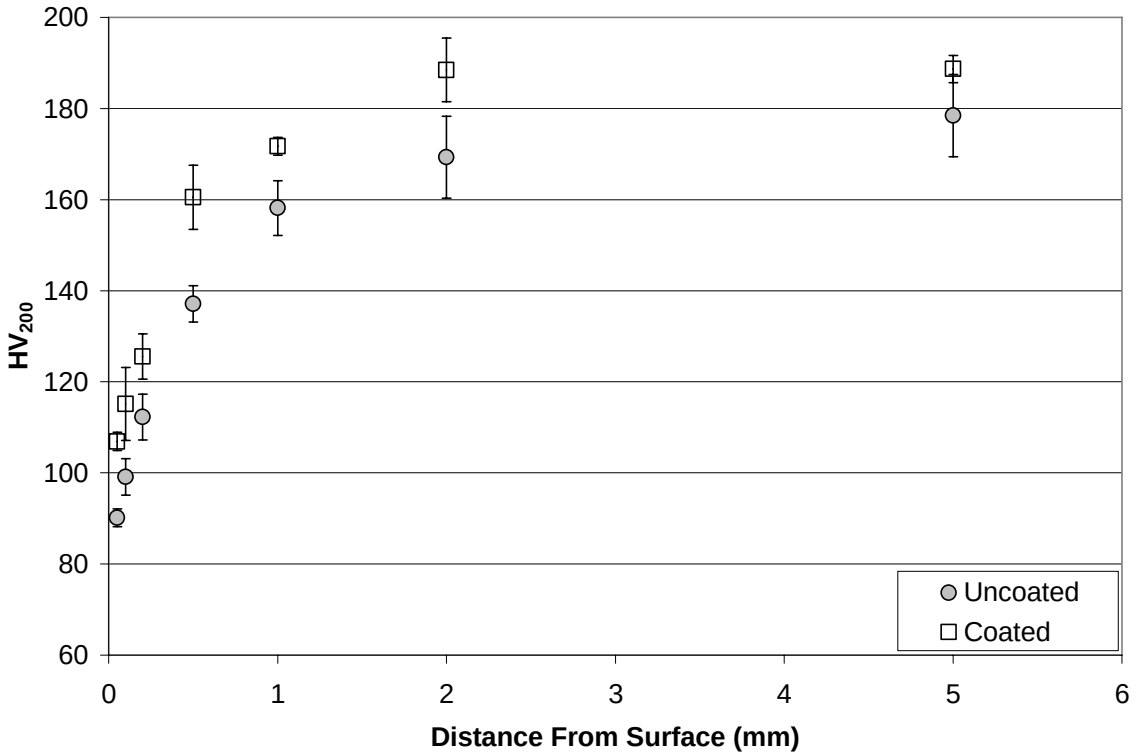

c)

Figure 4.5: Electrode hardness profile at a) 24, b) 100, and c) end of life

4.1.5 Coating as Thermal Barrier

As the heat generated at the electrode interface did not seem enough to cause additional softening of the electrode base material, the coating may have acted as a thermal barrier to prevent heat from being extracted through the electrode preventing softening as well as allowing larger nuggets to be formed. As discussed in section 2.1.1, the propagation of a heat wave generated at the faying interface was able to move very quickly through the material effectively making the thermal gradient in the direction parallel to the electrode axis very small. This makes the rate of heat extraction due to the heat sinking of the electrodes very critical. The presence of molten zinc at the electrode-work interface may also play a role in the thermal circuit of the system. As contact was improved with the liquid zinc layer, the rate of heat transfer to the electrodes would increase. To maximize the efficiency of the RSW process, it is desirable to generate heat at the faying interface as quickly as possible and retain it there, localizing the melting and reducing the negative thermal effects on the workpiece as well as the weld electrodes. As

the thermal diffusivity of copper is more than triple that of iron at room temperature [52], it follows that the electrode will sink a great deal of heat generated reducing the efficiency of the weld sequence.

Close inspection of the heat affected zones of the welds in Figure 4.3 revealed a thin layer of unaffected base metal very close to the electrode-work interface in the uncoated weld sample. This band of unaffected steel resembled the footprint of the electrode and was evidently due to the heat sinking properties of the uncoated electrode. This distinct band was not present in the coated electrode weld at the same parameters, suggesting that the rate of heat extraction was much lower. Water cooling of the electrodes is necessary to minimize damage to the electrodes caused by excessive heat, but may decrease the efficiency of the weld process by extracting heat needed at the faying interface. The copper electrodes are very good heat sinks and are able to pull heat away from the weld zone quickly. With the lower thermal conductivity coating present at the electrode workpiece interface, another layer was added to the thermodynamic system as well as another interface. Additionally, the small amount of heat generated at this interface due to the increased electrical resistance may also contribute to weld formation. From the discussion above, it has been shown that the coated electrode was able to preserve heat generated in the weld and protects the electrode base material from the same heat.

4.2 Electrode Life Testing

The following investigation explored the behaviour of the electrodes during an electrode life test prescribed by the AWS [15]. The electrodes' ability to form weld nuggets and electrode wear rates were tracked and discussed.

4.2.1 Electrode Life

Electrode life trials were conducted as per procedures outlined in Section 3.3. The same weld time was used for both electrode types and weld current was determined independently according to AWS standards [15]. This ensured that the button size at the beginning of the test was the same for both coated and uncoated electrodes. Electrode tip

life was tracked with peel samples taken every 100 welds. Figure 4.6 plots the size of the weld buttons versus the number of welds made with the electrode pair. The dashed line on the plot represents the minimum weld size and the point at which the electrodes will be considered to have failed once weld buttons fall below this size. Typical electrode tip failure occurred at 300 and 1100 welds for uncoated and coated electrodes respectively. Weld button diameter decreased as weld number increased for both sets of electrodes, however the coated electrodes were able to form more welds than the uncoated electrode. Repeated tests have yielded some variation and tip life was recorded in the range of 800-1200 welds for the coated electrodes and 300-500 for the uncoated electrodes. The TiC coating was able to improve the average electrode tip life by approximately 100 percent.

As the condition of the electrodes is mainly determined by the contact surface condition and tip diameter, tracking these attributes can give insight as to how the TiC coating was able to prolong the life campaign of the electrodes.

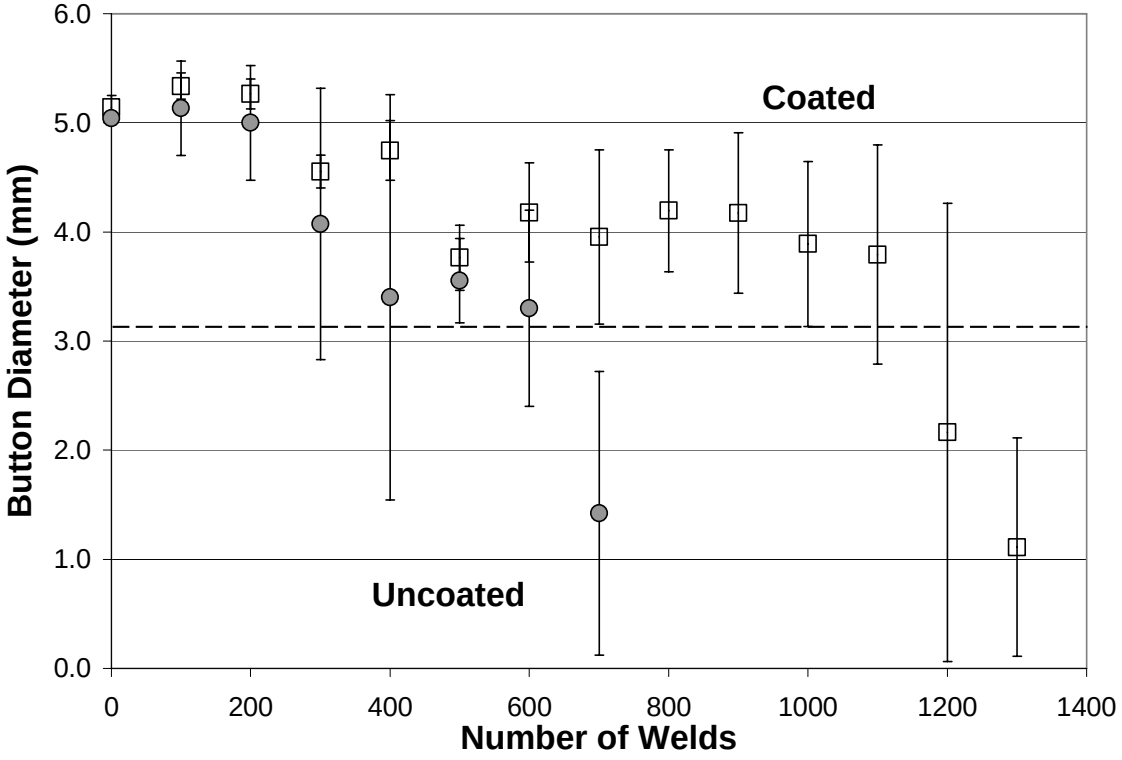

Figure 4.6: Weld peel button size vs. weld number. Dashed line represents the minimum weld size. Electrode life represented by number of welds before button size falls below MWS line.

4.2.2 Electrode Face Diameter

Throughout the life tests conducted, the electrode contact face diameter was measured with carbon tip imprinting. Figure 4.7 shows the electrode carbon imprints for four typical life trials of each electrode type. Failure points are marked with an asterisk (*). The overall shape of the electrode contact region remained round and did not show irregular deformation. Severe electrode pitting was seen only in the coated electrodes. The presence of pits on the electrode surface did not seem to play a large role in the overall performance of the electrodes.

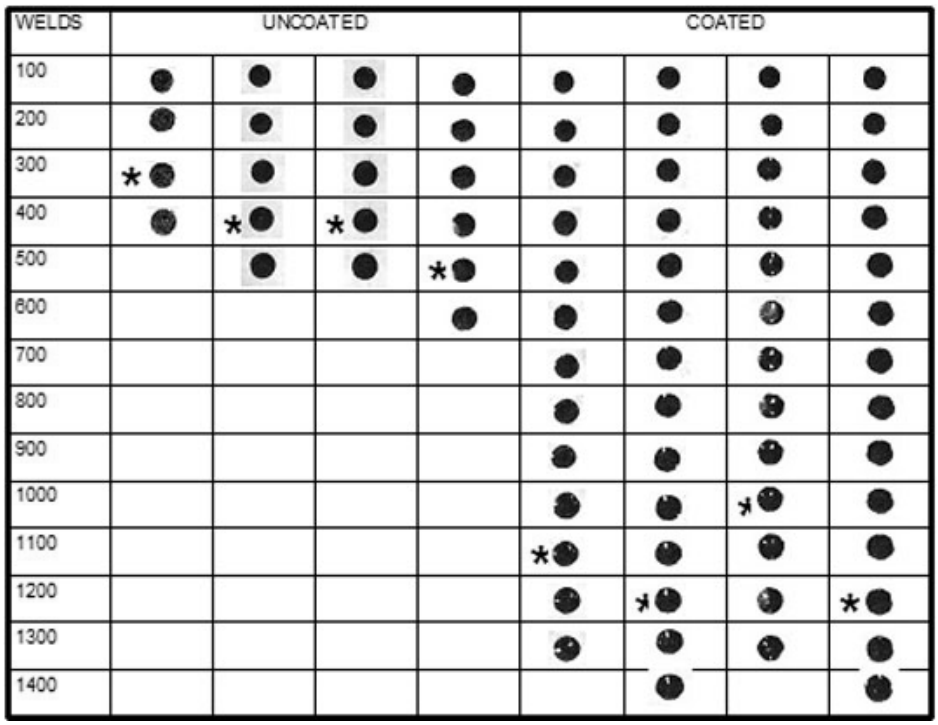

Figure 4.7: Uncoated and Coated Electrode Tip Carbon Imprints. Failure points are shown with an (*).

Figure 4.8 shows the trend of tip face diameter as measured from the carbon tip imprints versus the number of welds for both a typical set of coated and uncoated life tests. The slope of the curves indicates the rate at which the tip face grows due to degradation. The uncoated electrode displayed a high rate of growth as expected when welding zinc coated steels. The coated electrode did not experience a high growth rate as compared to the uncoated electrode. Instead, the growth rate was slower and steady until

failure. The uncoated electrode experienced a *0.13mm/100 welds* tip growth rate while the coated electrode exhibited a rate of *0.08mm/100 welds*. With a slower rate of tip growth, the current density of the coated electrodes decreased at a slower rate than the uncoated electrodes and was responsible for the ability to form welds at longer life. Electrode failure was found to occur when the coated electrodes reached a tip diameter large enough to reduce the current density to a point where a satisfactory weld could no longer be formed. This point was reached after roughly 0.6 and 0.8mm of tip growth for uncoated and coated electrodes respectively. The coated electrode again displayed the ability to weld beyond the limits of the uncoated electrode. This difference in growth rate and in tip diameter (hence area) was believed to be directly linked to the life improvement of the coated electrodes.

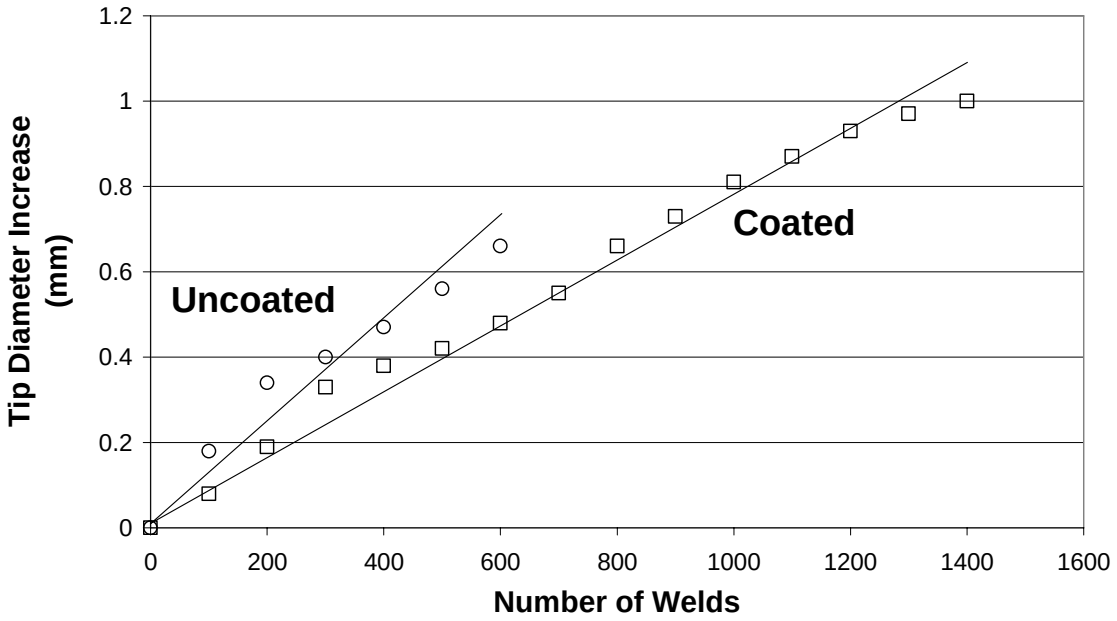

Figure 4.8: Tip growth vs. number of welds. Tip diameter growth rates are represented by the slope of the tip growth curves.

4.2.3 Electrode Length Reduction

Figure 4.9 shows the electrode length decrease versus the number of welds of a typical set for both coated and uncoated electrodes. It was immediately clear that the coated electrode had the ability to reduce the rate of length reduction of the electrode. As tip length and tip diameter are closely linked through geometry, this result was consistent

with the tip growth curve. Approximate length reduction rates of 0.02mm/100 welds and 0.006mm/100 welds were seen for the uncoated and coated electrodes respectively. The uncoated curve was sharp and roughly linear, showing steady length reduction until failure. The coated curve was also roughly linear, showing a slower rate of length reduction.

It is important to note that the total length reduction of the coated electrode was more than the initial thickness of the TiC coating. As length reduction may have been caused by factors other than material loss, this does not necessarily mean that the coating was completely removed. This phenomenon is further discussed in Chapter 5.

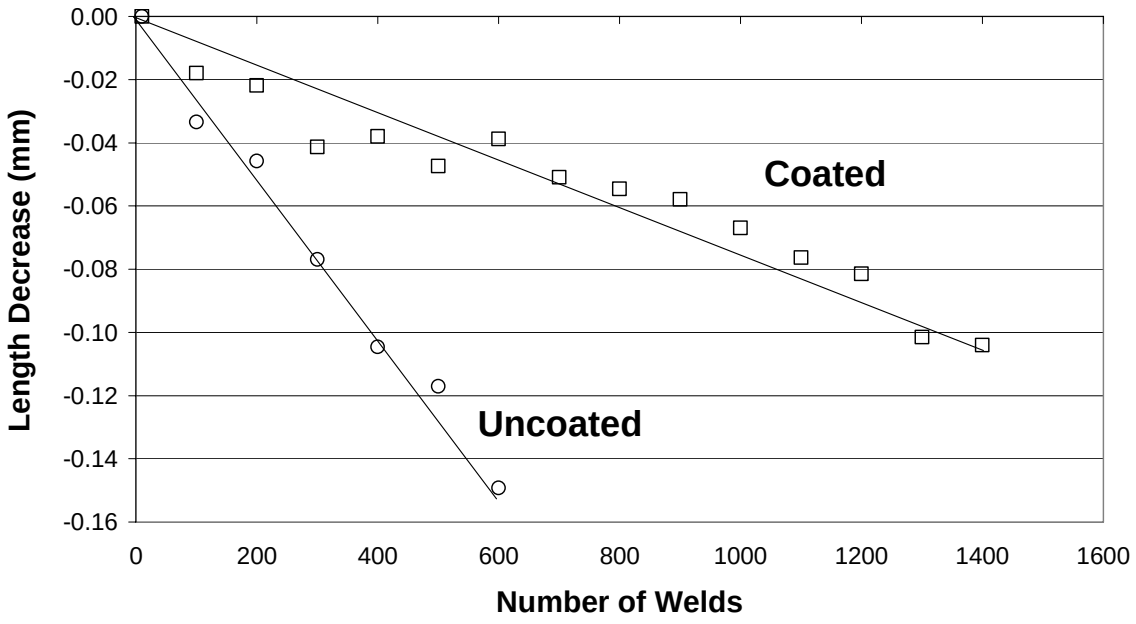

Figure 4.9: Electrode length reduction vs. number of welds. Length reduction rates are given by the slope of the length reduction curves.

4.2.4 Deformation

Figure 4.10 shows both coated and uncoated electrodes cross sectioned at the end of life condition. Macro inspection of the cross sections revealed that only a very small amount of plastic flow or mushrooming of the electrode faces occurred for both electrode types. This agrees with previous experience with this electrode geometry [5,20] as well as with the predicted tip growth trends. The TiC coating did not seem to have an adverse affect on the deformation character, however since gross deformation was not expected

with this electrode geometry, electrode base material softening was monitored during the electrode life. The softening curves discussed in Section 4.1.2 also showed that the coating did not cause an increased rate of softening of the electrode base material. Neither of the electrodes used experienced macro-deformation in the conventional "mushrooming" style associated with truncated cone electrodes.

It was also noted from Figure 4.10 that the wear profile of the electrodes at the end of life remained to be flat. The concave wear pattern seen by Saito et al. [9] was not apparent in the life trials.

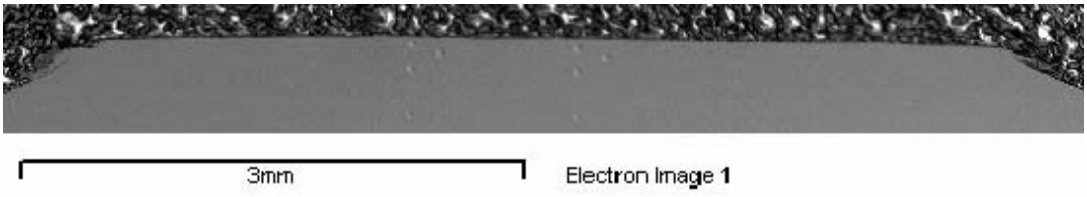

a)

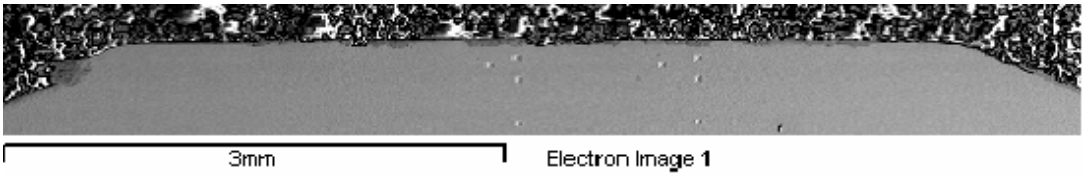

b)

Figure 4.10: Electrode surface cross sectioned at end of life condition showing little macro deformation. 18x. a) uncoated, b) coated.

Chapter 5

Electrode Degradation Study

The weldability and welding behaviour has been characterised in the previous chapter. The mechanism by which the coated electrode degrades and eventually fails was investigated and discussed through analysis of test results and metallographic study.

5.1 Coating as Diffusion Barrier

5.1.1 Material Interaction

The evolution of the surface layers that caused the growth of the tip face is due to the interaction of the zinc steel coating and the copper electrode material. If the zinc were not allowed to interact with the copper electrode material, the degradation would be decreased and the tip life extended. The TiC coating shown in Figure 5.1 was meant to provide a barrier to prevent the zinc from interacting with the copper. Without the interaction, the mass transfer and resultant length reduction would be theoretically reduced.

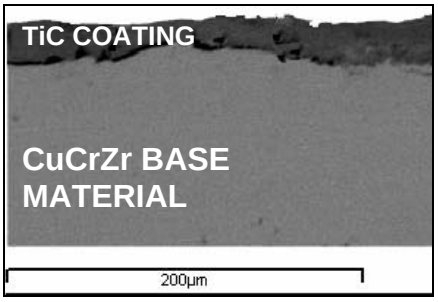

Figure 5.1: Coated electrode surface cross section showing electrode base metal and TiC coating. 0 welds.

Electrode contact surface scans by EDS show that zinc had adhered to the tip face early in the life of the electrode. Figures 5.2, and 5.3 show the SEM micrographs and accompanying EDS elemental mappings of the uncoated and coated electrode at 100 welds. The coated electrode was not able to prevent the zinc from adhering to the surface of the electrode. The titanium was still present on the coated electrode surface, except around the periphery where the zinc had accumulated on top of the coating preventing detection. Both coated and uncoated electrodes had also accumulated aluminum on the surface. The steel coating contained small amounts of aluminum which are deposited and collect on the electrode surface. Aluminum has a zinc equivalence of approximately six, meaning that from an alloy formation perspective, a given concentration of aluminum is as detrimental as six times that concentration of zinc [45]. Iron from the steel had also been transferred to the electrode surfaces. Copper from the base material was also seen on the electrode surfaces.

After cross sectioning, the progression of zinc into the electrode could be tracked by EDS line scans. Figure 5.4 shows the elemental line scan traces through the surface layers of the coated and uncoated electrodes at 100 welds. The uncoated electrode line scan in Figure 5.4a showed the penetration of Zn into the electrode which formed an alloy layer to a maximum depth of approximately 10μm. The coated electrode line scan shown in Figure 5.4b displays the titanium rich surface coating and the slight mixing of copper in this layer. The TiC coating interface with the electrode material was clearly seen as the sharp drop in Ti content and rise in Cu. The zinc trace was also seen to penetrate 10μm into the coating, however at much lower intensity and far from the copper base material. With the coating intact and continuous, the interaction of zinc and copper was prevented by the coating which acted as a diffusion barrier.

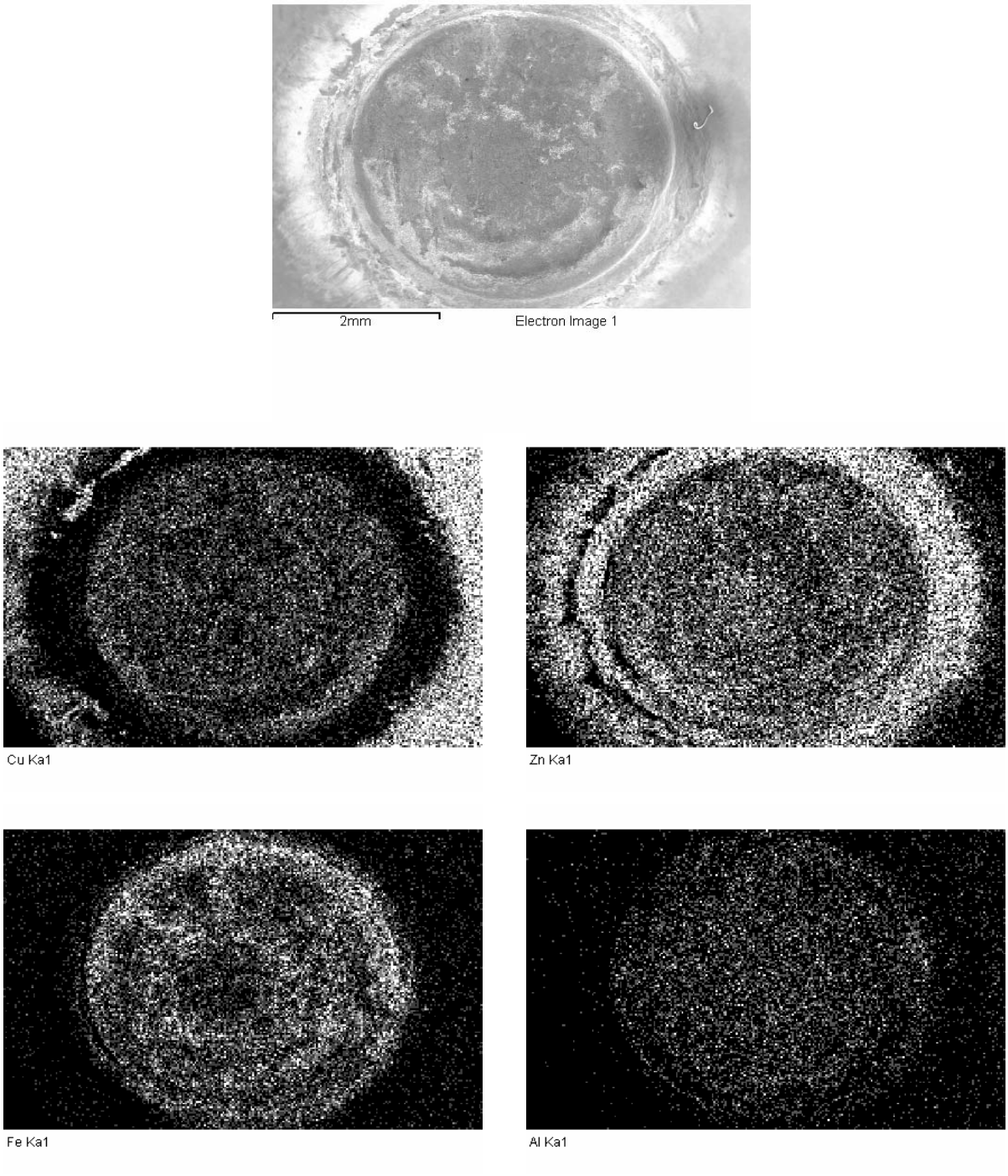

Figure 5.2: SEM image and EDS elemental mapping of uncoated electrode surface at 100 welds.

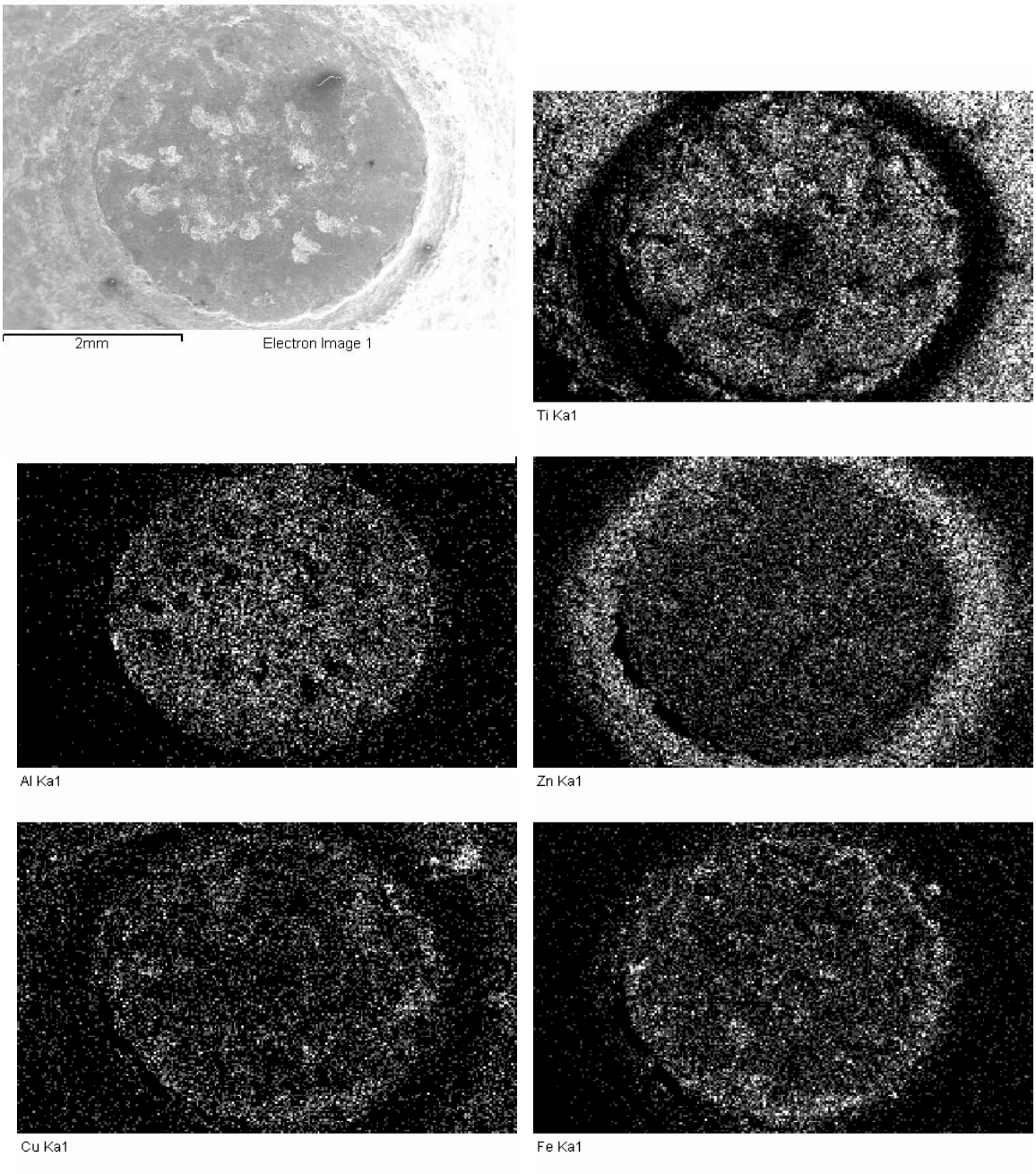

Figure 5.3: SEM image and EDS elemental mapping of coated electrode surface at 100 welds.

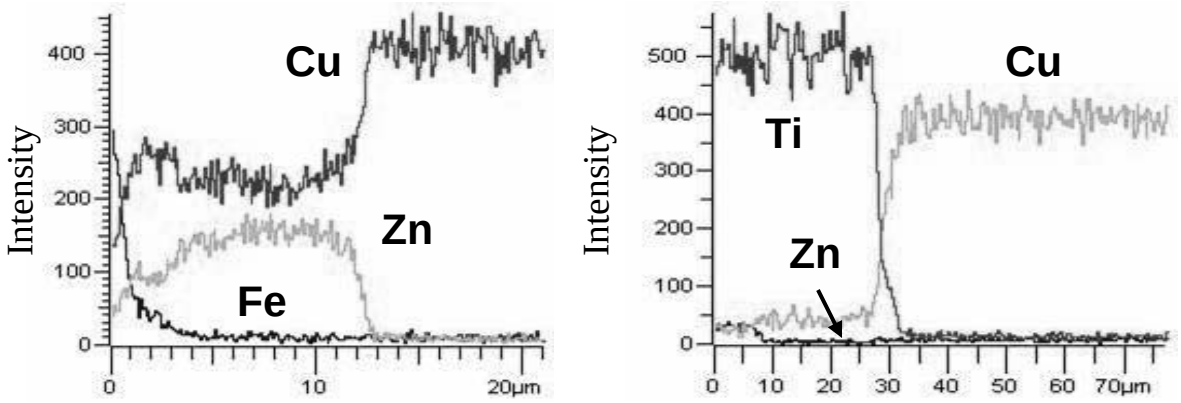

Figure 5.4: EDS elemental line scans of electrode surface at 100 welds. Line scans taken parallel to electrode axis. a) uncoated b) coated

The evolution of the alloy layers was tracked at four stages of the electrode campaign. Very early in the life, at only 24 welds, both coated and uncoated electrodes were cross sectioned and observed under SEM. Figure 5.5a showed the uncoated electrode with a thin alloy layer continuous along the surface. This alloy layer was suspected to be the beta brass layer seen in literature. Figure 5.5b showed the coated electrode with no alloy layer detected on the surface or underneath the coating.

a)

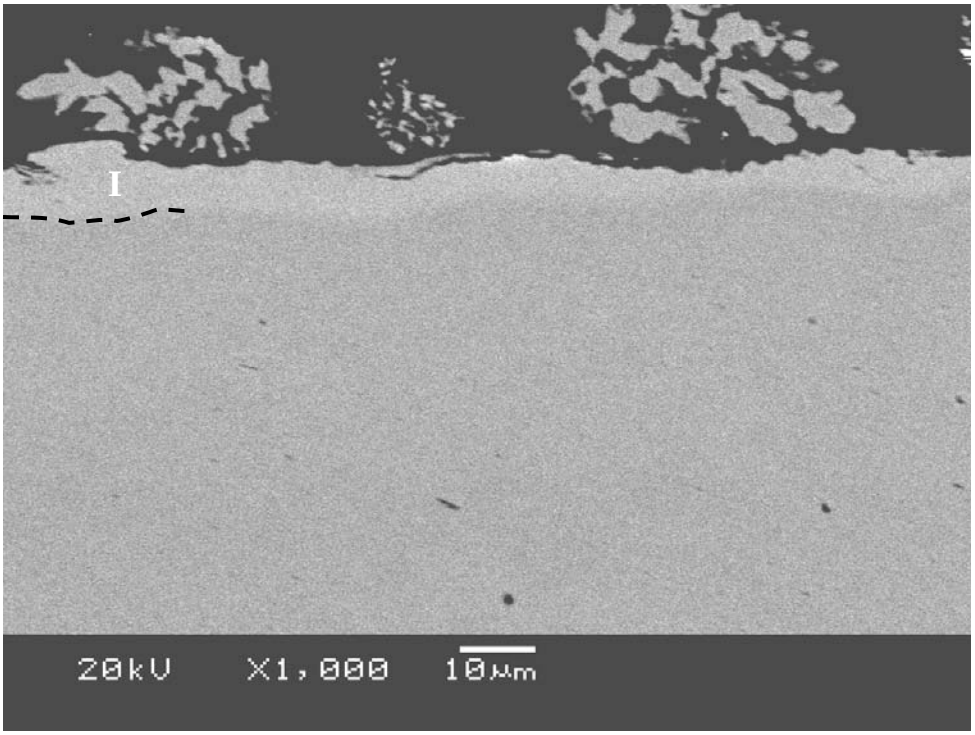

b)

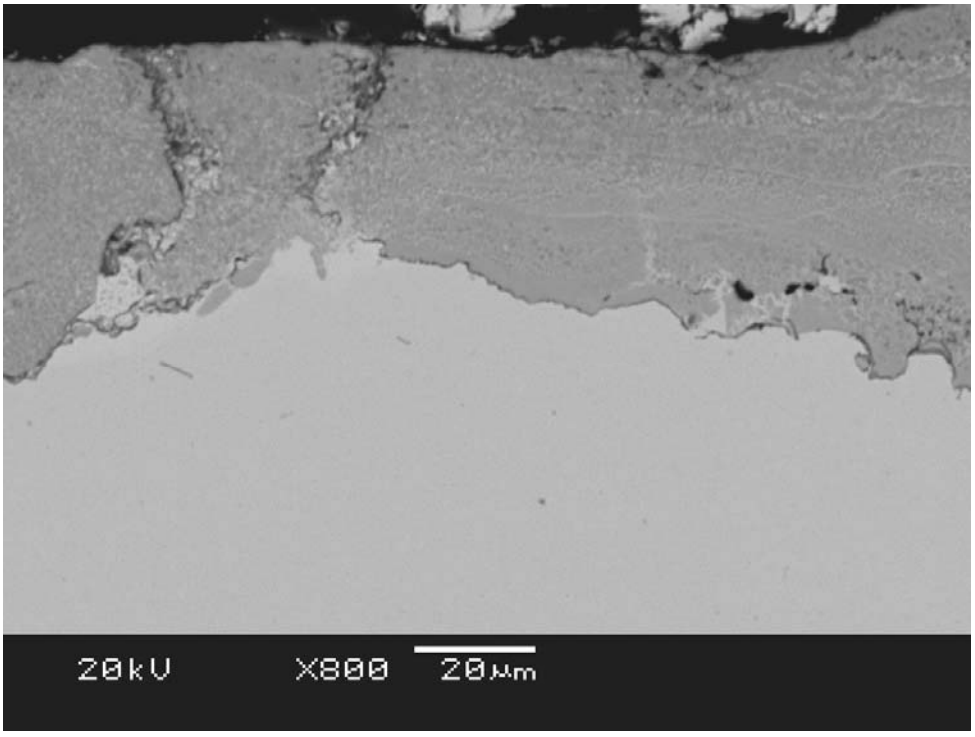

Figure 5.5: Electrode surface cross section micrographs. 24 welds. a) uncoated, dotted line shows alloy interface, b) coated.

At 100 welds, the uncoated electrode had developed a thicker multi-phase alloy layer as shown in Figure 5.6a. Using SEM backscatter imagery, the alloy layers were easily distinguished in the high magnification image and were seen to consist of four separate layers on top of the base material. At this stage, the uncoated electrode surface had reached the fully developed alloy formations as seen by Parker et al.[5]. Corresponding to alloy formations seen in literature the layers have been labelled I, II, III, IV, and V corresponding to copper, beta brass, gamma brass, outer mixed layer and zinc. The coated electrode at the same number of welds in Figure 5.6b had not yet formed a continuous alloy layer. The TiC coating at this stage was still intact; however some areas showed reduced thickness and minor damage.

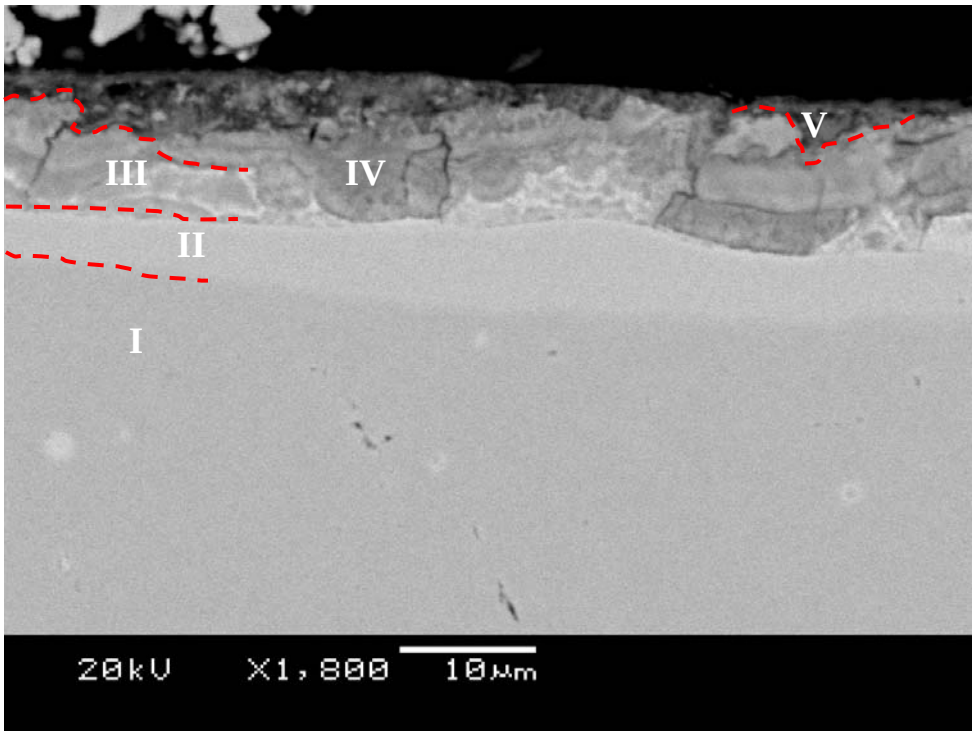

a)

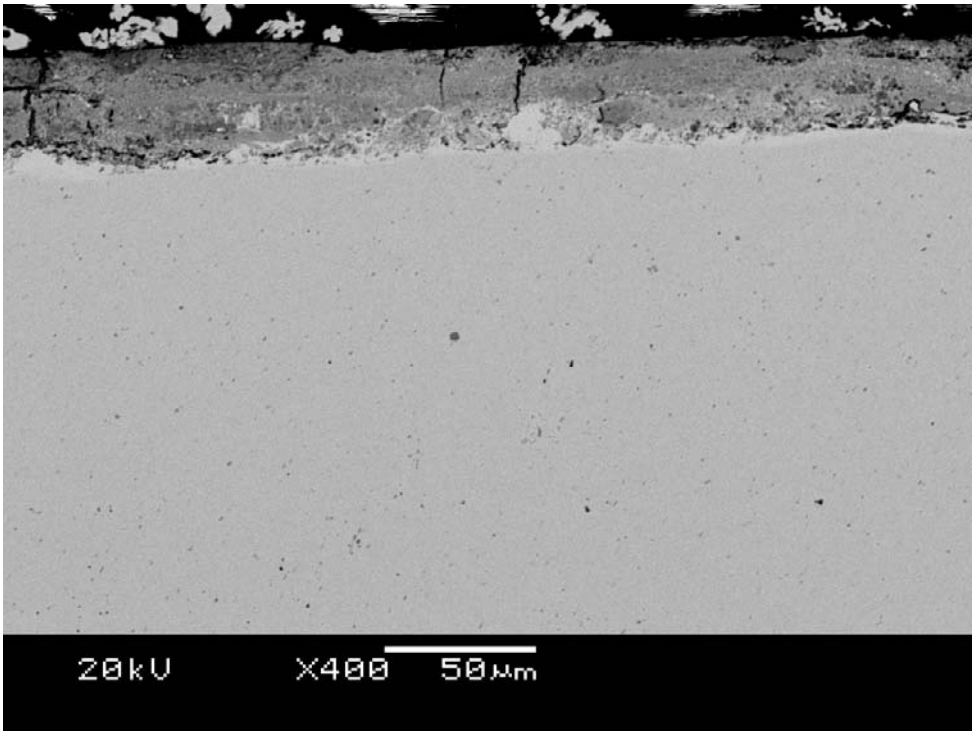

b)

Figure 5.6: Electrode surface cross section micrographs. 100 welds. a) uncoated electrode showing complex alloy layers on surface. b) coated electrode showing thin alloy layer under coating.

At 400 welds, the uncoated surface in Figure 5.7a showed fewer alloy layers than the 100 weld case. The depth of zinc penetration into the base material was approximately 16 micrometers, very similar to the 100 weld case. The many layers seen in the 100 weld image were evidently removed by the sticking and stripping mechanism leaving a thicker β brass layer behind labelled I on the figure, with some gamma brass and thin regions of zinc. At this stage, the uncoated electrode was very close to failure. The tip growth that had occurred reduced current density and local heating at the electrode interface which slowed the progression of zinc into the copper base material.

The TiC coating at this stage was broken and discontinuous. Alloy layers had formed underneath the coating which caused the coating to be lost in many areas. Continuous alloy layers were now seen in the SEM backscatter image in Figure 5.7b. Two separate brass layers believed to be beta and gamma brass were shown to exist in areas underneath the remaining coating. The area on the left of the image had experienced damage to the coating which allowed zinc (labelled V) to flow beneath the coating. To the right of the image, intact sections of the TiC coating (labelled MMC) could be seen above the alloy layers, which served to protect the alloy layers from becoming deposited to the steel sheet. In large areas without the TiC coating, the alloy layers and copper base material were exposed as an uncoated electrode.

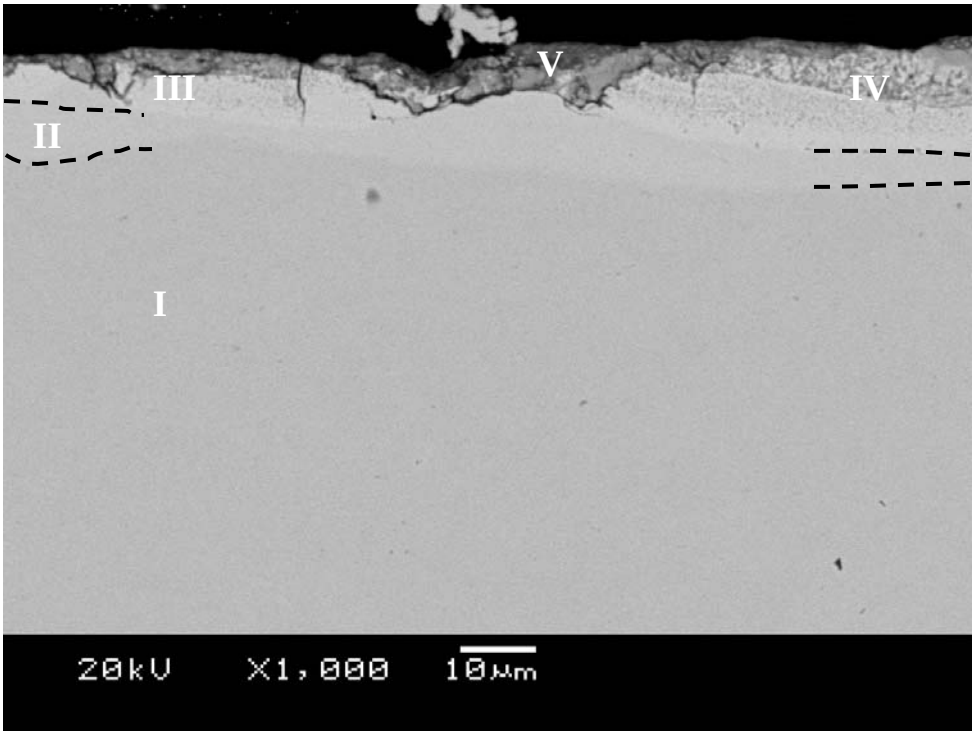

a)

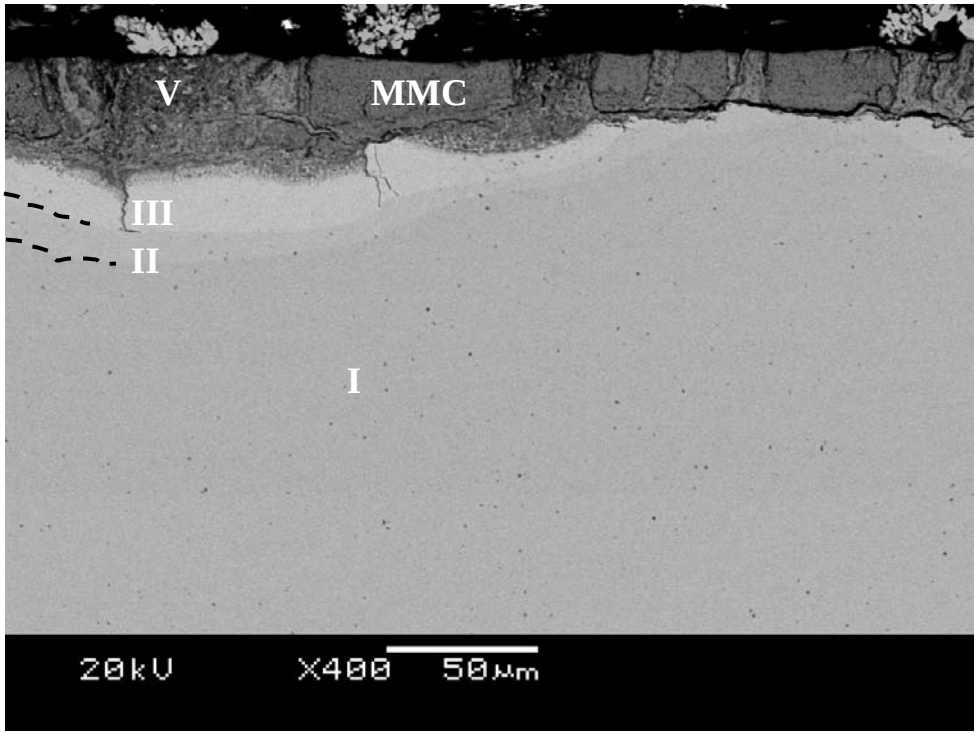

b)

Figure 5.7: Electrode surface cross section micrographs. 400 welds. a) uncoated, showing alloy layers. b) coated, showing dual alloy layer beneath the coating. The TiC coating is not continuous throughout the electrode surface.

At the end of life condition, the uncoated electrode was very similar to that of the 400 weld case. Figure 5.8a shows the cross-sectioned electrode after failure had occurred. Thin alloy layers were seen with a layer of zinc on the surface of the contact face. The coated electrode surface at end of life was very similar to the uncoated electrode. The TiC coating had been almost completely removed from the electrode surface as shown in Figure 5.8b. The surface of the electrode was covered in zinc with copper-zinc alloy layers underneath. It is believed that some of the TiC remained underneath the zinc and alloy layers however were difficult to find with cross sectioning techniques.

Elemental mapping of the contact faces of the electrodes showed further similarities between the coated and uncoated electrodes. Figure 5.9 shows surface images and scans at end of life condition for both coated and uncoated electrodes. The surfaces were seen to be composed mainly of iron and zinc, with low amounts of copper present. The Ti was almost completely removed from the surface. Very few indications of Ti were seen on the surface at this point, however the few points may be indication that some of the coating had remained under the zinc and alloy layers. As the TiC coating was compromised and no longer able to act as an effective alloy barrier, the electrode became susceptible to degradation as an uncoated electrode and had ended its life campaign in the same state as the uncoated electrode.

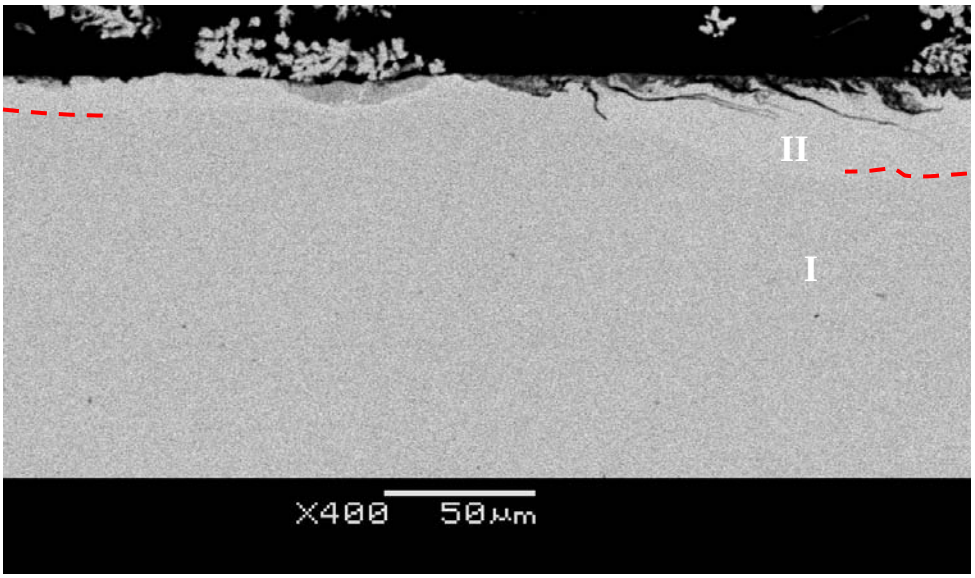

a)

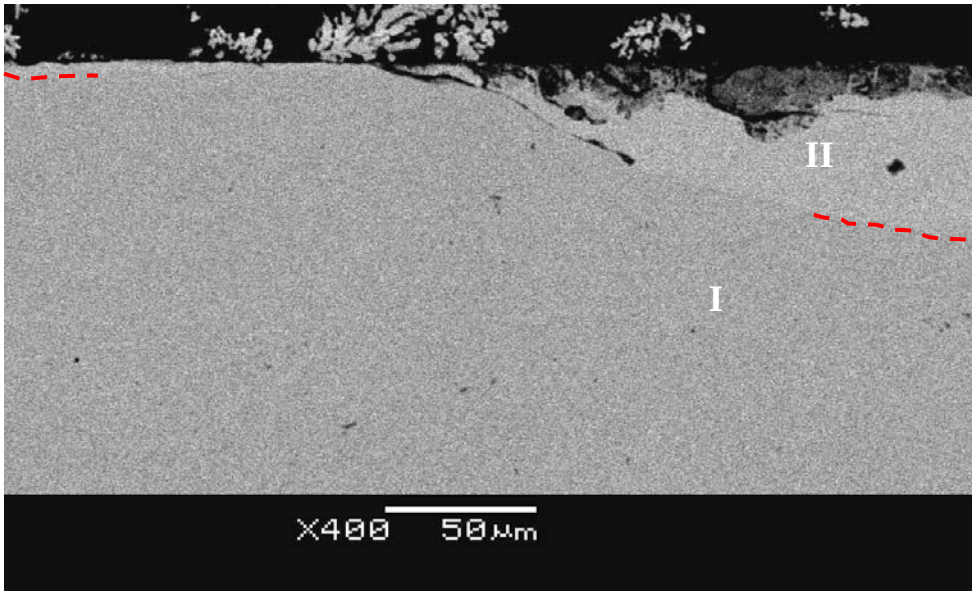

b)

Figure 5.8: Electrode surface cross section micrographs. End of life stage. a) uncoated, showing alloy layers. b) coated, showing continuous alloy layer and loss of coating along surface.

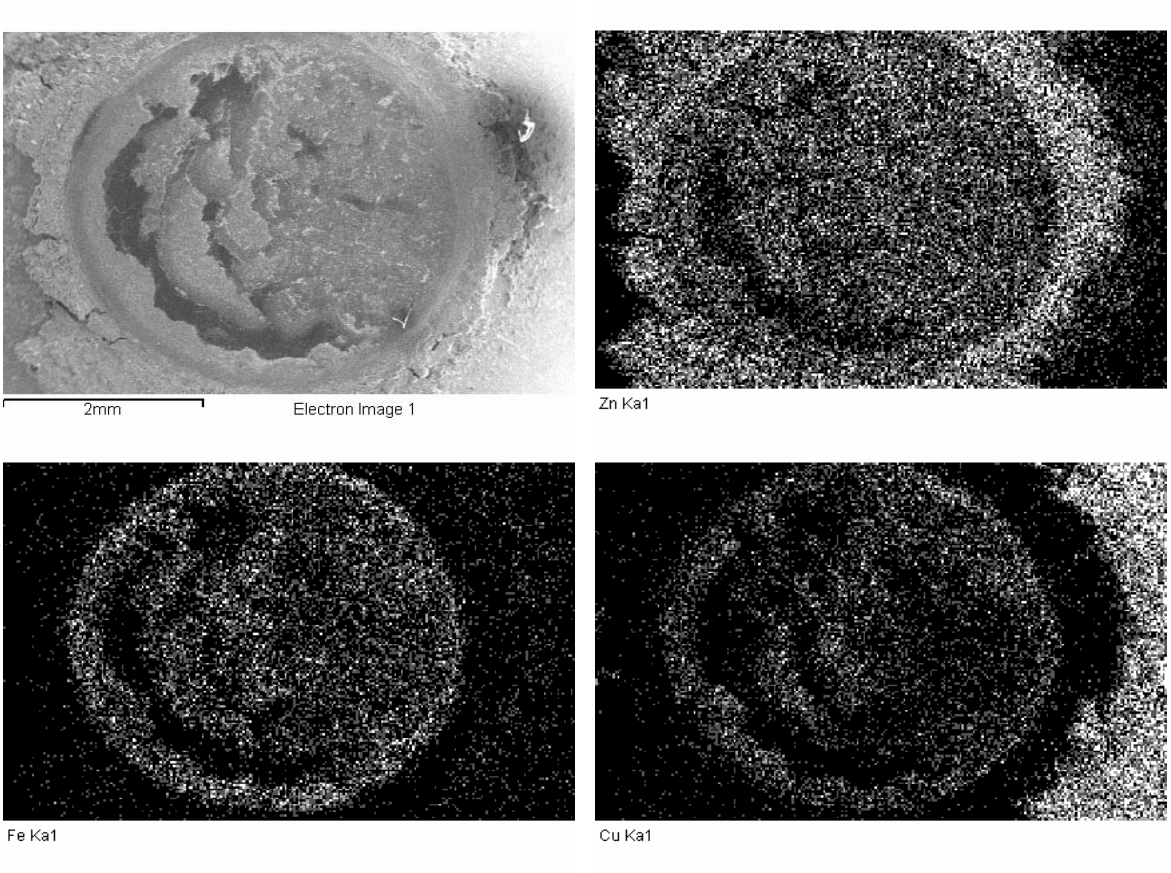

a)

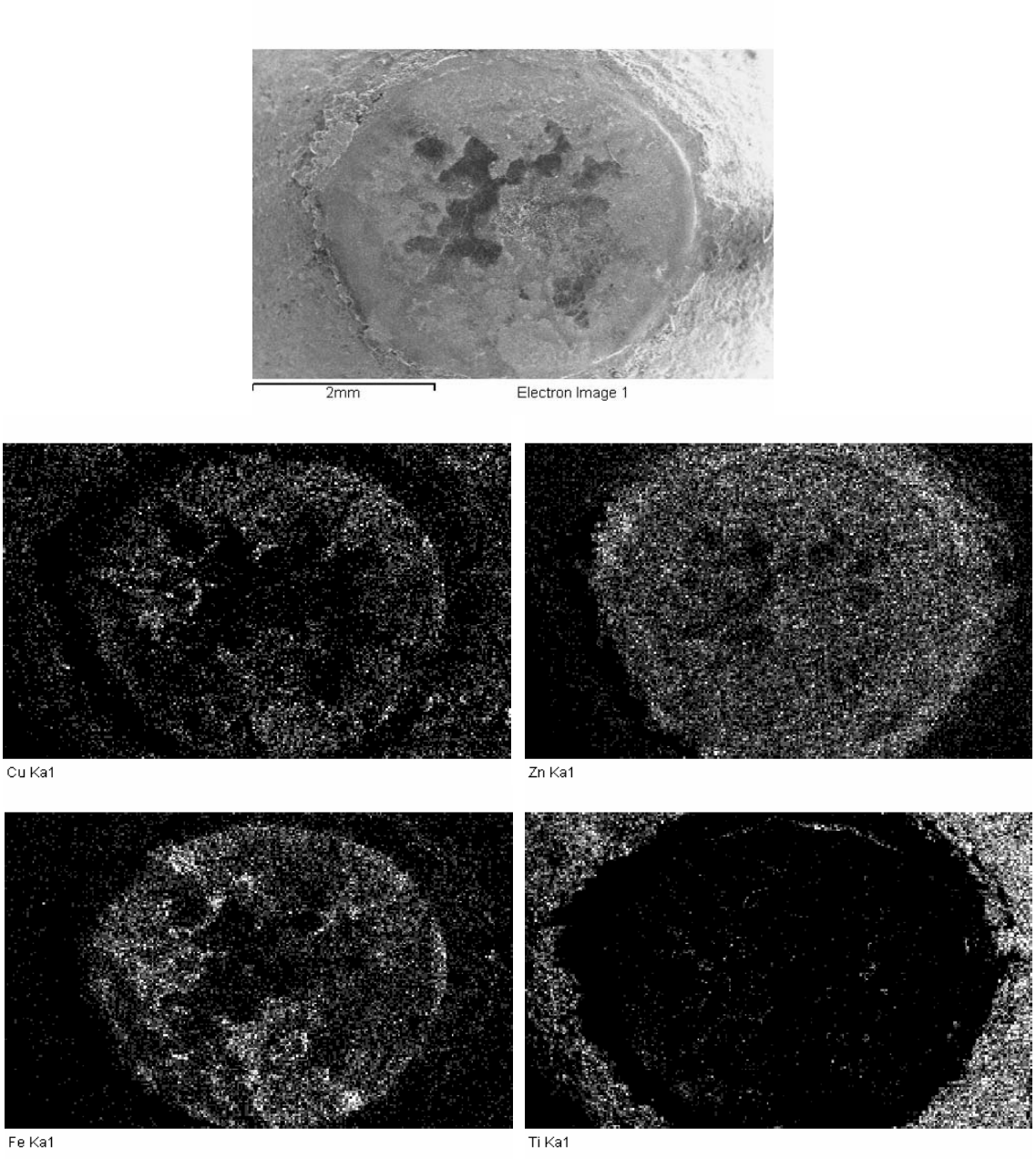

b)

Figure 5.9: SEM/EDS electrode surface images and scans at end of life condition. a) uncoated electrode. b) coated electrode.

5.1.2 Material Loss

As the effectiveness of the electrode coating to prevent the zinc from interacting with the copper electrode was diminished with degradation, alloying would eventually occur. However, the electrode would only become degraded if the alloy layers formed were allowed to be lost to the steel sheet. Uncoated electrodes have been seen to begin to deposit copper to the steel sheet on the very first weld. The combination of intimate contact between copper and zinc as well as the high temperatures in the early life of the electrode led to a high probability of alloy deposition. As shown above, the coated electrode developed alloy layers later in the electrode life and at that point, heating at the interface was less intense and less material transfer was observed. SEM/EDS analysis was used to scan the average amount of copper on the surface of the welds. Five consecutive welds from the tests were scanned for both coated and uncoated electrode trials and then averaged for each point in Figure 5.10. The uncoated electrode showed a high degree of alloy deposition, or brassing early in the electrode life followed by a steady decrease in the amount of copper deposited as welding continued until failure. The coated electrode showed a much smaller peak at 100 welds into the life. This may have been due to a local area of coating loss which exposed the copper underneath the coating. Copper deposition may also have been due to the small amounts of copper found in the coating matrix. Localized coating damage and coating removal could contribute to the copper deposits on the sheet surface. After this peak, the amount of copper dropped to a nominal level where it remained until failure of the electrode. This drop was due to the same reason as the uncoated electrode, the tip face had grown and heating at the electrode-sheet interface had been reduced as a consequence. With reduced heating, the amount of mass transfer which occurred at the interface was also reduced [6].

Due to the eventual penetration of zinc through coating defects to the base copper, the TiC coating was most effective in the early stages of the electrode life, where it was able to delay the formation of alloy layers. Later in the electrode life, after the alloy layers had formed underneath the coating, it was able to protect them from being lost to the sheet. This result clearly showed the coated electrode's ability to reduce tip growth by alloy formation and subsequent length reduction as seen in the slope of the tip growth curve of Figure 4.8.

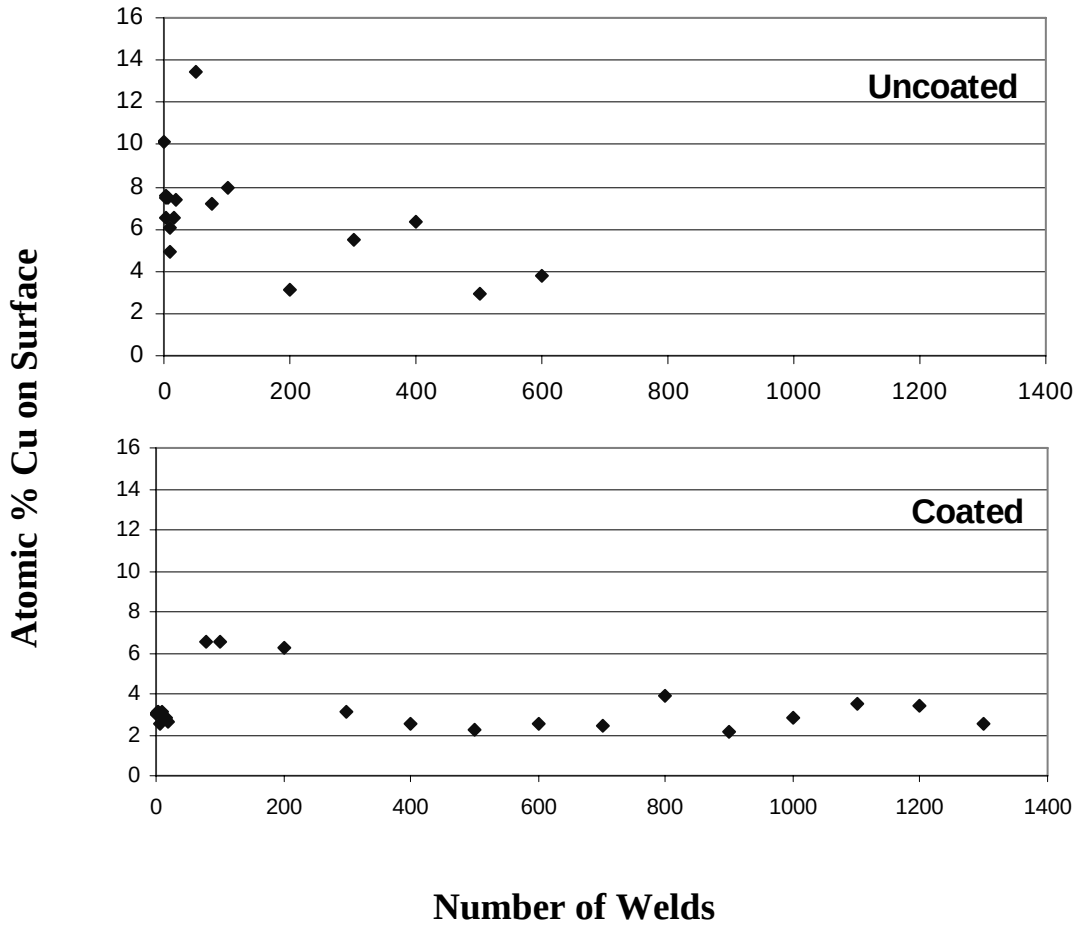

Figure 5.10: Amount of atomic copper deposited to the electrode surface at progressing welds. Top uncoated, bottom coated electrode.

5.2 Electrode Failure

As discussed previously, degradation of the electrodes is the loss of ability to perform its functions. Typical electrode degradation occurs when the tip diameter of the electrode grows too large to convey adequate current density to the workpiece. The cause of failure of the coated electrode was explored in this section with the mechanisms of degradation in the following section.

5.2.1 Tip Growth and Current Density

To gauge the degradation behaviour of the coated and uncoated electrodes, typical button size was plotted against the tip growth in Figure 5.11. Up to a tip growth of 0.7mm in diameter, both electrodes behaved similarly, with a steady decrease in button size as tip diameter and hence current density decreased. After 0.7mm of tip diameter growth, the uncoated electrode was no longer making satisfactory nuggets. The coated electrode was able to make satisfactory nuggets after 0.7mm of tip growth and continued to 0.9mm of tip growth where failure occurred. This increase was believed to be due to the increased weldability of the coated electrode. The button size appeared to be a function of the electrode tip diameter for both coated and uncoated electrodes. Besides the slight increase in tip diameter increase seen with the coated electrodes, the behaviour was similar for both electrode types.

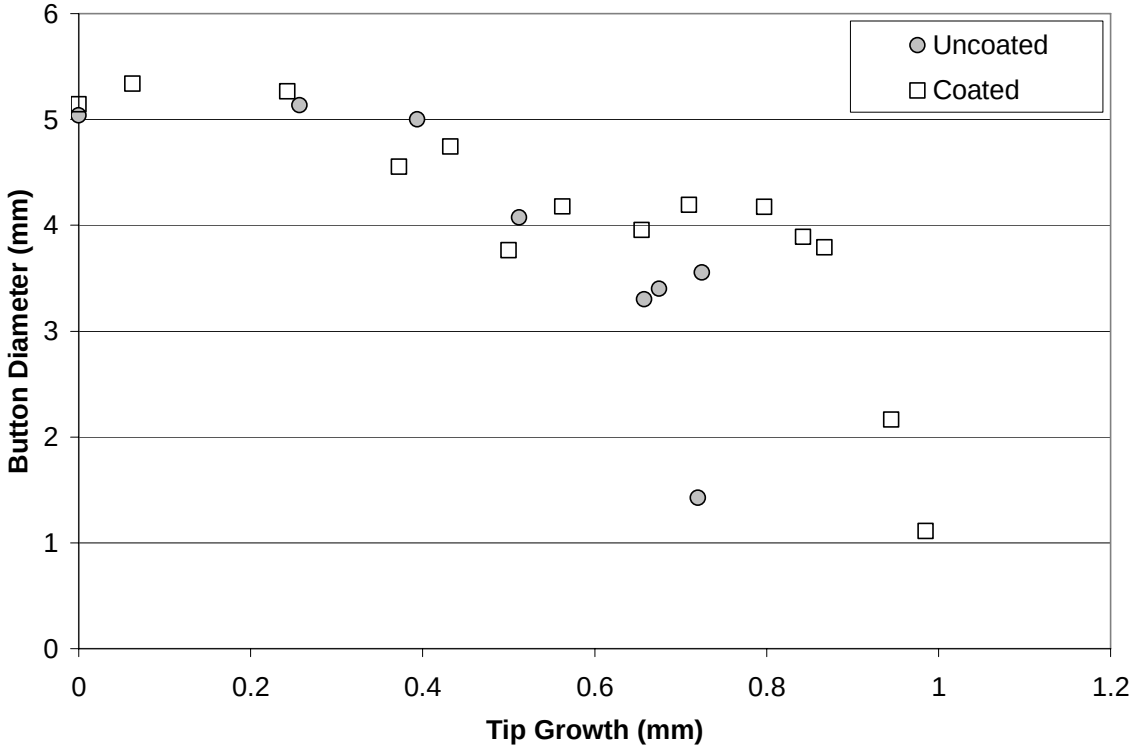

Figure 5.11: Button size vs. tip growth for both uncoated and coated electrodes

Estimating current density based on the nominal weld current and measured tip face diameters, Figure 5.12 plots the calculated current density versus button size. At the beginning of life, the current density was at its highest on the plot, as welding progressed,

the electrode contact face grew and the current density dropped due to the increase in area without an increase in current. The coated electrodes were able to achieve the same button sizes at a lower current density, again, consistent with the previous results. This also helped to explain the coated electrode's ability to form welds at a larger tip growth, as lower current densities were needed.

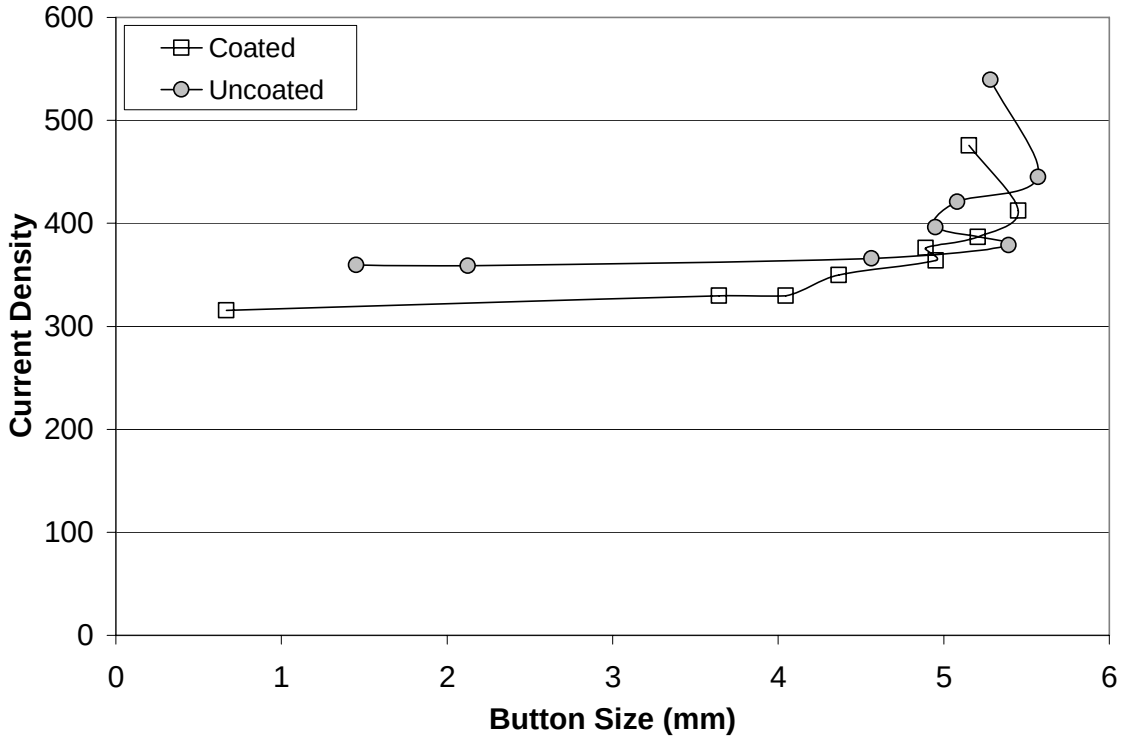

Figure 5.12: Calculated current density vs. button size for both uncoated and coated electrodes

The initial drop of approximately 100A/mm^2 did not seem to affect the button size of either electrode drastically. At the beginning of the electrode life campaign, the electrodes were forming welds that were larger than the tip diameters. This is possible to the point where the weld force is no longer able to contain the molten weld nugget and expulsion occurs. The slight increase in button size with a drop in the current density was due to the slight increase in tip diameter allowing for a larger nugget to be formed before the onset of expulsion.

As the calculated current density dropped below 400A/mm^2, the uncoated electrode behaviour became very unstable. In the range of 350 to 400A/mm^2, button diameters

were found in the range of 5.4 to 1.5mm. This large variation in button size indicated the onset of the end of life of the electrode. The coated electrode showed a steady decrease in current density and a more stable button size until approximately 345A/mm^2 where the process became out of control and end of life occurred.

In the previous chapter, the increased resistance of the coated electrode was shown to slightly increase the heat input and served to act as a thermal barrier to facilitate larger welds. At the end of life, the static resistance of the uncoated electrodes was very similar to that of the unused state. The coated electrode resistance was reduced somewhat approaching that of the uncoated electrodes. Table 5.1 showed the resistances of the uncoated and coated electrodes at the end of life. As the condition of the TiC coating was severely compromised at the end of life stage, it was logical to observe the resistances of both uncoated and coated electrodes approach the same value at this stage. The overall magnitude of the circuit resistances suggested that alloying and degradation of the contact face had little effect on the static resistance.

Table 5.1: Electrode Static Resistance at End of Life

Static Resistance (micro ohm)			
	Electrode Only	One Sheet	Two Sheets
Uncoated Electrodes	13.8 ±0.8	20.8 ±0.7	34.7 ±1.1
Coated Electrodes	18.4 ±0.5	26.9 ±0.8	35.1 ±1.3

The mechanism of failure for both electrodes remained to be the development of alloy products on the surface and the resultant tip erosion leading to area growth which caused a drop in current density. The coated electrode was able to withstand a larger tip growth before failure and weld at a lower current density. The ability to extend electrode life as seen thus far stemmed from the evolution of the alloy layers and the material interaction involved causing length reduction. The following study was conducted to determine what factors contributed to the growth of the electrode tip.

5.2.2 Length Reduction and Mass Loss Correlation

Interactions between the steel coating and electrode surface led to erosion of the tip face and material loss. The presence of low melting point alloys at the electrode-work interface led to electrode sticking and net loss of material which caused the electrode to decrease in length. The amount of mass lost to the workpiece could be directly correlated to the length reduction through the density of the material and the volume change experienced by the electrode. Volume loss was predicted by the length reduction and the geometry of the electrode given in Equation 5.1 for the volume of a spherical zone [53].

$$V = \frac{1}{6}\pi h\left[3\left(\frac{D1}{2}\right)^2 + 3\left(\frac{D2}{2}\right)^2 + h^2\right] \qquad (5.1)$$

where, D2 is the final tip diameter

D1 is the initial tip diameter

h is the length reduction

Using the length reductions given in Figure 4.9, and the initial and final tip diameters of the life trails, the predicted volume loss was calculated and multiplied by the approximate density of the copper base alloy to predict mass loss. Electrode mass was measured before and after life test trials. During welding, zinc flash was found to have accumulated around the periphery of the electrode adding mass. This flash was not removed during welding to mimic industrial conditions, however was removed at the end of life to facilitate a more accurate mass measurement. Table 5.2 shows the change in mass as measured by the scale as well as the calculated value derived from the length decrease. The coated electrode mass loss matched reasonably with the predicted value. The density of the electrode coating was found to be 6.05mg/mm^3, slightly less dense than the copper at 8.93mg/mm^3[52]. This was close enough to assume that any coating material loss would result in the same mass and length reduction relationship. The close match between predicted and measured mass changes suggested that length reduction of the coated electrode was primarily due to net loss of material from the electrode surface. This result supported the results of the previous chapter in that the electrode coating acted as a diffusion barrier to slow the alloying of the material in turn caused the reduction in material transfer rates and hence length reduction which caused the electrode tip to grow and loss of function to occur.

Table 5.2: Electrode Mass Change

	Coated	Uncoated
Measured Mass Change (g)	-0.0188	-0.0155
Predicted Mass Change (g)	-0.0175	-0.0243

The uncoated electrode had a net change in mass that was less than the predicted value. The undermatching of mass loss could stem from two factors: length reduction of the uncoated electrode was caused by more than material loss alone, or the zinc pickup around the contact face offset the mass loss by increasing the mass of the electrode. Length reduction could also be caused by deformation of the material at the contact face, however observations in Section 4.2.4 do not support the scale of deformation required to have caused length reductions that would cause false predictions of mass transfer. Deformation processes would also cause an associated tip growth. To determine the degree to which deformation has an influence on the length reduction behaviour of both types of electrodes, the length reduction and tip growth relationship was studied.

5.2.3 Length Reduction and Tip Growth Correlation

From the geometric relation schematically shown previously in Figure 2.11, the approximate tip diameter can be calculated based on length reduction alone. The predicted tip diameter could be found using Equation 5.2 shown below [53]. This would yield a predicted tip growth rate according to length data measured and can be compared to the actual tip diameter growth rate. Figure 5.13 plots the predicted tip growth versus the number of welds for both coated and uncoated electrodes using length loss data from Figure 4.8.

$$D' = 2 * \sqrt{R^2 - (\sqrt{R^2 - \left(\frac{D1}{2}\right)^2} - h)^2} \qquad (5.2)$$

where, D' is the predicted tip diameter

R is the radius of curvature of the dome

D1 is the initial tip diameter

h is the length reduction

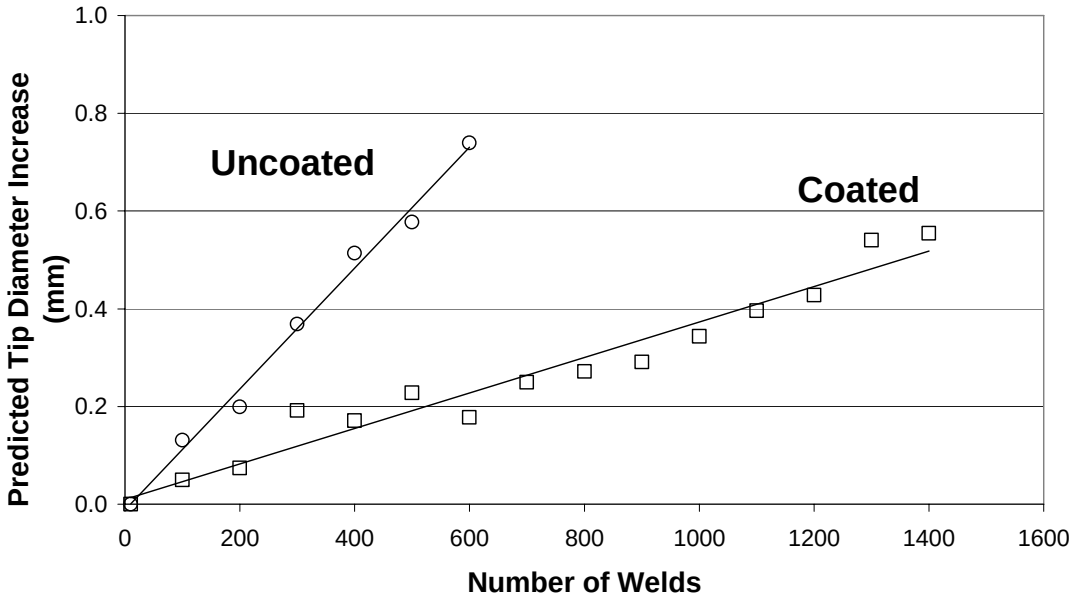

Figure 5.13: Predicted tip growth curves from length reduction measurements

The predicted tip growth rates were approximately *0.12mm/100 welds* for the uncoated electrode while the coated electrode should exhibit a rate of *0.04mm/100 welds* on this basis. Compared to the rates reported for tip growth in Section 4.2.2 (0.13*mm/100* for uncoated and 0.08*mm/100* for coated), the predicted rate for the uncoated electrode matched well. This suggested that the tip growth of the uncoated electrode was due to length reduction and geometric growth alone. If the length reduction accounted for the tip growth, it follows that deformation was not a factor in the tip growth of the electrode. The unmatched mass loss prediction has evidently been due to zinc pickup processes as shown in Figure 5.9 illustrating the pickup of zinc around the periphery of the uncoated electrode, while very little appears on the coated electrode.

The predicted growth rate of the coated electrode tip diameter based on length loss was half of the measured rate. This discrepancy was indication that a process other than geometric growth was involved in the tip growth and failure of the electrode. The matched prediction of the mass loss to actual mass loss in the previous section suggested that the mechanism of tip growth did not contribute significantly to the length reduction of the electrode. As macro-deformation of the electrode tip was not seen, there must have been another mechanism which led to the growth of the electrode tip.

5.3 Coated Electrode Tip Growth Mechanism

The previous section has shown that the failure of the coated electrode was due to processes other than net mass loss leading to length reduction and geometric tip face growth or macro-deformation of the tip face. The presence of the TiC coating on the surface of the electrode was not consistent throughout the life campaign of the electrode. To understand the mechanism in which the electrode failed, the means by which the TiC coating was degraded was investigated.

5.3.1 TiC Coating Loss

The condition of the coating was monitored during the life and analysed to observe how it was affected by the repeated welding cycles. In the as-coated condition, the TiC coating had very many surface defects. Figure 5.14 shows some examples of these defects. Cracks, pits and unfused layers were present allowing molten zinc to penetrate. These inherent defects in the coating provided an initiation point for further defects to develop and compromise the coating.

The first weld was very important in the life of a coated electrode. If the coating was not well fused to the electrode, large areas of the coating could have been easily removed from the surface which exposed the base copper. Such a phenomenon was seen in Figure 5.15. Inspection of the coated electrode revealed an area where the coating was missing. That portion of the coating was found on the sheet steel surface, attached by a zinc braze that was stronger than the coating bond to the electrode. If such damage were to occur in the first weld or early in the life of the electrode, the capacity for the coating to act as a thermal and diffusion barrier would have been compromised and life would be short (similar to that of an uncoated electrode). Although problematic and detrimental to the life of the electrode, this phenomenon did not occur on a regular basis and was not typical of the electrodes tested.

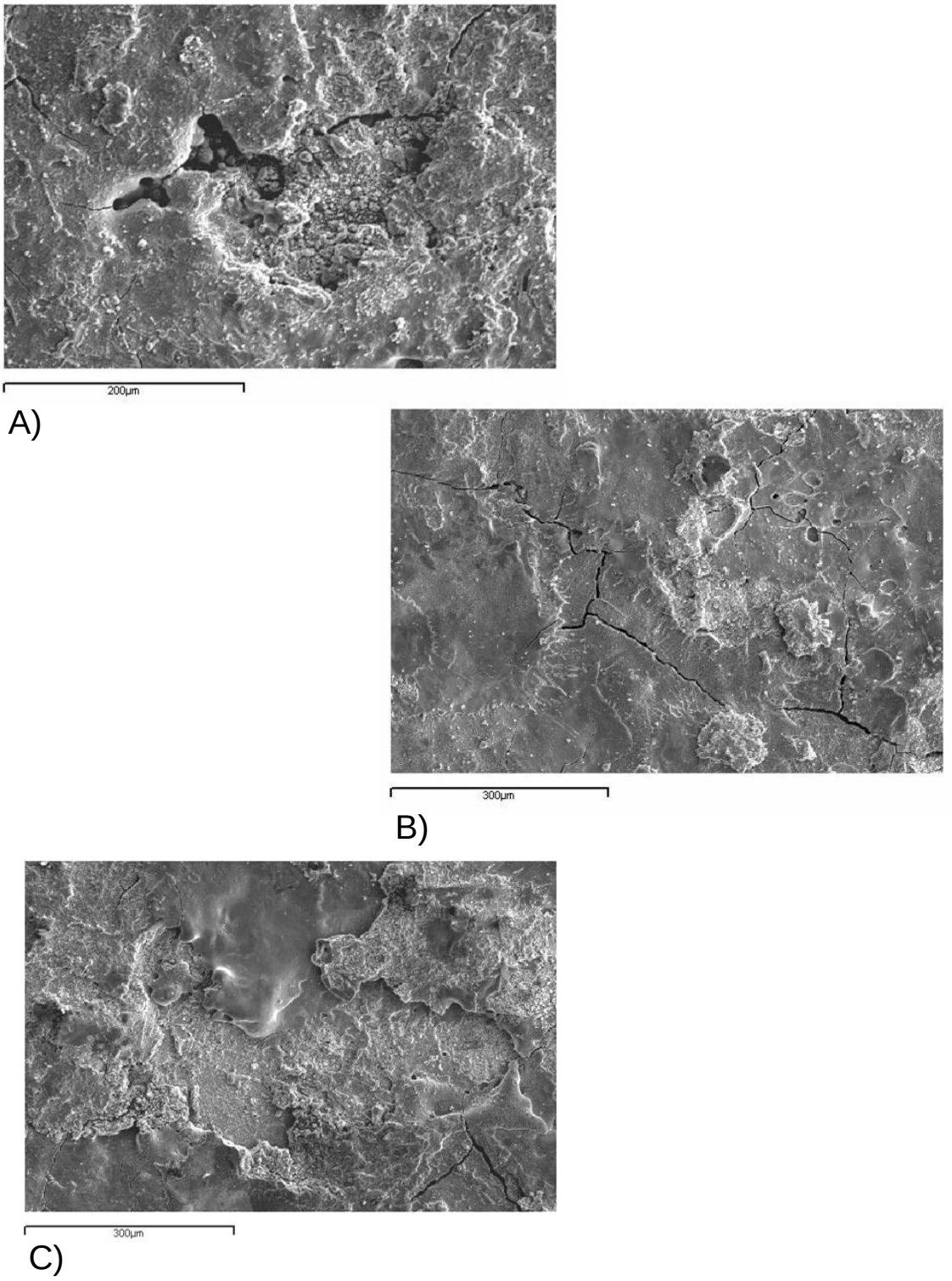

Figure 5.14: TiC coating defects. A) Pits/voids. B) Cracks. C) Delamination. 0 welds.

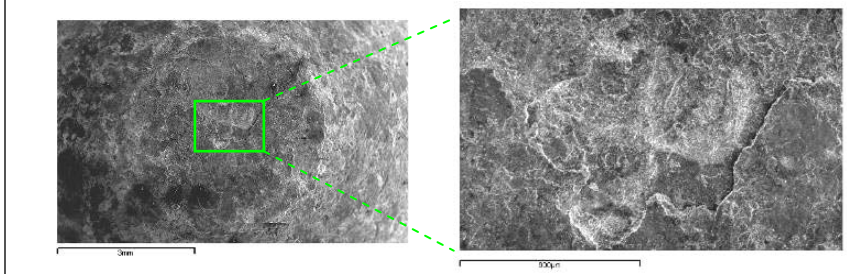

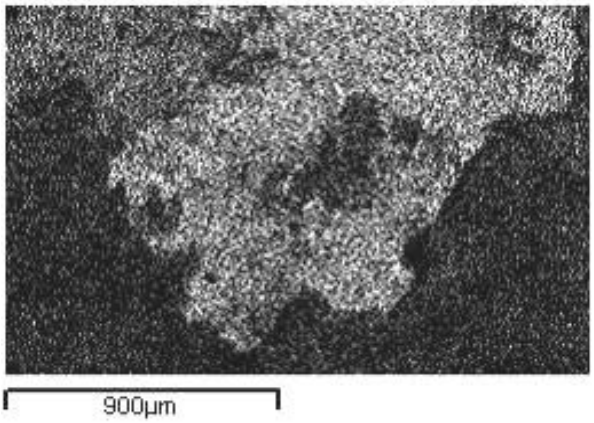

Cu

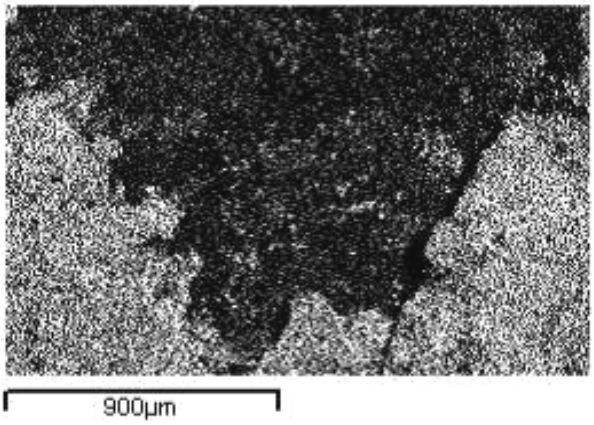

Ti

a)

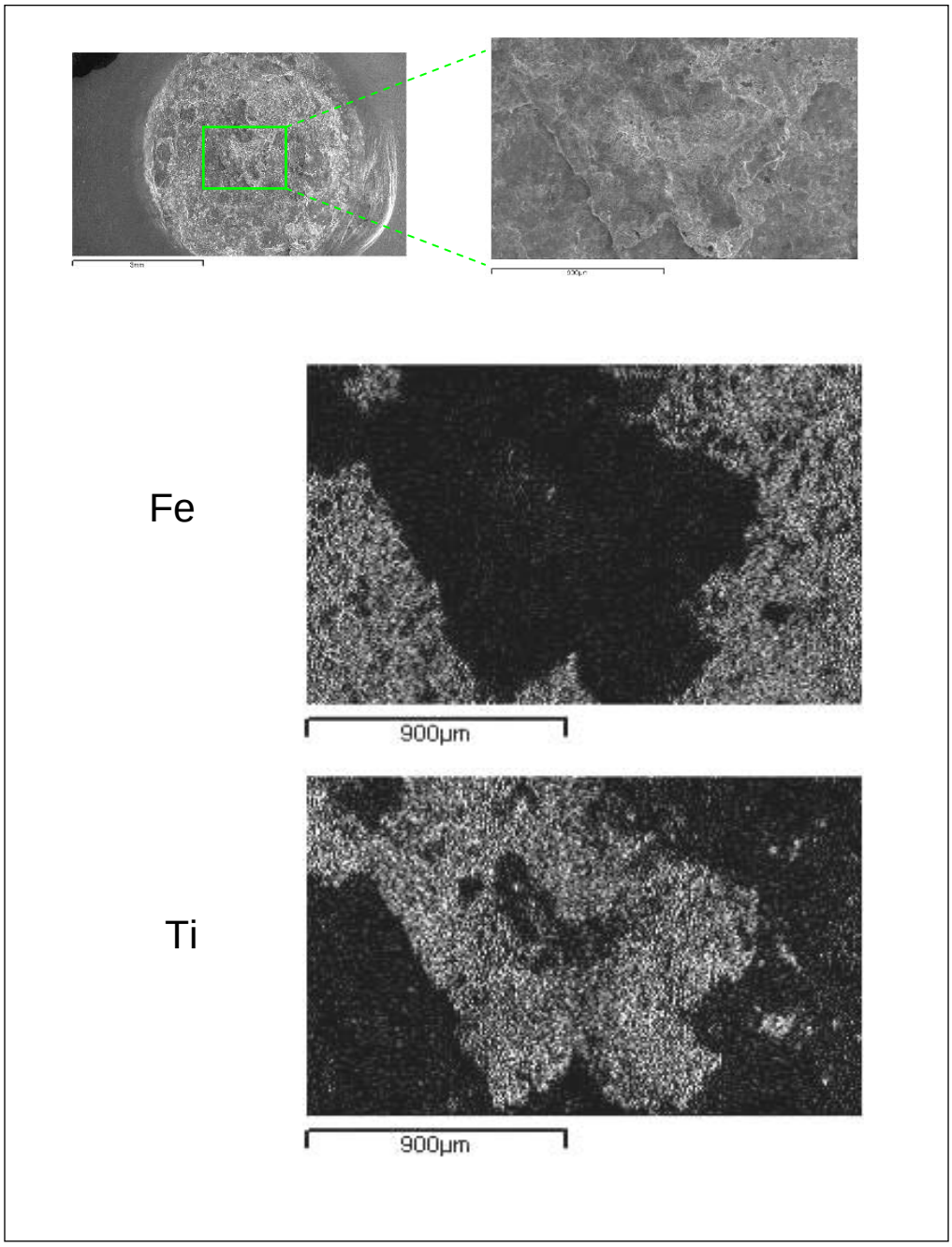

b)

Figure 5.15: TiC coating loss mechanism showing coating deposit on sheet steel surface. Image and elemental mapping of, a) coated electrode surface, b) sheet steel surface.

SEM/EDS were used to determine the amount of elemental Ti present on the surface of the electrode. Due to the low penetration depth of the EDS scan, Ti that may have been underneath alloy layers or zinc on the surface of the electrode was not detected. As seen in Figure 4.12 of Chapter 4, Ti was still found on the surface in abundance indicating the TiC coating was still intact and present at the surface after 100 welds. Figure 5.9 shows the coated electrode elemental mapping at the end of life condition. Titanium was no longer detected on the electrode surface, yet whether it had been lost to the steel sheet or was covered by a zinc and/or brass layer was not known. Several electrodes were scanned at intermediate life stages and the amount of elemental titanium varied from 9-36%. There was no way to determine if the next weld would have removed some alloy layers and revealed more Ti, or if the next weld would remove some of the coating by sticking and reduce the amount of Ti on the surface. Cross sections at the end of life revealed that most of the TiC coating had been removed and very little remained.

If the TiC were hidden under the surface, it may still have been able to function as a thermal barrier thereby preventing the electrode from failing. When the TiC coating fails to function as a thermal barrier, the electrode will function thermally as an uncoated electrode. The ability of the coating to function as a diffusion and alloy barrier was slowly diminished due to damage to the coating and penetration of the zinc to the base copper.

At 24 welds, the electrode coating was still intact, and little zinc had accumulated on the surface as seen in Figure 5.16. Closer inspection of this electrode in Figure 5.17 showed deep cracks in the coating where zinc was able to penetrate. In these damaged areas of the coating, zinc was able to penetrate and interact with the copper as shown in Figure 5.18. The zinc appeared to diffuse easily along the coating/electrode interface, slowly interacting with the copper beneath the coating. This would eventually have led to a layer of brass alloy underneath the coating.

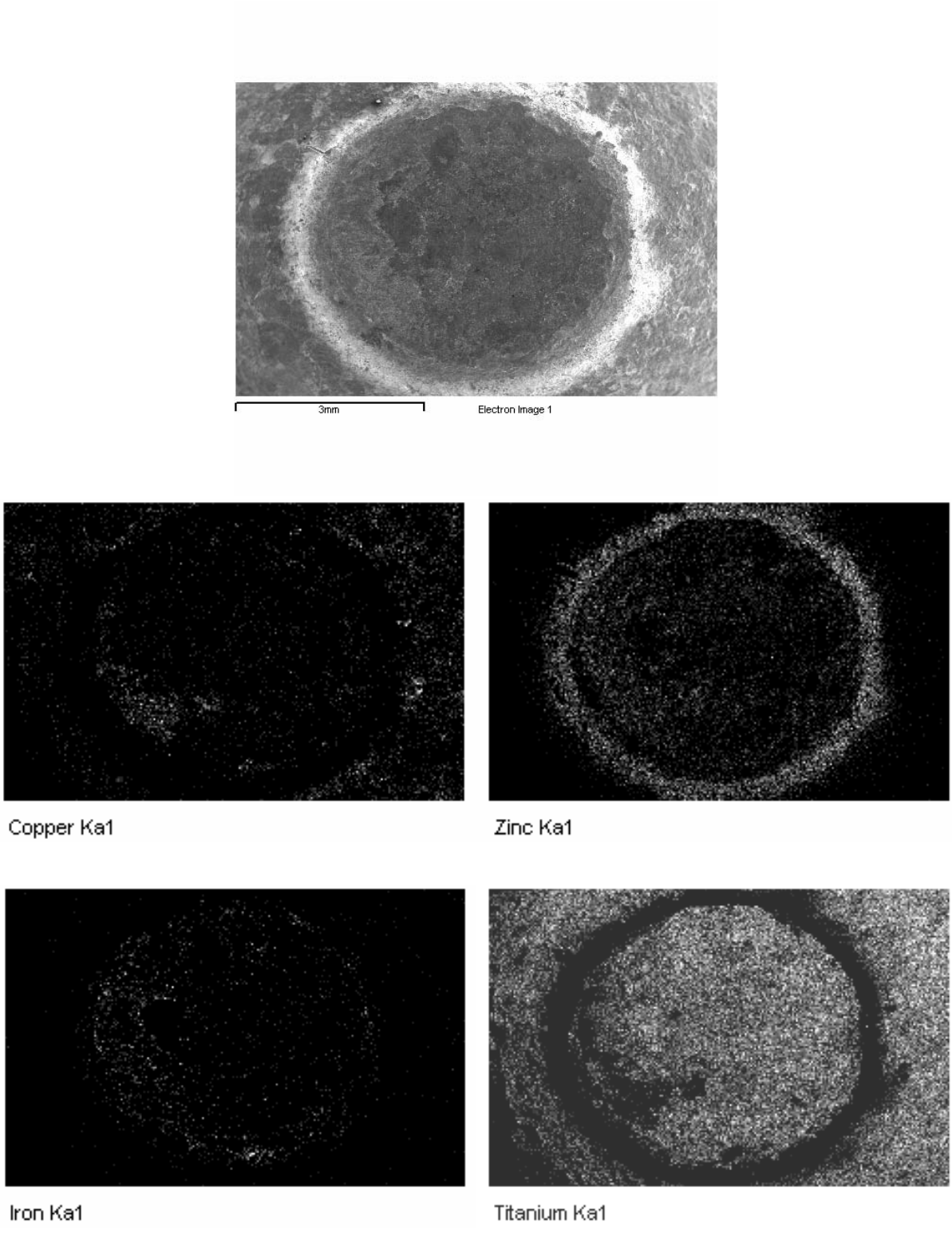

Figure 5.16: Coated electrode surface at 24 welds. SEM image and EDS elemental mapping.

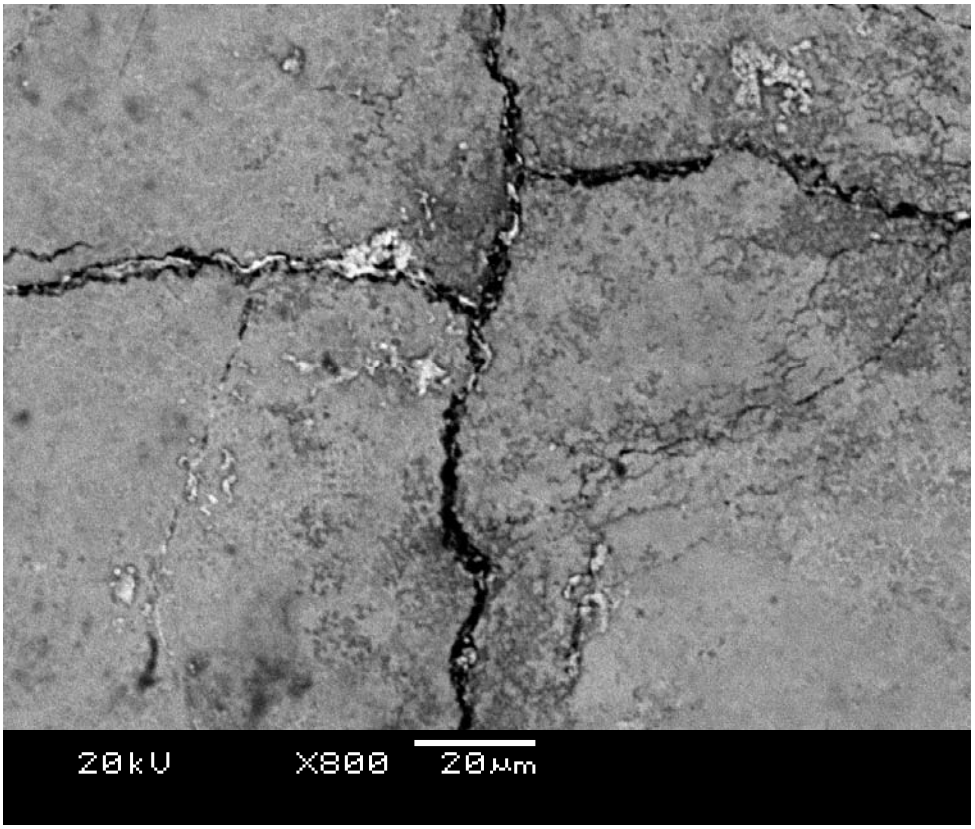

Figure 5.17: Coated electrode surface at 24 welds showing fissure cracks.

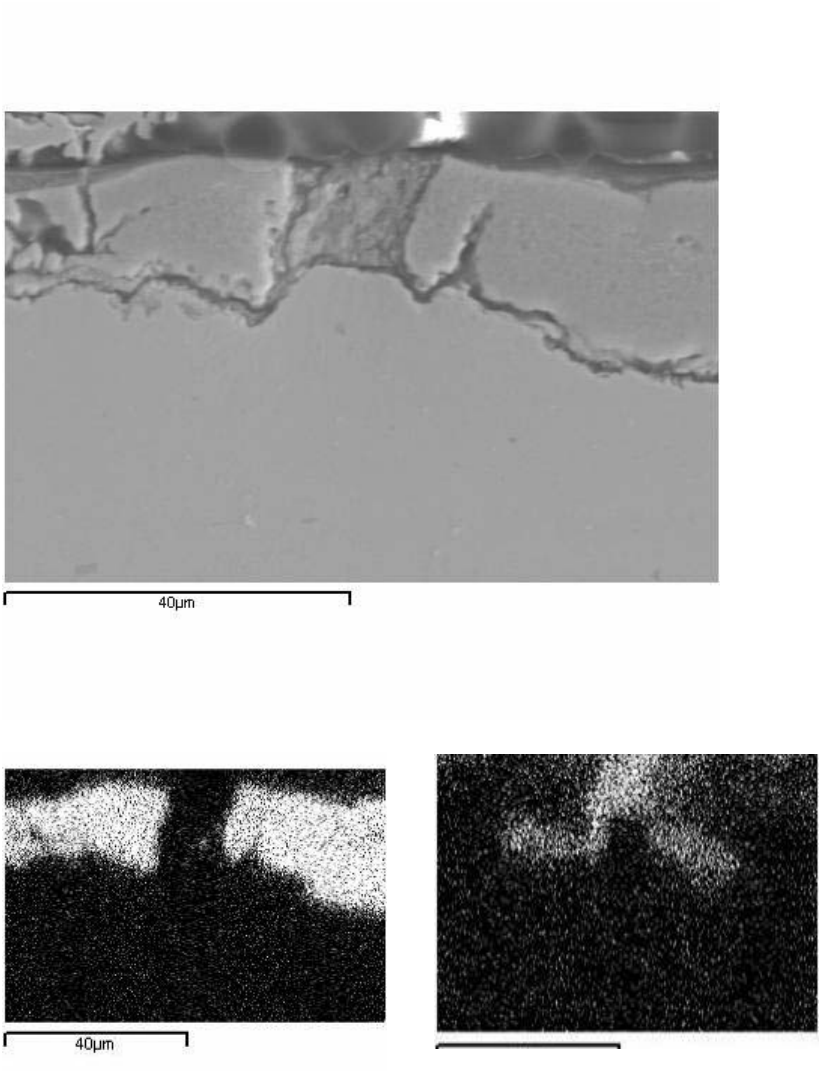

Figure 5.18: SEM image and EDS elemental mapping of coating damage area showing zinc penetration and migration along coating/electrode interface. 200 welds.

Inspection of the coated electrode surface after 250 welds revealed a highly fractured coating surface. Figure 5.19 shows the SEM image with EDS mappings. The coating had broken into islands with the fissures between them filled in with zinc. Soft alloy layers had formed underneath the hard TiC coating due to the zinc penetration and diffusion mentioned above. With repeated application of high welding forces on the TiC

coating while on top of a softer alloy layer, the coating was believed to fragment and extrude the alloy layer around the fragments and to the surface leaving the TiC particles embedded in the electrode.

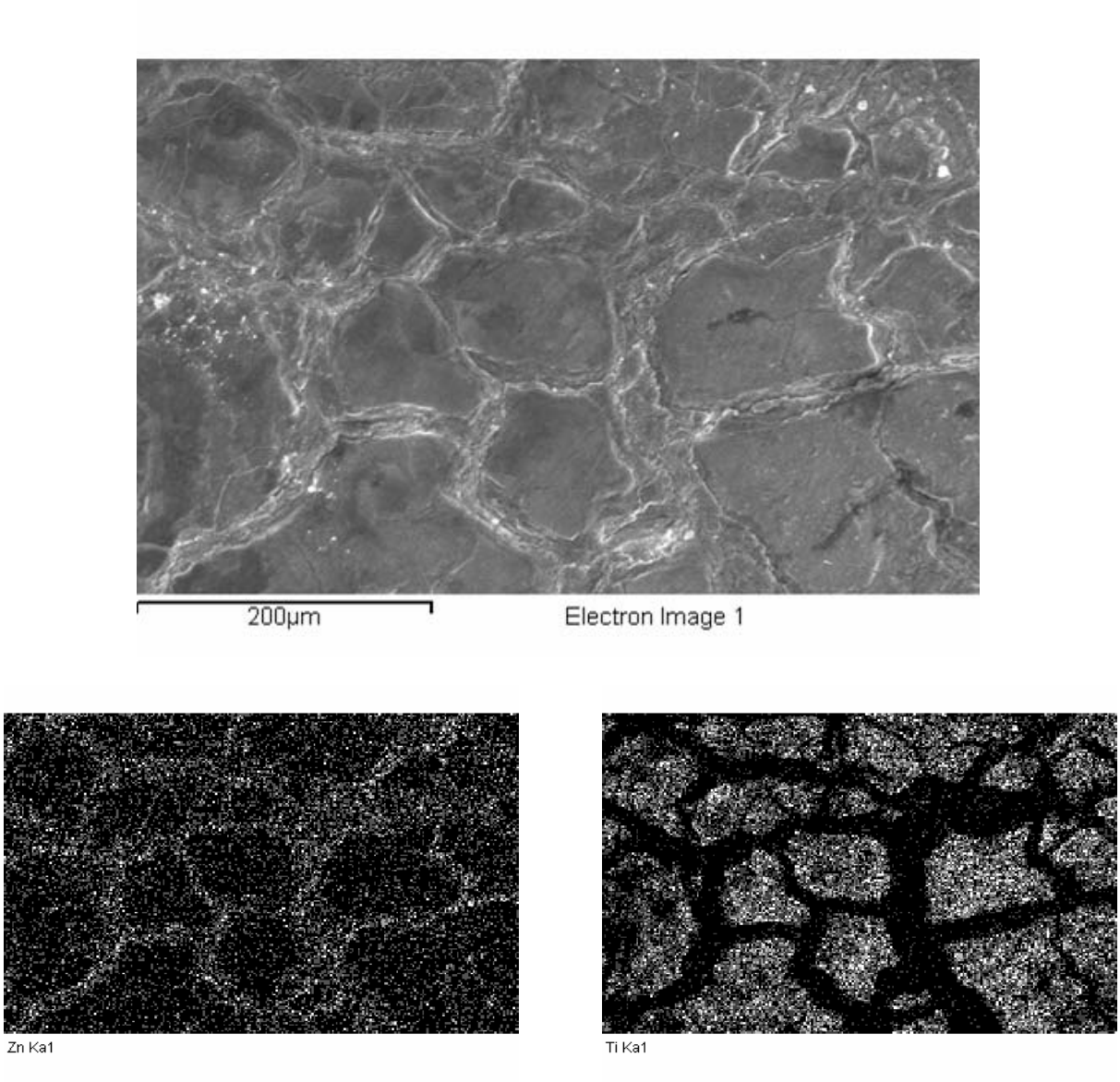

Figure 5.19: Coated electrode surface at 250 welds. SEM image and EDS elemental mapping showing TiC coating break up.

Forging brass is a copper-zinc alloy that is rated 100 out of 100 for hot forgability. The composition of forging brass (UNS C37700) is approximately 38% zinc, 2% lead and the remainder copper [48]. This composition is very close to that of beta brass,

suggesting that at elevated temperatures, the layer of beta brass underneath the TiC coating may have become extremely soft and have been displaced by the TiC coating. Figure 5.20 shows an area near the periphery of the same electrode shown in Figure 5.19. This area of the electrode appears as if the brass was being pushed to the lower right hand corner of the image. Evidence of the coating material being embedded into the softer brass was seen in Figure 5.21. At 250 welds, the particle of TiC coating has pushed aside the beta brass layer and was almost in contact with the base copper. The displaced brass has been forged around the particle and was flush with the top surface of the TiC particle.

Upon further welding, the beta brass present at the surface encountered more zinc from the sheet steel and could easily form the brittle gamma brass phase. Without the continuous diffusion barrier, zinc could diffuse around the coating particle and surround it with gamma brass. As discussed in Ch. 2, gamma brass is the phase that was continuously removed and replenished on the uncoated electrode surface which caused material loss. When surrounded by gamma brass, the TiC coating particles were likely to break off and become deposited to the steel sheet along with the brass.

The phenomenon of TiC embedding explains how the coated electrode length reduction could be greater than the initial coating thickness. The length reduction of the electrode can be greater than the coating thickness without complete coating loss because the coating is being depressed further into the electrode.

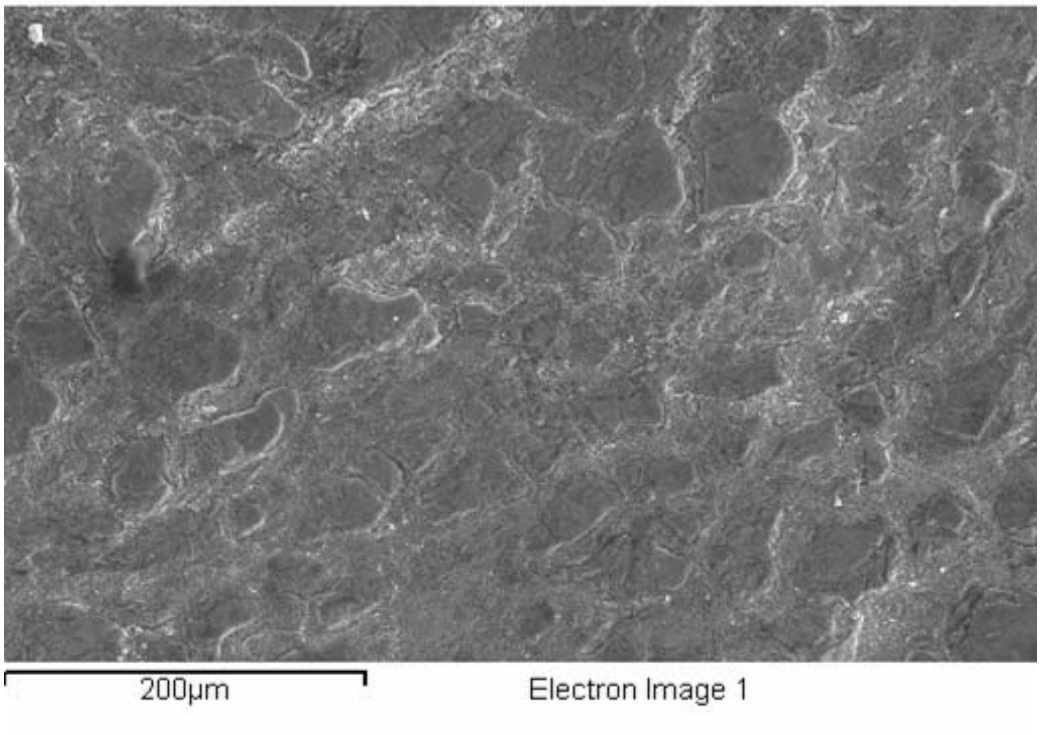

Figure 5.20: Coated electrode surface at 250 welds. SEM image and EDS elemental mapping showing TiC coating break up.

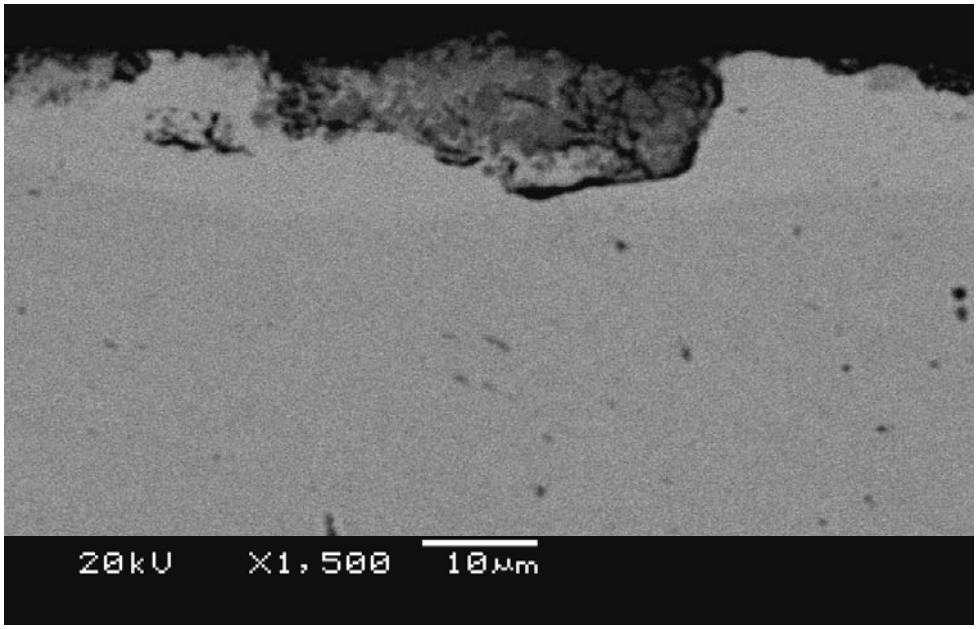

Figure 5.21: Coated electrode at 250 welds. A portion of the TiC coating has been embedded into the softer alloy layer.

5.3.2 Micro-deformation

The mechanism of TiC depression and extrusion of the beta brass layer can be viewed as micro-deformation, or deformation and displacement mechanism on the micron scale. At the end of life of the coated electrode, the length reduction was less than that of the uncoated electrode, yet the tip diameter growth was larger. This phenomenon as well as the unexplained tip growth with very little length reduction association could be explained by micro-deformation. The fragmented islands of TiC coating appeared to have been originally joined together to form the continuous coating in the as-coated condition. Figure 5.22 shows the same electrode surface seen in Figure 5.19, with the areas of zinc between the Ti islands isolated for image analysis. These areas accounted for approximately 40% of the image area according to image analysis. If the original coating surface was now depressed into a softer beta brass layer, conservation of volume would dictate that the surface area be enlarged, assuming that the brass was incompressible. A sample calculation for a $1mm^2$ area of the coated electrode surface, with a coating thickness of 30µm, and an alloy thickness of 10µm, given a depression of 5µm into the alloy layer and no loss of coating material, yields a 16% or $166\mu m^2$ increase

in surface area. The associated length reduction with the theoretical calculation is only 5μm.

Figure 5.22: Coated electrode surface at 250 welds from Figure 5.11 with contrast enhanced to reveal dark areas as new surface area.

The process of micro-deformation is shown schematically in Figure 5.23. Diagram a) in the figure shows the coating atop an alloy that had formed due to zinc penetration. In b), the force of repeated welds has caused the coating to break. These cracks are formed due to the unique situation of having a very hard layer supported by a much softer layer underneath. Heat and pressure from further welding causes the brass alloy underneath the coating to become forged into the cracks which pushed the coating aside. Figure 5.23c) shows the electrode surface after micro-deformation has taken place. The newly exposed area and enlargement are roughly quantified by *x1* and *x2*, where the associated length reduction is expressed as *h*. In practice, the thickness of the alloy layer and penetration of the coating was not uniform across the electrode surface and so becomes difficult to predict.

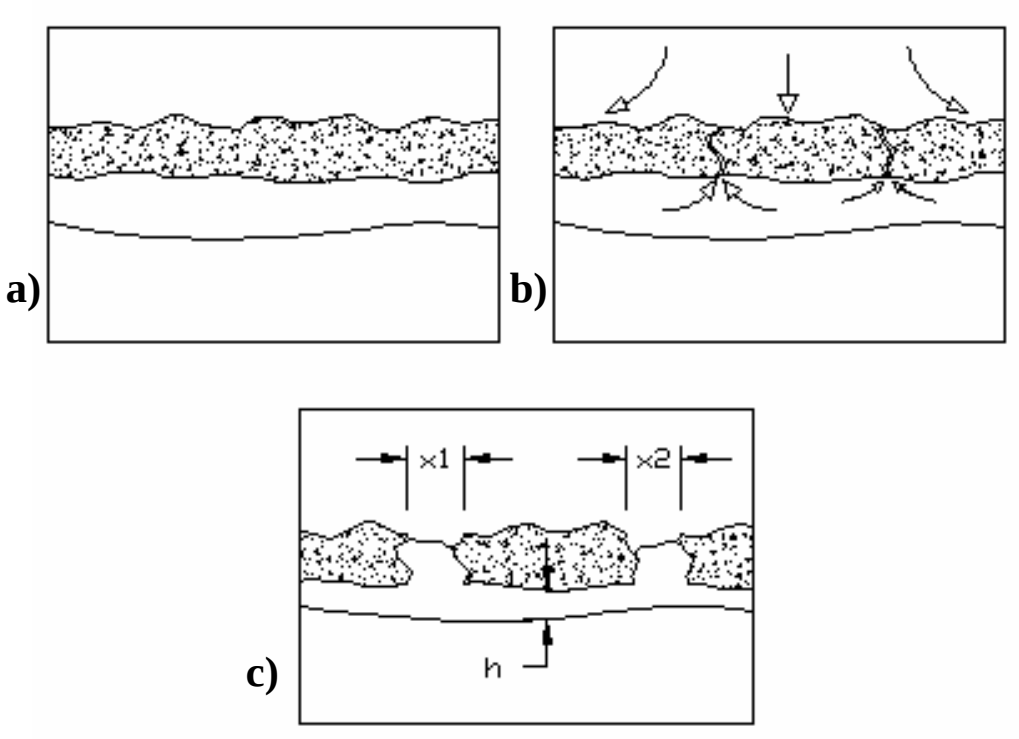

Figure 5.23: Schematic diagram of micro-deformation tip growth mechanism. a) The TiC coating sits atop a layer of beta brass. b) Cracks develop in the coating due to weld force. c) The coating is pressed into the soft alloy and the brass is extruded. x1 and x2 represent the new surface area exposed, h is the length reduction of the process.

Eventually, the exposed brass and copper brought to the surface by micro-deformation led to degradation similar to the uncoated electrode. Having the TiC particles embedded in the soft brass matrix may have helped to keep them on the electrode longer and prevented the coating from being lost to the steel sheet. Without the diffusion barrier in the fissures between coating fragments however, gamma brass was able to form easily. When the coating fragments were surrounded by sufficient gamma brass, loss of the entire fragment along with the surrounding gamma brass would occur. This was shown in Figure 5.24, where the fragmented surface of the coated electrode had lost a large section of coating due to alloy formation.

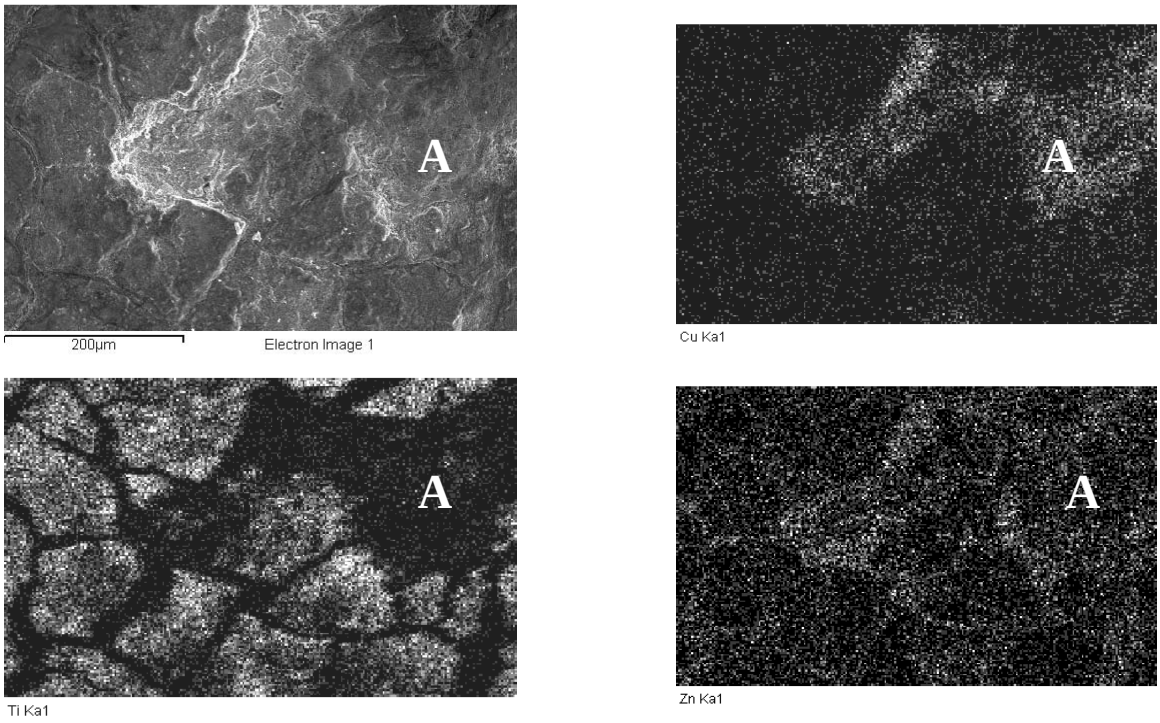

Figure 5.24: SEM/EDS image of coated electrode surface at 250 welds showing region of TiC coating fragment loss. Area labeled A has lost coating fragment due to sticking and stripping of coating fragment along with surrounding brass alloy

Chapter 6

Conclusions and Recommendations

This chapter summarizes the findings of this work with respect to the weldability and wear mechanisms affecting a TiC MMC coated cap electrode for the RSW of zinc HDG steels. The domed nose coated electrodes were tested in parallel with conventional RWMA Class II material electrodes and were shown to improve the robustness of the RSW system as well as improve electrode tip life. Typical wear mechanisms that afflict the conventional electrodes were delayed however a new mechanism was discovered which eventually led to the failure of the coated electrodes. Suggestions are also made of directions that this work may take to be extended for further study.

6.1 Coated Electrode Weldability

Lower weld current was necessary when using the coated electrodes. The decrease in power needed and increase of the range of acceptable parameters indicated the increase of the robustness of the coated electrode welding system. Electrode life testing proved that the coated electrodes could reduce the degree of wear and degradation of the electrode improving the tip life. Electrode softening and deformation was not affected by the presence of the TiC coating. The resistance circuit of the system with the addition of the electrode coating was investigated and the TiC coating was found to act as a thermal barrier insulating the weld.

- The coated electrodes made buttons of the MWS at 10300A of weld current where the uncoated electrodes required 10700A. The range of current where acceptable buttons was also improved to 600A over the 400A of the uncoated electrodes.
- Necessary weld time was also reduced to 166.7ms (10 cycles), 67ms less than the 233ms (14 cycles) weld time needed for the uncoated electrodes to achieve MWS. Also the acceptable weld time range was increased to 100ms (6 cycles) with the coated electrodes over the 67ms (4 cycles) of the uncoated electrodes.
- During the weld sequence, the heat generated at the faying interface was theoretically able to travel very quickly through the thickness of the steel and into the electrodes. The presence of the TiC coating at the electrode-sheet interface worked to insulate this interface and retain the heat in the weld. For this reason, the coated electrode was able to form larger nuggets than the uncoated electrode with the same heat input.
- Electrode tip life was improved from 300-1100 welds by using the coated electrode.
- The formation of alloy layers was delayed hence reducing the rate of material loss and length reduction. Tip growth rates were reduced by approximately 38% and as a result and electrode life was extended.
- Electrode softening was apparent after only 24 welds, with the coated electrode experiencing the same degree as the uncoated electrode. The degree of macro-deformation at the end of electrode life was very minor, not contributing to the failure mechanism of the electrodes.

6.2 Coated Electrode Failure

The processes by which the coated electrode was degraded differed from that of the uncoated electrode. Erosion of the coated electrode tip face and resulting tip face growth was accompanied by a form of surface deformation unique to the coated electrode.

Eventual penetration of the zinc, and breakdown and loss of the TiC coating caused the coating and hence the electrode to fail.

- The brittle TiC electrode coating cracked easily due to defects present from the coating process. These cracks allowed the penetration of zinc in localized areas which diffused along the coating electrode interface which formed a layer of brass underneath the coating.
- Upon successive weld force cycles, the hard coating on top of the soft brass layer broke apart easily and extruded the underlying brass into the cracks formed between coating plates. With copper alloys in direct contact with the molten zinc coating presented upon each weld, the development of gamma brass led to the loss of material as well as areas of TiC coating.
- Continued pressure from the weld force cycle embedded the broken plates of TiC coating further into the alloy layers on the electrode surface. The embedded TiC was not detected by EDS surface scans resulting in inaccurate readings of remaining elemental Ti on the electrode surface.
- Tip diameter growth due to the depression and extrusion of the brass layer termed micro-deformation occurred only with the coated electrodes and explained the phenomenon of tip diameter growth with little electrode length reduction. As the coating was broken and depressed into the electrode slightly, the original area occupied by the coating is spread out with the brass that was extruded around it increasing the area by up to 40% in some areas.

6.3 Future Work

Findings from this study have prompted questions on the possible improvement of the electrode coating. Although the coating was able to delay the interactions of zinc and copper, eventual damage to the coating undermined the coating caused the electrodes to fail. It was believed that improving initial coating quality would improve tip life as the

initial defects would be eliminated, however in light of the evidence of new cracks forming after very few weld cycles, the production of an initially defect free coating may prove to be useless.

Optimization of the coating thickness and composition can be performed with the aid of the knowledge gained in this study. Increasing the coating thickness on the electrode surface may force the zinc to travel further to reach the copper base material and provide a thicker thermal insulating barrier to assist in weld formation, but may also increase the surface resistance of the electrode and cause overheating. Explorations into the use of materials other than ceramic particles can be made in order to create a more elastic coating that is able to withstand the heat, force, and current of the weld cycles without fracturing. If the zinc can be effectively kept away from the copper, the extremely harmful interactions can be halted and the tip life of the electrodes can begin to approach that of uncoated steels.

Appendix A

Experimental Data

This section presents the data measured from the various experiments that were performed for the study. Experiments were conducted for weldability testing and electrode life testing. Data has been grouped by weld or electrode characteristic and is presented as measured.

Weldability Testing

Weld Current Testing

Test trials conducted on 1.0mm thick HDG steel sheets. A new electrode pair was used for each test. All other welding parameters were held constant while weld current was adjusted. Weld current, peel button diameter, and weld condition was recorded in Table A.1.

Table A.1: Weld Current Test Results at 13 cycle Weld Time

	SET 1		SET 2	
	Button Size / Joint Condition		Button Size / Joint Condition	
Weld Current (A)	Coated Electrode	Uncoated Electrode	Coated Electrode	Uncoated Electrode
10000	0	0	0	0
10100	Interfacial Failure	0	0	0
10200	3.1	0	Interfacial Failure	0
10300	4.2 (MWS)	0	2.8	0
10400	4.84	0	4.1 (MWS)	0
10500	5.6	Interfacial Failure	4.9	0
10600	5.8	3.6	5.25	0
10700	6.16	4.5 (MWS)	5.9	Interfacial Failure
10800	6.2	5.57	6.4	3.6
10900	6.5 (Expulsion)	5.8	6.7 (Expulsion)	4.5 (MWS)
11000		6.3		5.3
11100		6.45 (Expulsion)		6.2
11200				6.65 (Expulsion)

Weld Time Testing

Test trials conducted on 1.0mm thick HDG steel sheets. A new electrode pair was used for each test. All other welding parameters were held constant while weld time was adjusted. Weld time, peel button diameter, and weld condition was recorded in Table A.2.

Table A.2: Weld Time Test Results at 10500A Weld Current

		SET 1		SET 2	
Weld Time		Button Size / Joint Condition		Button Size / Joint Condition	
(ms)	(cycles)	Coated Electrode	Uncoated Electrode	Coated Electrode	Uncoated Electrode
17	1	0	0	0	0
33	2	0	0	0	0
50	3	0	0	0	0
67	4	0	0	0	0
83	5	0	0	0	0
100	6	0	0	No Fusion	0
117	7	Interfacial Failure	0	Interfacial Failure	0
133	8	3.46	0	3.1	0
150	9	3.74	0	3.8	0
167	10	4.7 (MWS)	0	4.25 (MWS)	0
183	11	5.09	0	4.95	0
200	12	5.2	0	5.36	0
217	13	5.6	Interfacial Failure	5.7	Interfacial Failure
233	14	6.15	4 (MWS)	6.06	3.66
250	15	6.53 (Expulsion)	5.2	6.45 (Expulsion)	4.12 (MWS)
267	16		6.46		5.86
283	17		6.6 (Expulsion)		6.04
300	18				6.52 (Expulsion)

Electrode Life Testing

Life tests were conducted as per the AWS Recommended practices for electrode life testing using coated steels [15]. The following tables present the data as recorded from the test sets

Table A.3: Uncoated Electrode Weld Button Size

Weld Number	Uncoated Electrode Weld Button Diameter							
	SET 1		SET 2		SET 3		SET 4	
	x	y	x	y	x	y	x	y
6	5.78	5.85					4.8	5.23
7	5.91	5.98					4.4	4.76
8	5.68	5.8	4.77	5.3	4.47	5.06	4.99	5.2
9	5.6	5.85	4.71	5.24	4.66	5.2	5.4	5.6
10	5.78	5.92	4.69	5.33			4.7	5.28
96	5.8	6.05					5.25	5.65
97	5.57	6.08					4.94	5.68
98	5.58	5.95	4.96	5.76			5.05	5.28
99	5.6	5.87	4.88	5.51			5.15	5.92
100	5.56	6.08	5.05	5.48			5.03	5.5
196	2.98	4.98					3.93	5.5
197	5.56	6.02					3.9	5.2
198	5.72	6.03	4.35	5.36			3.11	5.01
199	5.69	6.09	3.98	5.36	4.84	5.24	3.74	5.4
200	5.48	6.04	3.78	5.62	2.93	4.8	3.5	5.15
296	2.5	5.5					2.66	4.81
297	3.03	4.75					2.9	4.91
298	3.89	5.28	3.56	4.07			2.6	5.2
299	0	0	2.94	4.52			2.9	4.8
300	2	4.5	2.6	5.2			2.3	4.6
396	0.8	1.72					1.76	3.47
397	0	0					1.66	3.73
398	1.75	3.3	2.13	3.55			1.5	4.14
399	2.04	4.3	1.89	4.25	1.6	5.01	1.85	3.55
400	0	0	2.41	4.61	1.5	4.59	1.3	4.04
496							3.46	3.46
497							2.7	2.7
498			1.2	4.47			2.93	2.93
499			0.9	2.2	0.8	1.68	2.66	2.66
500			1.33	4.81	1.02	1.09	1.2	3.37
596							2.15	4.8
597							3.13	4.96
598							2.6	4.9
599							2.6	4.66
600							2.75	4.69

Table A.4: Coated Electrode Weld Button Size

Weld Number	Coated Electrode Weld Button Diameter							
	SET 1		SET 2		SET 3		SET 4	
	x	y	x	y	x	y	x	y
6			5.41	5.44				
7			5.6	5.76				
8	5.34	5.12	5.61	5.81	5.08	5.09	5.16	5.18
9	5.13	5.22	5.35	5.51	5.26	5.19	5.04	5.06
10	5.31	5.17	5.25	5.48	5.2	5.18	5.09	5.33
96			5.16	5.65				
97			5.02	5.62				
98			5.04	5.69				
99			5.08	5.75				
100			5.35	5.5				
196			4.61	5.45				
197			4.62	5.45				
198	5.29	5.31	4.96	5.35	5.36	5.42	4.98	5.09
199	5.31	5.29	4.83	5.24	5.26	5.39	5.62	5.66
200	5.41	5.5	4.93	5.88	5.56	5.69	5.14	5.16
296			3.51	5.39				
297			3.84	5.48				
298			4.25	5.78				
299			4.72	5.68				
300			4.02	5.34				
396			2.79	5.17				
397			4.45	5.35				
398	5.01	5.13	3.32	5.34	5.07	3.68	4.71	5.01
399	5.27	5.22	4.5	5.6	5.23	5.37	4.77	4.63
400	5.09	5.26	3.24	5.25	5.36	5.08	4.59	4.6
496			3.09	5.13				
497			3.13	5.75				
498	4.84	5.11	3.01	5.24				
499	3.83	5.26	3.37	5.47				
500	4.99	5.2	2.19	5.12				
596			3.18	5.25				
597			3.31	4.49				
598	4.4	3.95	3.53	5.4	3.97	2.46	4.12	5.43
599	4.32	4.33	3.49	5.25	4.4	4.64	4.32	4.25
600	4.39	4.28	3.15	5.3	4.66	4.77	3.99	4.78
696			2.75	5.09				
697			3.49	5.18				
698	4.43	4.16	3.64	5.01	4.39	4.1		
699	2.19	4.07	3.46	4.94	4.53	3.55		
700	4.67	3.59	3.18	5.27	4.01	2.76		
796			2.59	5.09				
797			3.96	4.69				
798	4.48	2.96	3.65	4.67	3.05	4.26	4.32	2.79
799	1.5	4.67	3.57	4.68	2.17	4.32	3.72	5.12

800	4.66	3.44	2.77	4.81	4.79	2.24	4.87	3.88
896			2.29	5.04				
897			2.65	4.75				
898	4.62	3.68	3.31	5.02	3.31	3.97		
899	4.59	3.44	2.66	4.89	4.06	2.65		
900	4.35	4.02	2.55	5.02	3.53	5.29		
996			2.7	3.75				
997			2.85	4.78				
998	4.96	3.65	1.26	3.12	3.29	4.76	3.58	2.64
999	4.61	3.3	2.09	4.77	4.39	5.28	2.99	4.98
1000	4.86	3.29	2.9	4.6	5.07	4.46	3.25	4.85
1096			3.38	4.62				
1097			2.9	4.6				
1098	4.19	2.96	2.78	4.78	5.51	3.78	4.89	3.45
1099	4.61	3.12	3.1	4.97	1.19	2.02	3.87	3.71
1100	4.64	3.07	1.82	4.55	4.76	1.07	3.92	5.23
1196			2.87	4.7				
1197			3.1	4.44				
1198	0.99	3.69	1.89	3.09	2.93	4.34	4.03	3.47
1199	3.67	2.65	2.8	4.64	2.14	3.04	3.1	4.44
1200	4.03	3.47	0.87	4.5	1.08	4.96	3.67	2.65
1296			1.67	3.8				
1297			2.45	3.93				
1298	2.52	1.08	1.6	1.9	0	0	1.2	2.36
1299	2.31	3.91	1.56	3.63	1.65	4.03	1.6	2.02
1300	2.15	2.78	2.03	4.11	3.6	4.06	1.16	3.69
1396			0	0				
1397			0	0				
1398			0	0			1.2	0.9
1399			1.18	1.5			0	0
1400			1.5	3.43			0.7	0.9

Table A.5: Electrode Tip Diameter as Measured from Carbon Tip Imprints

	Uncoated Electrode				Coated Electrode			
WELDS	SET 1	SET 2	SET 3	SET 4	SET 1	SET 2	SET 3	SET 4
0	4.895	4.92	4.93	4.65	4.99	4.88	5.01	4.75
100	5.32	4.995	5.2	5.11	5.01	5.03	4.99	4.86
200	5.51	5.17	5.41	5.21	5.16	5.14	5.29	5.11
300	5.63	5.375	5.48	5.35	5.24	5.28	5.45	5.125
400	5.94	5.525	5.59	5.68	5.31	5.33	5.46	5.235
500		5.74	5.66	5.55	5.4	5.37	5.55	5.14
600				5.62	5.43	5.43	5.57	5.35
700					5.61	5.5	5.64	5.42
800					5.65	5.61	5.65	5.615
900					5.74	5.68	5.75	5.56
1000					5.75	5.76	5.79	5.58
1100					5.68	5.82	5.88	5.66
1200					5.81	5.88	5.97	5.88
1300					5.89	5.92	5.96	5.955
1400						5.95		5.88

Table A.6: Electrode Length Reduction

	Top Electrode Length Reduction (mm)			
	Coated SET 2	Coated SET 3	Uncoated SET 2	Uncoated SET 4
Welds				
0	0.000	0.000	0.000	0.000
100	-0.018	-0.050	-0.033	-0.080
200	-0.022	-0.140	-0.077	-0.110
300	-0.041	-0.100	-0.105	-0.170
400	-0.038	-0.050	-0.117	-0.120
500	-0.047	-0.060	-0.149	-0.090
600	-0.039	-0.050		-0.130
700	-0.051	-0.110		
800	-0.055	-0.103		
900	-0.058	-0.100		
1000	-0.067	-0.091		
1100	-0.076	-0.090		
1200	-0.082			
1300	-0.102			
1400	-0.104			

Table A.7: Elemental Copper Weight Percent on Steel Weld Top Surface

	Weight Percent Elemental Copper on Weld Surface				
Weld	**Coated Electrode SET 1**				
1	3.02	3.322	2.416	3.473	2.869
2	3.11	3.421	2.488	3.5765	2.9545
3	3.16	3.476	2.528	3.634	3.002
5	2.5	2.75	2	2.875	2.375
10	3.17	3.487	2.536	3.6455	3.0115
15	2.85	3.135	2.28	3.2775	2.7075
20	2.67	2.937	2.136	3.0705	2.5365
80	6.55	7.205	5.24	7.5325	6.2225
100	6.56	7.216	5.248	7.544	6.232
200	6.22	6.842	4.976	7.153	5.909
300	3.09	3.399	2.472	3.5535	2.9355
400	2.56	2.816	2.048	2.944	2.432
500	2.22	2.442	1.776	2.553	2.109
600	2.54	2.794	2.032	2.921	2.413
700	2.43	2.673	1.944	2.7945	2.3085
800	3.95	4.345	3.16	4.5425	3.7525
900	2.11	2.321	1.688	2.4265	2.0045
1000	2.79	3.069	2.232	3.2085	2.6505
1100	3.56	3.916	2.848	4.094	3.382
1200	3.4	3.74	2.72	3.91	3.23
1300	2.5	2.75	2	2.875	2.375
	Weight Percent Elemental Copper on Weld Surface				
Weld	**Uncoated Electrode SET 4**				
1	10.17	11.187	8.136	11.6955	9.6615
2	6.54	7.194	5.232	7.521	6.213
3	7.53	8.283	6.024	8.6595	7.1535
4	7.47	8.217	5.976	8.5905	7.0965
5	7.49	8.239	5.992	8.6135	7.1155
9	4.95	5.445	3.96	5.6925	4.7025
10	6.03	6.633	4.824	6.9345	5.7285
15	6.56	7.216	5.248	7.544	6.232
20	7.38	8.118	5.904	8.487	7.011
50	13.44	14.784	10.752	15.456	12.768
75	7.22	7.942	5.776	8.303	6.859
100	7.99	8.789	6.392	9.1885	7.5905
200	3.08	3.388	2.464	3.542	2.926
300	5.5	6.05	4.4	6.325	5.225
400	6.31	6.941	5.048	7.2565	5.9945
500	2.96	3.256	2.368	3.404	2.812
600	3.83	4.213	3.064	4.4045	3.6385

Table A.8: Electrode Hardness Measurements on Sacrificed Electrodes

	Uncoated Electrode Vickers Hardness (HV)					
Distance from surface (mm)	24 welds		100 welds		End of Life	
0.05	107.96	111.09	75.18	77.36	90.15	92.77
0.1	124.03	127.63	82.70	85.10	99.18	102.05
0.2	147.59	151.87	91.71	94.37	112.26	115.52
0.5	167.26	172.11	126.38	130.05	137.14	141.11
1	167.32	172.17	140.26	144.32	158.17	162.75
2	183.55	188.87	153.04	157.48	169.31	174.22
5	169.33	174.24	148.77	153.09	178.43	183.61
	Coated Electrode Vickers Hardness (HV)					
Distance from surface (mm)	24 welds		100 welds		End of Life	
0.05	134.36	138.26	99.54	102.43	106.89	109.99
0.1	147.76	152.05	105.67	108.73	115.12	118.45
0.2	154.81	159.30	122.72	126.28	125.57	129.21
0.5	169.53	174.45	149.36	153.69	160.51	165.17
1	174.21	179.26	157.04	161.60	171.72	176.70
2	171.58	176.56	165.28	170.08	188.46	193.92
5	178.69	183.87	171.58	176.56	188.67	194.15

Table A.9: Electrode Circuit Electrical Static Resistance at Beginning and End of Life

	Beginning of Life			End of Life		
	Electrodes Only	One Sheet	Two Sheets	Electrodes Only	One Sheet	Two Sheets
Uncoated Electrodes	12.5	22.8	32.5	13.8	20.8	34.7
	13.0	21.6	32.9	13.6	20.7	33.2
	13.6	23.8	33.4	14.9	21.3	34.9
	11.8	22.5	33.8	12.6	19.4	35.6
	12.9	23.0	31.2	13.5	21	34.7
Coated Electrodes	36.1	33.9	36.0	18.4	26.9	35.1
	36.9	34.8	37.1	19.7	27.8	36.4
	34.8	33.1	36.2	18.2	26.1	34.1
	37.2	32.9	35.7	17.9	25.4	36.9
	36.5	35.0	34.8	19.3	28	33.8

Table A.10: Electrode Cap Mass at Beginning and End of Life

	Uncoated Electrode Mass (g)			
	0 welds		End of Life	
Measurement	Top Electrode	Bottom Electrode	Top Electrode	Bottom Electrode
1	24.5988	24.6872	24.584	24.6874
2	24.5987	24.6872	24.5826	24.6872
3	24.5988	24.6874	24.5839	24.6871
	Coated Electrode Mass (g)			
Measurement	Top Electrode	Bottom Electrode	Top Electrode	Bottom Electrode
1	24.7625	24.5917	24.7438	24.5693
2	24.7622	24.5918	24.7436	24.5691
3	24.7626	24.5917	24.7438	24.5694

Appendix B

Sample Calculations

Calculations for electrode volume and mass loss predicted from measured electrode length reductions are given below. Geometric equations used were taken from *Mark's Standard Handbook for Mechanical Engineers* [53].

Predicted Mass Loss

To determine the amount of mass theoretically lost from the electrode face, measured electrode length is used with measured face diameter before and after welding to determine volume change of the electrode. Volume is then multiplied by an approximate density of the material lost to yield a predicted net mass change.

The volume of a spherical zone is given by:

$$V = \frac{1}{6}\pi h\left[3\left(\frac{D1}{2}\right)^2 + 3\left(\frac{D2}{2}\right)^2 + h^2\right] \qquad (5.1)$$

where, D2 is the final tip diameter

D1 is the initial tip diameter

h is the length reduction

For example, using the measured length reduction for h, and the measured initial and final tip diameters, actual volume lost for the uncoated top electrode of SET 4 assuming no deformation has occurred was found:

h (mm)	D1 (mm)	D2 (mm)
-0.13	4.65	5.62

$$V = \frac{1}{6}\pi(-0.13)\left(3\left(\frac{4.65}{2}\right)^2 + 3\left(\frac{5.62}{2}\right)^2 + (-0.13)^2\right) \text{ [mm}^3\text{]}$$

$V = \text{-}2.717\,\text{mm}^3$

Taking the volume loss and knowing the approximate density of copper [52], mass loss can be found as the product of density and volume. The predicted mass loss was found:

ρ copper
8.93mg/mm^3

$m = \rho V$
$m = 8.93(-2.717)\,[\text{mg}]$
$m = -0.0243\,\text{mg}$

Predicted Tip Diameter

To predict the diameter of the electrode tip face at any time during the electrode life, equation 5.2 can be used knowing the initial measured tip diameter, measured length reduction, and radius of curvature of the electrode dome portion as follows:

$$D' = 2 * \sqrt{R^2 - (\sqrt{R^2 - \left(\frac{D1}{2}\right)^2} - h)^2} \qquad (5.2)$$

where, D' is the predicted tip diameter
R is the radius of curvature of the dome
D1 is the initial tip diameter
h is the length reduction

Again, using measurements from uncoated SET 4 at end of life, variables are given below. Note that h is a positive value for length reduction.

R (mm)	D1 (mm)	h (mm)
8.0	4.65	0.13

$$D' = 2 * \sqrt{8^2 - (\sqrt{8^2 - \left(\frac{4.65}{2}\right)^2} - (0.13))^2} \text{ [mm]}$$

$$D' = 5.433 \text{ [mm]}$$

References

1. RWMA Handbook, Fourth Edition, 1989

2. Howe, P., Kelly, S. C., “A Comparison of the Resistance Spot Weldability of Bare, Hot-Dipped, Galvannealed, and Electrogalvanized DQSK Sheet Steels”, International Congress and Exposition, Detroit Michigan, February 29-March 4, 1988.

3. Gedeon, S. A., Eagar, T. W., “Resistance Spot Welding of Galvanized Steel: Part I. Material Variations and Process Modifications”, Metallurgical Transactions B, Vol. 17B, Dec. 1986, pp. 879-885.

4. Gedeon, S. A., Eagar, T. W., “Resistance Spot Welding of Galvanized Steel: Part II. Mechanisms of Spot Weld Nugget Formation”, Metallurgical Transactions B, Vol. 17B, Dec. 1986, pp. 887-901.

5. Parker, J. D., Williams, N. T., Holliday, R. J., “Mechanisms of electrode degradation when spot welding coated steels”, Science and Technology of Welding and Joining, 1998, Vol. 3, No. 2, pp. 65-74

6. Holliday, R.J., Parker, J. D., Williams, N. T. (UK), “Relative contribution of electrode tip growth mechanism in spot welding zinc coated steels”, Welding in the World, Vol. 37, No. 4, pp. 186-193, 1996

7. Holliday, R.J., Parker, J. D., Williams, N. T. (UK), “Electrode deformation when spot welding coated steels”, Welding in the World, Vol. 35, No. 3, pp. 160-164, 1995.

8. Ikeda, R., Yasuda, K., Hashiguchi, K., Okita, T., Yahaba, T., “Effect of Electrode Configuration on Electrode Life in Resistance Spot Welding of Galvannealed Steel and Aluminum Alloy For Car Body Sheets”, IBEC 1995, Advanced Technologies and Proceedings, pp. 144-151

9. Saito, T., Takahashi, Y., Nishi, T., “Electrode Tip Life in Resistance Spot Welding of Zinc and Zinc Alloy Coated Sheet Steels”, Nippon Steel Technical Report, No. 37 April 1988, pp. 24-30

10. Friedman, L. M., McCauley, R. B., “Influence of Metallurgical Characteristics on Resistance welding of Galvanized steel”, Welding Journal, Supplement, Oct. 1969, pp. 454s-462s

11. Tanaka, Y., Sakaguchi, M., Shirasawa, H., Miyahara M., and Nomura, S., “Electrode Life in resistance spot welding of zinc plated sheets”. Int. J. of Materials and Product Tech, vol. 2, no. 1, 1987. pp. 64-74

12. Natale, T.V., “ A review of the resistance spot welding behaviour of galvanized steels”, Sheet Metal Welding conference III, Detroit, USA, October 1988, Paper No. 1

13. Howe, P., “Resistance Spot Weldability and Electrode Wear Mechanisms of ZnNi EG® Sheet Steel”, SAE Technical Paper Series, 910192, 1991.

14. Lane, C. T., Sorensen, C. D., Hunter, G. B., Gedeon, S. A., Eagar, T. W., “Cinematography of Resistance Spot Welding of Galvanized Steel Sheet”, Welding Journal, Supplement, September 1987, pp. 260s-265s.

15. ANSI/AWS/SAE/D8.9-97, “Recommended practices for test methods for evaluating the resistance spot welding behaviour of automotive sheet steel materials”, AWS/SAE, 1997

16. Calva, C. M., Eager, T. W., “Enhancement of the weldability in resistance spot welding”, Sheet Metal Welding Conference IV, Conference Proceedings, 1990

17. Lu, F., Dong, P., “Model for estimating electrode face diameter during resistance spot welding”, Science and Tech. of Welding and Joining, Vol. 4, No. 5, 1999, pp. 285-289

18. Kaiser, J. G., Dunn, G. J., Eagar, T. W., “The Effect of Electrical Resistance on Nugget Formation During Spot Welding”, Welding Journal, Supplement, June 1982, pp. 167s-174s.

19. Babu, S.S., Santella, M. L., and Peterson, W., “Modeling Resistance Spot Welding Electrode Life”. Oak Ridge National Laboratory, 2000??

20. Huys Industries Limited, < http://www.huysindustries.com/ >, 2004

21. Product Knowledge Seminar Publication, BHP Steel, Sheet and Coil Products, 1990

22. Finlay, M. R., “Resistance Spot Welding of Metallic Coated Steels and PVD Coated Electrodes”, CRC Australia and WTIA, CRC No. 18, 1996

23. Gould, J. E., Peterson, W. A., “Resistance Welding Research Evaluations of Coated Steels. Part Three: Nugget Development Studies”, EWI Research Report, MR8814, August 1988.

24. ASM Binary Phase Diagrams, Vol. 1, 1987

25. Dong, S., Zhou, Y., “Effects of TiC Composite Coating on Electrode Degradation in Microresistance Welding of Nickel-Plated Steel”, Metal. And Materials Trans. A., Vol. 34A, July 2003, pp. 1501-1511

26. Orts, D.H., “The Effect of Zinc Coating in Resistance Spot Welding Galvanized Steel”, Master’s Thesis, Ohio State University, 1967

27. Morita, A., Inour, S., Takezoe, A., “Spot Weldability of Zinc Vapour Deposited Steel Sheets”, Journal of Metal Finishing Society, Japan. Vol. 39, No. 5, pp270-275.

28. Dickinson, D.W., “Welding in the Automotive Industry”. AISI Report SG81-5, August, 1981.

29. Kimchi. M., Gould, J., “Effects of Coating Weight on the Resistance Spot Weldability of Galvanized Steel”, SAE Technical Paper Series, No. 860436, 1986.

30. Nealon, C.S., Lake, J.S.H., “Resistance Spot Welding Tip Lives for Zincalume Coated Qualities”, BHP Steel Research and Technology Centre, Research Report No. 950, January 1987.

31. Jud, R.W., “Joining Galvanised and Galvannealed Steels”, SAE Technical Paper Series, No. 840285, 1984.

32. Kimchi, M., Gould, J.E., “The Evaluation of Resistance Spot Welding Electrode Materials for Welding Galvanised Steels”. Sheet Metal Welding Conference III, Detroit, USA, October 1988.

33. Kumagai, M., Nagata, K., “Spot Weldability of Aluminium Oxide Dispersion Strengthened Copper Electrodes for Alternate Welding of Mild Steel Sheets and Galvanised Steel Sheets”, Sumitomo Light Metals Technical Report, Vol. 31, No. 4, Oct. 1990, pp18-26.

34. Lavery, R.C., Williams, N.T., “Resistance Spot Welding of Galvanized Steels”, Sheet Metal Industries, March, 1970. pp201.

35. Gould, J.E., Kimchi, M., Campbell, D.H., “Weldability and Electrode Wear Characteristics of Hot Dip Galvanised Steel With and Without a Ferrophos Containing Primer”, SAE Technical Paper Series, 880370, 1988.

36. Saito, T., “Resistance spot weldability of coated sheet for automotive application”, Welding International 1992, Vol. 6 No. 9, pp 695-699

37. Roswell, S.L., “Resistance welding of hot-dipped galvanized steel”, Metal Construction, April 1978, pp. 163-169

38. Chatterjee, K.L., “Extending electrode life by tip design and dressing”, Welding and Metal Fabrication, Vol. 68, no. 8, pp. 12, 14. Sept. 2000

39. Takahashi, Y., Saito, T., “Development of Spin electrode spot welding. Report 2: Investigation of mechanism of electrode tip life improvement in coated steel sheet spot welding”, Quarterly Journal of the Japan Welding Society, Vol. 11, issue 1, 1993 pp. 61-67.

40. Nadkarni, V., Weber, E.P., “A New Dimension in Resistance Welding Electrode Materials”, Welding Journal, Supplement, November 1977, pp. 331s-338s.

41. Nadkarni, V., “Sticking Behavior of Common Electrode Materials and Electrode Designs in Welding Coated Steels”, SMWC VI, Proceedings, 1994.

42. Key, J.F., Courtney, T.H., “Refractory Metal Composite Tips for Resistance-Spot Welding of Galvanized Steel”, Welding Journal, Supplement, June 1974, pp. 261s-266s

43. Tanaka, Y., Naguchi, M., “An alumina dispersion strengthened copper composite electrode for spot welding”, Welding International, No. 11, 1987, pp. 1074-1078

44. De, A., Dorn, L., Gupta, O.P., Chang, I., “Advanced Electrode Design for Resistance Spot Welding of Galvanized Steel – a Numerical and Experimental Study”, Eurojoin 3, third European Conference on Joining Technology, April 1998

45. West, E.G., “Copper and its Alloys”, Ellis Horwood Ltd., John Wiley & Sons Canada Ltd., 1982.

46. Finlay, R., Samandi, M., Howes, S., “PVD Coating of Resistance Spot Welding Electrodes”, Welding Research Supplement, Australian Welding Journal, Vol 42, First Quarter, 1997.

47. Roach, B.W., “Resistance Welding of Modern Coated Materials”, Welding Review, November, 1988, pp226-230.

48. Copper Development Association, 260 Madison Avenue, New York, New York 10016, 2003

49. Newbury, D., Joy, D., Echlin, P., Fiori, C., Goldstein, J., “Advanced Scanning Electron Microscopy and X-Ray Microanalysis”, Plenum Press, New York. 1986.

50. White, C.L., Gugel, M.D., Kimchi, M., “Mechanisms of resistance welding electrode wear on galvanized steel”, Automation Ltd., Vol. 2, 1996, pp 839-850

51. Carslaw H.S., Jaeger J.C., “Conduction of Heat in Solids”, Oxford University Press, London, second edition, 1959.

52. Tslaf, A., “Combined Properties of Conductors”, Elsevier Scientific Publishing Company, New York, 1981.

53. Avallone, E.A., Baumeister III, T., Editors, “Mark’s Standard Handbook for Mechanical Engineers”, 9th Edition, McGraw Hill, New York, 1979.